REDOX-ACTIVE POLYMERS AS CATHODE MATERIALS FOR ELECTROCHEMICAL ENERGY STORAGE SYSTEMS

A Dissertation

Presented to the Faculty of the Graduate School

of Cornell University

In Partial Fulfillment of the Requirements for the Degree of

Doctor of Philosophy

by

Thanh-Tam Thi Truong

August 2015

REDOX-ACTIVE POLYMERS AS CATHODE MATERIALS FOR ELECTROCHEMICAL ENERGY STORAGE SYSTEMS

Thanh-Tam Thi Truong, Ph. D.

Cornell University 2015

The world's rising energy needs and finite fossil-fuel resources demand the development of new methods of generating and storing energy. For renewable energy sources, which are inherently intermittent, to be successfully implemented in a sustainable energy future requires the development of energy storage technologies. The next-generation of electrochemical energy storage (EES) technologies needs to have higher energy and power densities, long cycle life, while also being a safer and more sustainable alternative than current devices. The bottleneck for Li-ion batteries, the highest energy density EES devices, is the cathode material. Consequently, the improvement of the performance of cathode materials can have a dramatic effect on the overall performance of EES devices. Organic compounds are promising alternative materials to existing inorganic cathode materials due to their high theoretical gravimetric capacities, energy and power densities, and abundance. The development of new organic cathode materials is discussed in this work. The polyarylamines investigated display multiple reversible redox couples and good cycling performance.

BIOGRAPHICAL SKETCH

Thanh-Tam Truong was born in Vietnam in 1988 and moved to Washington State when she was six-years old with her two older brothers and parents. The adjustment to a new country and culture was difficult – she refused to attend the first day of school in the States – but her curiosity to learn aided her transition. Especially important to her growth was discovering a passion for reading thanks to several programs promoted by McCarver Elementary School. Her interest in chemistry started in general chemistry class at Foss High School due to the hands-on laboratory experiments, such as identifying mystery inorganic compounds. Two more years of chemistry classes in the International Baccalaureate Program convinced her to consider a career in chemistry. Her college search focused on liberal arts colleges with rigorous academic programs and a supportive, involved, well-rounded student body, and she found a great fit in Whitman College. Entering Whitman, she contemplated completing a 3-2 program where she would transfer to another university after three years at Whitman to complete her chemical engineering degree. However, the chemistry department at Whitman was exceptional with new, enthusiastic professors and she decided to stay in Walla Walla, Washington to finish her Bachelor of Arts. After completing a summer research experience at IBM Almaden in 2009, she knew she wanted to continue working in a chemistry lab and applied to graduate schools. She moved across the country to Ithaca, New York in 2010 for her graduate studies in chemistry at Cornell University with Professors Héctor Abruña and Geoffrey Coates. Upon completion of her Ph.D., she will be a postdoctoral researcher at Savannah River National Laboratory. She is looking forward to living in another region of the US!

Dedicated to those who lift as they rise

ACKNOWLEDGMENTS

I would like to thank my committee for their guidance, support, and thoughtful discussions during my time at Cornell University. I am so grateful to have joined the Héctor Abruña research group and worked alongside amazing scientists under the direction of a great boss. I have learned so much about electrochemistry and energy materials in the last five years, but sadly, not Spanish. Our discussions about the role of professor/mentor/advisor have really influenced me and I shall carry the same philosophy to always treat others with respect and generosity. The enthusiasm and energy Professor Abruña brings everyday for chemistry is unmatched and have countless times encouraged me to continue working and to stay motivated. Professor Abruña has always stated that his legacy as a scientist is the students, postdocs and visiting scientists in his group, and I'm honored to say that I am a member of the growing Abruña academic family tree. I am also a student in the Geoffrey Coates research group, and I am lucky to have worked with many fantastic organic chemists. I learned a lot from his example as a scientist, professor and advisor. I usually come away from meetings with Geoff with new ideas and directions to pursue. Geoff has a very discerning eye for data presentation and I have improved tremendously on how to communicate data in presentations and in articles. I thank Will Dichtel for insightful discussions and suggestions, and I have enjoyed my collaborations with the Dichtel group and use of their instruments. I am very glad to have Brett Fors as a proxy on my committee and for his help with cross-coupling chemistry.

I would not have completed 21 years of education without the support of my parents and two brothers. My parents left everything that was familiar and dear to them in Vietnam to move to the United States in order to provide more opportunities for my siblings and me. I cannot thank them enough for their strength and courage. My older brothers are the scouts of my life; they guide and advise me to find the right

path based upon their experience. I remember I refused to attend the first day of school in the US, and they convinced me to go the next day by describing how much fun it was. Thanks Tan and Tuan for always having my back.

I am so appreciative of the people who made the daily grind of graduate school more enjoyable and broadened my chemistry knowledge. My dearest friends, Deepti and Yuki, have been with me since the beginning of graduate school; literally in the case of Yuki since I sat down next to her on the first day of TA training during the summer of 2010. I aspire to have Deepti's positive attitude, levelheadedness and kindness, and Yuki's compassion, strength and generosity. Our friendship has helped me so much and had the most effect on my personal growth in the last five years. Thanks for all of the memories and delicious meals!

My fellow electrochemists are amazing people, scientists and coworkers. Thanks to Stephen and Michele for introducing me to the Abruña group; Nikki, Eric and Joaquin for countless meals and discussions; Sean and Gaby for their constant help in synthesis and electrochemistry; Joanna, Dave, Michael and Jie for their support and assistance. Special thanks to my batch mates, Kenny and Katie, for their willingness to lend a hand and an ear. Best of luck to Abby, Ryo, Rebecca, Johary, James P., James M., Hongsen, Luxi, Dong, Na and Yin. I know you'll do well during the rest of your time at Cornell and beyond. Luxi, you've been an amazing person to work with and I have enjoyed watching your growth. As the boss says, let 'er rip!

The people in the Coates group made coming into lab, even on the worse of days, worth it. I've lucked out on office mates in 570 – you are the best. Yuki, thanks for being my desk neighbor for five years and sharing a snack drawer (and too many 11 lb bags of ginger candy), and your valuable help in lab. Thanks to Giang for being my go-to consultant on organic synthesis; the good doctor, Pasquale, for being a steadying influence; Sarkar for all your advice and aid in chemistry and life. Tulaza

probably claims the title for most interesting person I've ever met. You have "short-circuited" my brain a lot but I'm so glad to have met you and thanks for making everyday interesting and memorable. Maria is one of the sweetest people in my life and I really cherish our friendship. As you are channeling your inner Tam, I have been channeling my inner Maria, too. James E. continued the trend of great post-docs working in 570 and he is a great conversationalist and chemist. Thanks for expanding our pop culture knowledge and music repertoire, as well as being a wealth of organic synthesis knowledge.

The rest of the Coates crew, past and present, made the fifth floor a wonderful work environment. Anne is a fantastic resource and sounding board. Our lab would not operate half as well without her. I really admire Rachna for her knowledge, straightforward personality and sense of humor. Angie was the first member of the group I've ever interacted with and she is one of the kindest people in my life. Thanks to Michael, Chad, C, Erin and Taz for their help, advice, and encouragement. I wish all the best for the current group members: Kyle, Masato, Jessica, Brandon, Michelle, Qi, Lilli, Julie, Xiaopeng and Leah. I will miss discussing hockey (and attending games) with Jessica. I am so lucky to have Ian, Kristina, Nate and Yuki as my batch mates; you are all such talented and amazing individuals. Thanks for always having my back and commiserating with me at the beginning of graduate school in classes and as we wrapped up our final year at Cornell. I look forward to hearing about your future accomplishments and adventures. And a big thank you to Kelly for all her assistance with ordering supplies, keeping the lab orderly and of course supplying us with snacks.

The staff in the chemistry department are amazing people to work with and are dedicated to fixing problems and smoothing any hiccups. I am grateful to Dave and Larry in building services for "keeping me out of trouble", Ivan and Tony in the NMR

facilities for their assistance on experiments, Pat in the front office for her support, and Josh for always greeting me with a smile and reminding me to enjoy every day.

I was fortunate to be an IGERT fellow for two years and thank CCMR for funding, and leadership and communication development. I learned valuable information about energy research conducted at Cornell and worldwide in EMC^2 meetings and symposiums.

Finally, I thank all of my friends for their help, support and encouragement: Eunji, Jill, Crystal, Ashma, Estela, Neda, Emily, Brian, Devin, Carmella, Chantal, Dave, Ashwath, Clint, Yuhua, Jenny, Kate, Shirley, Matt and Jeff.

TABLE OF CONTENTS

Biographical Sketch iv

Acknowledgements vi

Table of Contents x

List of Figures xii

List of Tables xviii

List of Abbreviations xix

List of Symbols xx

CHAPTER ONE - BRIEF OVERVIEW OF ORGANIC CATHODE MATERIALS FOR ENERGY STORAGE

1-1. Introduction 1

1-2. Organic Cathode Materials 5

1-3. Conclusions 9

REFERENCES 11

CHAPTER TWO - HIGH POWER ORGANIC CATHODES USING THIN FILMS OF ELECTROPOLYMERIZED BENZIDINE POLYMERS

2-1. Introduction 16

2-2. Results and Discussions 17

2-3. Conclusions 29

2-4. General Considerations 30

2-5. Materials 31

2-6. Electrochemical Measurements 39

2-7. ^{1}H and ^{13}C NMR Spectra 51

REFERENCES 57

CHAPTER THREE - POLYARYLAMINES: ORGANIC CATHODE MATERIALS FOR ELECTROCHEMICAL ENERGY STORAGE

3-1. Introduction 60

3-2. Results and Discussions 63

3-3. Conclusions 70

3-4. General Considerations 71

3-5. Materials 72

3-6. Electrochemical Measurements 76

3-7. Differential Scanning Calorimetry (DSC) Thermograms 87

3-8. ^{1}H and ^{13}C NMR Spectra of Poly(arylamines) 96

REFERENCES 104

CHAPTER FOUR - CONCLUSIONS AND FUTURE OUTLOOK

4-1. Overview 107

4-2. Future Studies 107

REFERENCES 112

LIST OF FIGURES

1-1	Schematic diagram of a capacitor in the charged state.	2
1-2	Schematic diagram of a lithium-ion battery during the discharging process.	3
1-3	The structure and redox mechanism of several types of organic cathode materials.	6
1-4	The discharge potentials and capacities of radical polymers (blue), organosulfur compounds (green) and carbonyl compounds (orange).	8
2-1	Redox reactions of (a) TMPD and (b) TMB and the corresponding cyclic voltammograms (CV) of 10 mM (c) TMPD and (d) TMB in $(^{n}Bu)_4N(ClO_4)/CH_3CN$ at 50 mV s^{-1}.	18
2-2	(a) The mechanism for the oxidative coupling of *N,N*-dimethylaniline to yield *N,N,N′,N′*-tetramethylbenzidine. (b) Using the analogous oxidative coupling to electropolymerize dianilinoalkanes, **DA-n**.	19
2-3	(a) Cyclic voltammograms (CV) of 10 mM monomer in 0.1 M $[NBu_4][PF_6]$ in CH_2Cl_2 on the 1st (solid line) and 2nd cycle (dashed line). (b) CVs of electrodes prepared from (a) cycled in 0.1 M $[NBu_4][PF_6]$ in CH_3CN. All CVs on 100 μA scale except as indicated. Scan rate: 20 mV s^{-1}.	20
2-4	Cyclic voltammograms of 10 mM **DA-6** in 0.1 M $[NBu_4][PF_6]$/solvent on the 1st (solid line) and 2nd cycle (dashed line). All CVs on 100 μA scale. Scan rate: 20 mV s^{-1}.	23
2-5	(a) Contour plot of the *in situ* UV-Vis spectroelectrochemistry of **PDA-6** deposited onto ITO electrode during one cycle. Inset: Corresponding CV of **PDA-6** film cycled in 0.1 M $[NBu_4][PF_6]$ in CH_3CN at 10 mV s^{-1} with Roman numeral markers relating designated potentials to UV-Vis spectra. UV-Vis spectra of **PDA-6** at designated potentials (b) between −0.10–0.22 V for the **PDA-6**/**PDA-6**$^{+\bullet}$ couple and (c) between +0.20–0.60 V for the **PDA-6**$^{+\bullet}$/**PDA-6**$^{2+}$ couple. (d) Pictures of **PDA-6** film on ITO in the neutral, cationic and dicationic states.	24
2-6	The performance of polymer films, deposited on GCE as in Figure 2-3a, cycled in 0.1 M $[NBu_4][PF_6]/CH_3CN$ at 20 mV s^{-1}.	25

2-7	(a) Discharge curves for **PDA-6** at various C rates. (b) The capacity (red) and Coulombic efficiency (blue) of **PDA-6** with different positive cutoffs in 0.5 M $[NBu_4][PF_6]/CH_3CN$ at rate of 1,000 C. Inset: Representative charge and discharge curves for **PDA-6** with different potential ranges. The range was −0.1–0.2 V (square) and −0.1–0.5 V (triangle) vs. Ag/Ag^+.	26
2-8	Discharge curves of **PTA-6** in 0.5 M $[NBu_4][PF_6]/CH_3CN$ at an applied current of 36 μA. Inset: The relative capacities between the two couples with cycling, where the first reduction occurs between +0.2 and −0.1 V and the second reduction is between +0.5 and +0.2 V vs. Ag/Ag^+.	28
2-9	(a) Sweep rate dependent CVs of 10 mM *N,N,N′,N′*-tetramethylbenzidine (TMB, Aldrich) in 0.1 M $[NBu_4][PF_6]/CH_3CN$. (b) The dependence of the peak currents of the two redox couples of TMB on the square root of the scan rate.	40
2-10	(a) The difference in peak potentials (ΔE_p) of the two redox couples of **PDA-6** at various scan rates. (b) The dependence of the anodic and cathodic peak currents (i_{pa} and i_{pc}, respectively) of the first and second couples of **PDA-6** on scan rates.	41
2-11	(a) Successive CVs of 5 mM **DA-6** in 0.5 M $[NBu_4][PF_6]/CH_2Cl_2$ during electropolymerization at 20 mV s^{-1}. (b) CVs of **PDA-6** films that were prepared by different deposition cycles, cycled in 0.5 M $[NBu_4][PF_6]/CH_3CN$ at 20 mV s^{-1}. (c) Dependence of the anodic and cathodic peak currents (i_{pa} and i_{pc}, respectively) of **PDA-6** on the number of deposition cycles during film preparation.	42
2-12	The cyclic voltammogram of **PDA-6** cycled in 0.5 M $[NBu_4][PF_6]/CH_3CN$ at 10 mV s^{-1}.	43
2-13	Dependence of the difference between peak potentials (E_p) and the formal redox potential ($E^{0\prime}$) on the logarithm of the scan rate (log(ν)).	44
2-14	Cottrell plot of **PDA-6** in 0.1 M $[NBu_4][PF_6]/CH_3CN$.	45
2-15	Simultaneously acquired (a) absorbance at 469 nm and (b) current measurements at set (c) applied potentials of **PDA-6** deposited onto an ITO electrode in 0.5 M $[NBu_4][PF_6]/CH_3CN$. The switching time between the neutral, colorless polymer film and the dicationic, marigold-colored **PDA-6**$^{2+}$ is 1.8 seconds.	47
2-16	Simultaneously acquired (a) absorbance at 400 nm and (b) current	48

measurements at set (c) applied potentials of **PDA-6** deposited onto an ITO electrode in 0.5 M $[NBu_4][PF_6]/CH_3CN$. The switching time between the neutral, colorless polymer film and the green-colored **PDA-6**$^{+\bullet}$ is 0.9 seconds.

2-17 Performance of **PDA-6** films cycled at various C rates over 100 cycles. The polymer films on GCE were galvanostatically charged and discharged in 0.5 M $[NBu_4][PF_6]/CH_3CN$ between −0.1–0.5 V. The |applied current| was the same for the charge and discharge except for 100 C which was charged at 1000 C and discharged at 100 C. 50

2-18 ^{1}H NMR spectrum (400 MHz, $CDCl_3$) of *N,N′*-dimethyl-*N,N′*-diphenylethylenediamine (**DA-2**). 51

2-19 ^{13}C NMR spectrum (125 MHz, $CDCl_3$) of *N,N′*-dimethyl-*N,N′*-diphenylethylenediamine (**DA-2**). 51

2-20 ^{1}H NMR spectrum (400 MHz, $CDCl_3$) of *N,N′*-dimethyl-*N,N′*-diphenyl-1,3-propanediamine (**DA-3**). 52

2-21 ^{13}C NMR spectrum (125 MHz, $CDCl_3$) of *N,N′*-dimethyl-*N,N′*-diphenyl-1,3-propanediamine (**DA-3**). 52

2-22 ^{1}H NMR spectrum (400 MHz, $CDCl_3$) of *N,N′*-dimethyl-*N,N′*-diphenyl-1,4-butanediamine (**DA-4**). 53

2-23 ^{13}C NMR spectrum (125 MHz, $CDCl_3$) of *N,N′*-dimethyl-*N,N′*-diphenyl-1,4-butanediamine (**DA-4**). 53

2-24 ^{1}H NMR spectrum (400 MHz, $CDCl_3$) of *N,N′*-dimethyl-*N,N′*-diphenyl-1,6-hexanediamine (**DA-6**). 54

2-25 ^{13}C NMR spectrum (125 MHz, $CDCl_3$) of *N,N′*-dimethyl-*N,N′*-diphenyl-1,6-hexanediamine (**DA-6**). 54

2-26 ^{1}H NMR spectrum (400 MHz, $CDCl_3$) of *N*-methyl-*N′*-[2-(methylphenylamino)ethyl]-*N*,*N′*-diphenyl-1,2-ethanediamine (**TA-2**). 55

2-27 ^{13}C NMR spectrum (125 MHz, $CDCl_3$) of *N*-methyl-*N′*-[2-(methylphenylamino)ethyl]-*N*,*N′*-diphenyl-1,2-ethanediamine (**TA-2**). 55

2-28 ^{1}H NMR spectrum (400 MHz, $CDCl_3$) of *N*-Methyl-*N′*-[6-(methylphenylamino)hexyl]-*N*,*N′*-diphenyl-1,6-hexanediamine 56

(**TA-6**).

2-29 ^{13}C NMR spectrum (125 MHz, $CDCl_3$) of *N*-Methyl-*N′*-[6-(methylphenylamino)hexyl]-*N*,*N′*-diphenyl-1,6-hexanediamine (**TA-6**). 56

3-1 Mechanism of redox processes of TMPD and arylamine analogs. 61

3-2 a) Pd-catalyzed polycondensation of diamines with dibromoarenes. b) Dibromoarenes investigated in this work. 62

3-3 Cyclic voltammograms (CV) of poly(**1**-**2a**) in 0.1 M $[NBu_4][ClO_4]$ in CH_2Cl_2 at 20 mV s^{-1}. All CVs on 10 μA scale. 64

3-4 Cyclic voltammograms (CV) of poly(**1d**-**2**) in 0.1 M $[NBu_4][ClO_4]$ in CH_2Cl_2 at 20 mV s^{-1}. All CVs on 10 μA scale. 67

3-5 a) Ten CV cycles of poly(**1d**-**2c**) in 0.5 M $LiBF_4$ in 1,3-dioxolane:dimethoxyethane (DOL:DME) at 20 mV s^{-1}. b) The electrochemical cycling of poly(**1d**-**2c**) in 0.5 M $LiBF_4$ in various solvents at 20 mV s^{-1}. 69

3-6 (a) A polymer film of poly(**1b**-**2a**) was adsorbed onto GCE by five CV cycles of 2 mM concentration in repeat unit of poly(**1b**-**2a**) in 0.1 M $[NBu_4][ClO_4]/CH_2Cl_2$ at 10 mV s^{-1}. (b) The CV of the modified electrode from a) cycled in 0.1 M $[NBu_4][ClO_4]/CH_3CN$ at 10 mV s^{-1}. 78

3-7 (a) A polymer film of poly(**1c**-**2a**) was adsorbed onto GCE by holding the potential at 0 V for 1 minute in 4 mM concentration in repeat unit of poly(**1c**-**2a**) in 0.1 M $[NBu_4][ClO_4]/ CH_2Cl_2$, after cycling to 0 V at 10 mV s^{-1}. (b) The CV of the modified electrode from a) cycled in 0.1 M $[NBu_4][ClO_4]/CH_3CN$ at 10 mV s^{-1}. 79

3-8 (a) A polymer film of poly(**1d**-**2a**) was adsorbed onto GCE by holding the potential at 0 V for 1 minute in 4 mM concentration in repeat unit of poly(**1d**-**2a**) in 0.1 M $[NBu_4][ClO_4]/ CH_2Cl_2$, after cycling to 0 V at 10 mV s^{-1}. (b) The CV of the modified electrode from a) cycled in 0.1 M $[NBu_4][ClO_4]/CH_3CN$ at 10 mV s^{-1}. 80

3-9 The CV of the modified electrode from Fig. 3-8b cycled in 0.1 M $[NBu_4][ClO_4]/CH_3CN$ at 10 mV s^{-1} to more negative potentials. 81

3-10 (a) A polymer film of poly(**1d**-**2b**) was adsorbed onto GCE by holding the potential at 0 V for 1 minute in 4 mM concentration in repeat unit of poly(**1d**-**2b**) in 0.1 M $[NBu_4][ClO_4]/ CH_2Cl_2$, after cycling to 0 V at 10 mV s^{-1}. (b) The CV of the modified electrode 82

from a) cycled in 0.1 M $LiClO_4$/tetraglyme at 20 mV s^{-1}.

3-11 (a) A polymer film of poly(**1d-2c**) was adsorbed onto GCE by 5 CV cycles in 4 mM concentration in repeat unit of poly(**1d-2c**) in 0.1 M $[NBu_4][ClO_4]$/ CH_2Cl_2. (b) The CV of the modified electrode from a) cycled in 0.1 M $[NBu_4][ClO_4]/CH_3CN$ at 20 mV s^{-1}. 83

3-12 A polymer film of poly(**1d-2c**) cycled in 0.1 M $LiPF_6$/tetraglyme at 50 mV s^{-1}. 84

3-13 (a) A polymer film of poly(**1d-2d**) was adsorbed onto GCE by 5 CV cycles in 4 mM concentration in repeat unit of poly(**1d-2d**) in 0.1 M $[NBu_4][ClO_4]$/ CH_2Cl_2. (b) The CV of the modified electrode from a) cycled in 0.1 M $LiClO_4$/tetraglyme at 20 mV s^{-1}. 85

3-14 (a) A polymer film of poly(**1d-2e**) was adsorbed onto GCE by 5 CV cycles in 4 mM concentration in repeat unit of poly(**1d-2e**) in 0.1 M $[NBu_4][ClO_4]$/ CH_2Cl_2. (b) The CV of the modified electrode from a) cycled in 0.1 M $LiClO_4$/tetraglyme at 20 mV s^{-1}. 86

3-15 DSC traces of poly(**1a-2a**) (Table 3-1, entry 1). 88

3-16 DSC traces of poly(**1b-2a**) (Table 3-1, entry 2). 89

3-17 DSC traces of poly(**1c-2a**) (Table 3-1, entry 3). 90

3-18 DSC traces of poly(**1d-2a**) (Table 3-1, entry 4). 91

3-19 DSC traces of poly(**1d-2b**) (Table 3-2, entry 1). 92

3-20 DSC traces of poly(**1d-2c**) (Table 3-2, entry 2). 93

3-21 DSC traces of poly(**1d-2d**) (Table 3-2, entry 3). 94

3-22 DSC traces of poly(**1d-2e**) (Table 3-2, entry 4). 95

3-23 ^{1}H NMR spectrum of poly(**1a-2a**) (Table 3-1, entry 1). 96

3-24 ^{13}C NMR spectrum of poly(**1a-2a**) (Table 3-1, entry 1). 96

3-25 ^{1}H NMR spectrum of poly(**1b-2a**) (Table 3-1, entry 2). 97

3-26 ^{13}C NMR spectrum of poly(**1b-2a**) (Table 3-1, entry 2). 97

3-27 ^{1}H NMR spectrum of poly(**1c-2a**) (Table 3-1, entry 3). 98

3-28 ^{13}C NMR spectrum of poly(**1c-2a**) (Table 3-1, entry 3). 98

3-29	^{1}H NMR spectrum of poly(**1d-2a**) (Table 3-1, entry 4).	99
3-30	^{13}C NMR spectrum of poly(**1d-2a**) (Table 3-1, entry 4).	99
3-31	^{1}H NMR spectrum of poly(**1d-2b**) (Table 3-2, entry 1).	100
3-32	^{13}C NMR spectrum of poly(**1d-2b**) (Table 3-2, entry 1).	100
3-33	^{1}H NMR spectrum of poly(**1d-2c**) (Table 3-2, entry 2).	101
3-34	^{13}C NMR spectrum of poly(**1d-2c**) (Table 3-2, entry 2).	101
3-35	^{1}H NMR spectrum of poly(**1d-2d**) (Table 3-2, entry 3).	102
3-36	^{13}C NMR spectrum of poly(**1d-2d**) (Table 3-2, entry 3).	102
3-37	^{1}H NMR spectrum of poly(**1d-2e**) (Table 3-2, entry 4).	103
3-38	^{13}C NMR spectrum of poly(**1d-2e**) (Table 3-2, entry 4).	103
4-1	The discharge curves for compounds that undergo (red) two-electron transfer and (blue) two one-electron transfers.	108
4-2	The cyclic voltammogram of the substituted benzidine polymer film in 0.5 M $[NBu_4][PF_6]$ in CH_3CN at 20 mV s^{-1}.	109
4-3	The charge (red) and Coulombic efficiency (blue) of PDA-6 deposited on high surface area reticulated vitreous carbon electrodes, cycled in 0.5 M $[NBu_4][PF_6]$ in CH_3CN at 10 mV s^{-1}.	110
4-4	The cyclic voltammogram of the substituted benzidine polymer film in 0.5 M $[NBu_4][PF_6]$ in CH_3CN at 20 mV s^{-1}.	111

LIST OF TABLES

2-1	The electrochemical values for polymer films from Figure 2-3b.	39
3-1	Pd-catalyzed polycondensation of alkyldiamines with dibromobenzene.	63
3-2	Pd-catalyzed polycondensation of hexamethylenediamine with dibromoarenes.	66
3-3	Polymerization of alkyldiamines with dibromobenzene.	73
3-4	Optimization of the polycondensation of poly(**1d**-**2a**).	74
3-5	The electrochemical values for polymer films from Figure 3-1.	77
3-6	The electrochemical values for polymer films from Figure 3-2.	77
3-7	The polymer properties of poly(arylamines).	87

LIST OF ABBREVIATIONS

Electrochemical energy storage	EES
Lithium-ion batteries	LIB
Poly(2,5-dimercapto-1,3,4-thiadiazole)	PDMcT
2,2,6,6-Tetramethyl pyridine-1-oxyl	TEMPO
N,N,N′,N′-Tetramethyl-*p*-phenylenediamine	TMPD
N,N,N′,N′-Tetramethylbenzidine	TMB
N,N-Dimethylaniline	DMA
Dianilinoalkane	DA-n
Indium tin oxide	ITO
Glassy carbon electrode	GCE
Nuclear magnetic resonance	NMR
High resolution mass spectrometry	HRMS
Cyclic voltammetry	CV
High-performance liquid chromatography	HPLC
Direct analysis in real time	DART
Ethylene carbonate	EC
Diethyl carbonate	DEC
1,3-Dioxolane	DOL
Dimethoxyethane	DME
Gel permeation chromatography	GPC
Differential scanning calorimetry	DSC

LIST OF SYMBOLS

E_p	Peak potential
ΔE_p	Peak to peak separation
Q	Charge
$E^{0'}$	Formal redox potential
i_{pa}	Anodic peak current
i_{pc}	Cathodic peak current
ν	Scan rate
α	Electron transfer coefficient
k_s	Electron transfer rate constant
n	Number of electrons
R	Ideal gas constant
F	Faraday constant
i	Current
A	Area
C	Concentration
D	Diffusion constant
ρ	Density
h	Film thickness
w	Mass of film
δ	Chemical shift
R_f	Retention factor
m/z	Mass to charge ratio

M_n	Number average molecular weight
M_w	Weight average molecular weight
T_g	Glass transition temperature
T_m	Melting temperature

CHAPTER ONE

BRIEF OVERVIEW OF ORGANIC CATHODE MATERIALS FOR ENERGY STORAGE

1-1. Introduction

The escalating energy needs of society and the depletion of fossil-fuel resources demand the development of new methods of generating and storing energy. It has been projected that the world energy consumption will double by 2050, from 14 TW to 28 TW.[1,2] This is the energy equivalent of 10^{10} tons of oil yearly. It is a global imperative to address this technological problem, while also factoring in environmental concerns about global warming and environmental stewardship. Renewable energy will play a major role in the development of a sustainable energy future. Renewable energy sources include wind, solar, hydropower, biomass, and geothermal energy but they are intermittent resources. Therefore, energy storage technologies are required to efficiently and effectively use and implement renewable energy sources.[3-6]

Pumped-storage hydroelectricity accounts for over 98% of the bulk-energy storage.[2] However, this only translates into 1% of the world energy consumption. The development of better energy storage technologies is vital if renewable energy resources will power the world. In addition to smart electrical grids and renewable energy, the growth of portable electronics and electric transportation motivates research on better performing electrochemical energy storage (EES) technologies.

The two major classes of EES devices are electrochemical capacitors and batteries, which store energy by two different types of mechanisms.[7] Capacitors store energy directly as charge on a pair of electrodes, while batteries store chemical energy. The difference in their performance stems from the two fundamentally different

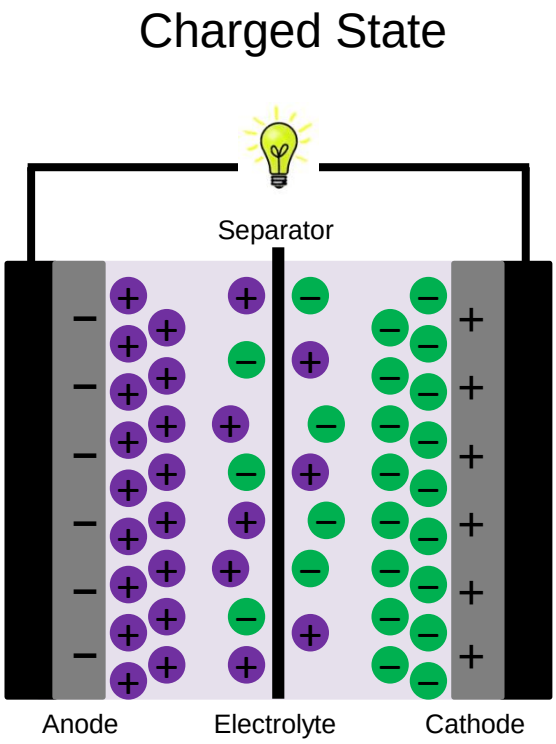

Figure 1-1. Schematic diagram of a capacitor in the charged state.

mechanisms. Electrochemical capacitors have high power densities (can be charged and discharged within seconds) and cyclability (can be cycled up to millions of cycles) because they are not limited by the kinetics of chemical reactions or structural changes in the electrode materials. However, they have much lower energy densities than batteries that can generate electrical energy from chemical reactions. These Faradaic processes involve redox reactions at the electrode/electrolyte interfaces. Correspondingly, the performance of the battery is connected to the properties of its components and the chemical and physical interactions between electrolyte and electrode materials.[8] The diversity of battery materials means they are used in a wide variety of applications, from portable electronics, to electric vehicles and grid applications.

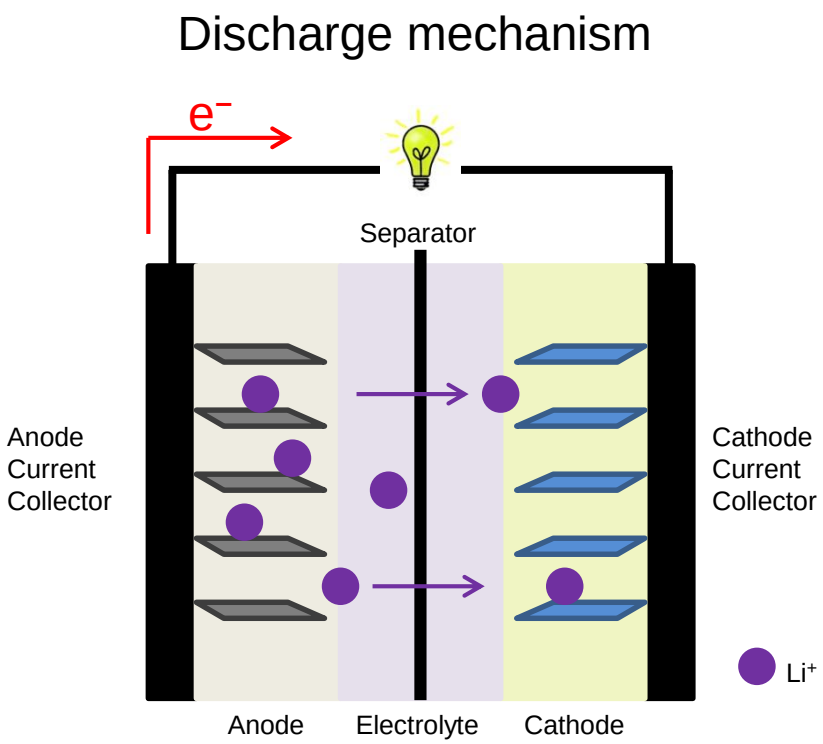

Figure 1-2. Schematic diagram of a lithium-ion battery during the discharging process.

Batteries are composed of an anode (electropositive material) and a cathode (electronegative material), which are divided by a separator and the electrolyte (Fig. 1-2). The two types of batteries are primary and secondary batteries. The former are single-use batteries (e.g., zinc/alkaline manganese dioxide batteries), while the latter can be recharged and used repeatedly (e.g., lithium-ion batteries). Lithium-ion batteries (LIB) were first commercialized by SONY[9] in 1991, and have recently dominated the portable electronics market because they have the highest volumetric and gravimetric energy densities of all commercial secondary batteries.[8] This is due to the fact that lithium is the most electropositive, as well as the lightest, metal. Fig. 1-2 depicts the general discharge mechanism for a LIB. During the discharging process, the anode is oxidized and electrons flow through the external circuit from the anode to the cathode. Concurrently, lithium ions are released from the anode and travel through

the electrolyte to the cathode to maintain charge balance. The reverse processes occur when the battery is charged.

The typical electrode materials for LIBs are ones that can intercalate and deintercalate lithium ions, such as lithium containing metal oxides (e.g., $LiCoO_2$, $LiFePO_4$) and carbonaceous materials (e.g., graphite).[10] However, there is an imbalance in the capacities of the cathodes and anodes. The practical capacities of inorganic cathodes are 120-160 mA h g^{-1}, compared to 372 mA h g^{-1} for LiC_6.[11,12] The disparity in capacities means that the battery cell requires approximately three times the amount of cathode material to anode material. Due to the reciprocal nature of the capacity of the cell (Eqn. 1), improvements in the capacity of the limiting component (i.e. cathode materials) will have a more dramatic effect on the overall cell capacity than improving the performance of the higher capacity electrode material. Furthermore, the costs of carbon anodes are a fraction of that of the inorganic cathode materials. Generally, cathode materials account for nearly half of the total materials cost of a cell.[13] The abundance of a material factors into its cost, which is especially important for larger applications like electric vehicles and grid energy storage, but it also impacts the long-term sustainability and availability of the battery. Ideally, political tensions and instabilities should not impact the supply of battery materials for electrochemical energy storage technologies.

$$\frac{1}{\text{capacity}_{cell}} = \frac{1}{\text{capacity}_{cathode}} + \frac{1}{\text{capacity}_{anode}} \quad (1)$$

Current commercial EES technologies do not meet the performance requirements for sustainable transportation using electric vehicles, efficient utilization of renewable energy, and grid load leveling.[3,14-16] The high paced word of consumer electronics also puts heavy demand on the development of longer lasting and faster-

charging batteries. One strategy to improve the energy and power density of EES technologies is to address the bottleneck for LIB performance (i.e. cathode) by developing novel electroactive cathode materials.

1-2. Organic Cathode Materials

The imbalance in capacities of the electrode materials, and the high cost and low capacities of inorganic cathodes motivate researchers to investigate alternative cathode materials. The pursuit of higher performing EES technologies should address the following four issues: energy density, cost, safety and cycling performance. Organic, redox-active compounds are promising candidates for next generation electrochemical energy storage applications. In contrast to inorganic cathode materials with practical capacities of 120-160 mA h g^{-1}, organic compounds can have theoretical capacities >400 mA h g^{-1}. Capacity is proportional to the number of electrons transferred and inversely proportional to the molar mass of the material. Thus, low molecular weight compounds that are capable of multiple electron transfers at high redox potentials can surpass the capacities (>160 mA h g^{-1}) and energy densities (>250 W h kg^{-1}) of commercial materials, although at lower volumetric energy densities.[17-19]

Organic compounds have attracted interest for EES applications because they can be designed and tuned through organic synthesis to maximize gravimetric capacity, energy and power density, and cycling performance. The redox processes of organic materials often have faster reaction kinetics than the metal ion insertion/deinsertion reactions of inorganic intercalation cathodes and hence, they can be used in high power applications. For example, a polymer with stable radical groups had good cycling performance when it was charged and discharged at 360 °C, meaning it took 10 seconds to charge/discharge the cell.[20] They are abundant and

Organic Cathode Material	Examples	Redox Mechanism
Conducting polymers	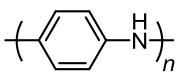	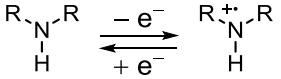
Organosulfur compounds	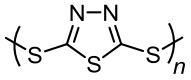	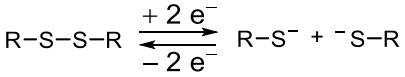
Carbonyl-based compounds	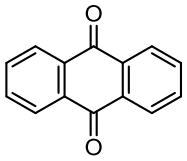	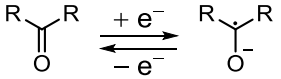
Radical polymers	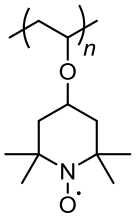	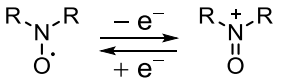

Figure 1-3. The structure and redox mechanism of several types of organic cathode materials.

potentially low-cost since redox-active organic compounds are composed mostly of carbon, oxygen, nitrogen and sulfur. Hence, they are sustainable and if derived from biomass, potentially renewable, alternatives to inorganic cathode materials.[1,21-24] The challenges of using organic compounds as electrode materials are due to their solubility in organic electrolytes, low electronic conductivities, and low volumetric energy densities.[18] In general, most organic electrode materials are insulators, with the exception of conducting polymers, and require conductive additives.[25] The addition of conductive carbon lowers the percentage of active material in the cathode to 20-85%, compared to 90% for inorganic cathode materials.[17] The low mass densities of organic materials are a disadvantage for certain applications, such as portable electronics and electric vehicles. They can be used for applications where volume is not a primary concern, such as thin film flexible electronics and back-up energy storage applications.

Electrode materials need to be in contact with the current collectors to facilitate charge transfer, and loss of active material during cycling due to dissolution dramatically reduces the capacity of the cell. Strategies to design insoluble electrode materials include using organic polymers[17-19,26,27] and organic salts.[23,24,28,29] The diversity of redox-active compounds means there are a variety of types of organic electrode materials that can be applied to EES devices, including conducting polymers, organosulfur compounds, stable radical polymers, and carbonyl-based compounds (Fig. 1-3).

Conducting polymers, such as polyaniline, polypyrrole, polythiophene and poly(*p*-phenylene) have been investigated as electrode materials since the 1980s.[25,30] The conductivity and insolubility of conducting polymers are attractive features, and the polymers can be cycled thousands of times. Research on conducting polymers has led to the commercialization of a polyaniline battery.[31] The success of the commercialized battery and conducting polymers were limited because of its low capacities, due to low doping levels and sloping charge/discharge curves.[32] Researchers are investigating methods of improving the capacity by attaching redox-active groups[33-38] or as a cathode for supercapacitors.[39-41]

The redox reactions of organosulfur compounds can provide more energy than the doping mechanism of conducting polymers. Visco *et al.*[42-45] and Oyama *et al.*[46-48] investigated symmetric materials with disulfide bonds that can be reversibly cleaved and re-dimerized. Poly(2,5-dimercapto-1,3,4-thiadiazole) (PDMcT) has attracted the most attention due to its high theoretical capacity (362 mA h g^{-1}) at high reduction potentials. However, organosulfur compounds suffer from slow reaction kinetics, and poor cycling performances due to dissolution of the active material during cycling. Abruña and coworkers demonstrated that conducting polymers (e.g., poly(3,4-ethylenedioxythiophene) can accelerate the charge/discharge reactions of DMcT by a

factor of ~12,000.[49-52] Investigators synthesized polymers with disulfide bonds in the side chains to improve the cycling retention because main chain disulfide polymers reduced to thiolate ions that readily dissolved in organic electrolytes. Unfortunately, these polymers suffered from sluggish kinetics due to slow re-formation of the disulfide bond.[53,54] Researchers must address the challenges of slow kinetics and poor capacity retention for organosulfur compounds to be considered practical cathode materials for electrochemical energy storage applications.

Carbonyl-based compounds have been studied as cathode materials for battery applications since the 1960s.[55] Researchers have immobilized carbonyl-based compounds by incorporating the molecules into polymer networks[56-59] and by salt formation.[23,24,28,29] The compounds can typically undergo one-electron reduction per

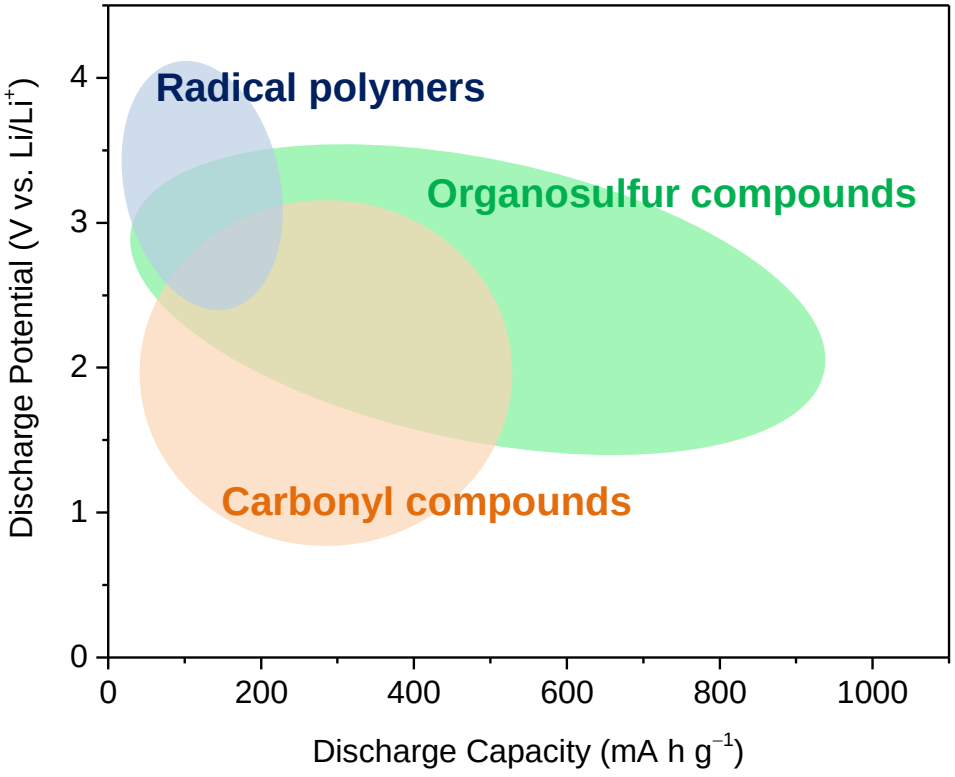

Figure 1-4. The discharge potentials and capacities of radical polymers (blue), organosulfur compounds (green) and carbonyl compounds (orange).

carbonyl group, and multi-electron reactions, and consequently, high capacity materials are possible. Tarascon *et al.* have demonstrated a renewable, rechargeable battery using a biomass-derived dilithiated oxocarbon, which retained 85% of its initial capacity after 25 cycles.[23] In general, carbonyl-based compounds exhibited high capacities and good cycling performances but their discharge potentials are lower than other organic cathode materials, and hence these materials have low energy densities. Some carbonyl-based compounds have redox potentials low enough to be potential anode materials (e.g., 0.5-1.5 V vs. Li/Li^+).[60,61]

In contrast to carbonyl-based compounds, stable radical polymers exhibit high discharge potentials (~3.5 V vs. Li/Li^+).[26,27,62] Nitroxide-based (e.g., 2,2,6,6-tetramethyl pyridine-1-oxyl, TEMPO) polymers are the most common radical polymers studied for EES applications since it was first reported in 2002.[62] TEMPO is the well known stable radical that can reversibly oxidize to the oxoammonium cation. Radical polymers typically have excellent cycling retention (e.g., 89% capacity retention after 1000 cycles) and high power capability (e.g., charge and discharge under one minute) due to the stability of the radicals and the fast kinetics of the redox reactions.[63,64] However, radical batteries only exchange one electron per redox-active moiety, and thus, they have lower capacities than inorganic cathode materials (e.g., 110 mA h g^{-1}).

1-3. Conclusions

Current lithium-ion batteries do not meet the performance requirements for efficient utilization of renewable energy, grid energy storage, and electric vehicles.[3] The development of higher capacity cathode materials can considerably improve cell performance. Organic compounds are promising candidates due to their high theoretical capacities, energy and power densities. The discharge potentials and

capacities of the different types of organic cathode materials are summarized in Fig. 1-4. Practical organic cathode materials need to have high discharge capacities, (>160 mA h g^{-1}), high redox potentials (>3.0 V vs. Li/Li^+), fast redox kinetics, and good cycling stability. The reviewed organic cathode materials need to have better performances to successfully compete with inorganic cathodes and in order to be commercialized. The diversity of redox-active organic materials means that there are many pathways to develop cathode materials that meet the demands listed above. In order to develop high performing cathode materials for electrochemical energy storage applications, we began by identifying organic molecules with promising properties (e.g., high capacities, multiple electron transfer reactions at high redox potentials and fast rates). Then, we explored different methods to synthesize redox-active polymers containing the promising moieties. They were characterized electrochemically to test their performance as cathode materials. We used our understanding of the system and the redox reactions to provide insight into the design and development of new materials with improved performance.

REFERENCES

(1) Larcher, D.; Tarascon, J. M. *Nat. Chem.* **2015**, *7*, 19-29.

(2) Lewis, N. S. *MRS Bull.* **2007**, *32*, 808-820.

(3) Goodenough, J. B.; Abruña, H. D.; Buchanan, M. V. *Basic Research Needs for Electrical Energy Storage. Report of the Basic Energy Sciences Workshop on Electrical Energy Storage*, 2007.

(4) Goodenough, J. B. *Energy Environ. Sci.* **2014**, *7*, 14-18.

(5) Yang, Z.; Zhang, J.; Kintner-Meyer, M. C. W.; Lu, X.; Choi, D.; Lemmon, J. P.; Liu, J. *Chem. Rev.* **2011**, *111*, 3577-3613.

(6) Dunn, B.; Kamath, H.; Tarascon, J.-M. *Science* **2011**, *334*, 928-935.

(7) Winter, M.; Brodd, R. J. *Chem. Rev.* **2004**, *104*, 4245-4270.

(8) Reddy, T. B.; Linden, D. *Handbook of Batteries*; McGraw-Hill: New York, 2011.

(9) Yoshino, A.; Sanechika, K.; Nakajima, T., Japanese Patent 1989293, 1985.

(10) Goodenough, J. B.; Park, K.-S. *J. Am. Chem. Soc.* **2013**, *135*, 1167-1176.

(11) Tarascon, J. M.; Armand, M. *Nature* **2001**, *414*, 359-367.

(12) Chen, J.; Cheng, F. *Acc. Chem. Res.* **2009**, *42*, 713-723.

(13) Dillon, S. J.; Sun, K. *Curr. Opin. Solid State Mater. Sci.* **2012**, *16*, 153-162.

(14) Goodenough, J. B.; Kim, Y. *Chem. Mater.* **2009**, *22*, 587-603.

(15) Etacheri, V.; Marom, R.; Elazari, R.; Salitra, G.; Aurbach, D. *Energy Environ. Sci.* **2011**, *4*, 3243-3262.

(16) Yoo, H. D.; Markevich, E.; Salitra, G.; Sharon, D.; Aurbach, D. *Materials Today* **2014**, *17*, 110-121.

(17) Liang, Y.; Tao, Z.; Chen, J. *Adv. Energy Mater.* **2012**, *2*, 742-769.

(18) Song, Z.; Zhou, H. *Energy Environ. Sci.* **2013**, *6*, 2280-2301.

(19) Gracia, R.; Mecerreyes, D. *Polym. Chem.* **2013**, *4*, 2206-2214.

(20) Suga, T.; Ohshiro, H.; Sugita, S.; Oyaizu, K.; Nishide, H. *Adv. Mater.* **2009**, *21*, 1627-1630.

(21) Tarascon, J. M. *ChemSusChem* **2008**, *1*, 777-779.

(22) Armand, M.; Tarascon, J. M. *Nature* **2008**, *451*, 652-657.

(23) Chen, H.; Armand, M.; Demailly, G.; Dolhem, F.; Poizot, P.; Tarascon, J.-M. *ChemSusChem* **2008**, *1*, 348-355.

(24) Chen, H.; Armand, M.; Courty, M.; Jiang, M.; Grey, C. P.; Dolhem, F.; Tarascon, J.-M.; Poizot, P. *J. Am. Chem. Soc.* **2009**, *131*, 8984-8988.

(25) Novák, P.; Müller, K.; Santhanam, K. S. V.; Haas, O. *Chem. Rev.* **1997**, *97*, 207-282.

(26) Oyaizu, K.; Nishide, H. *Adv. Mater.* **2009**, *21*, 2339-2344.

(27) Janoschka, T.; Hager, M. D.; Schubert, U. S. *Adv. Mater.* **2012**, *24*, 6397-6409.

(28) Wang, S.; Wang, L.; Zhang, K.; Zhu, Z.; Tao, Z.; Chen, J. *Nano Lett.* **2013**, *13*, 4404-4409.

(29) Song, Z.; Qian, Y.; Liu, X.; Zhang, T.; Zhu, Y.; Yu, H.; Otani, M.; Zhou, H. *Energy Environ. Sci.* **2014**, *7*, 4077-4086.

(30) Nigrey, P. J.; MacInnes, D.; Nairns, D. P.; MacDiarmid, A. G.; Heeger, A. J. *J. Electrochem. Soc.* **1981**, *128*, 1651-1654.

(31) Matsunaga, T.; Daifuku, H.; Nakajima, T.; Kawagoe, T. *Polym. Adv. Technol.* **1990**, *1*, 33-39.

(32) Nyholm, L.; Nyström, G.; Mihranyan, A.; Strømme, M. *Adv. Mater.* **2011**, *23*, 3751-3769.

(33) Park, K. S.; Schougaard, S. B.; Goodenough, J. B. *Adv. Mater.* **2007**, *19*, 848-851.

(34) Kunz, T. K.; Wolf, M. O. *Polym. Chem.* **2011**, *2*, 640-644.

(35) Aydın, M.; Esat, B.; Kılıç, Ç.; Köse, M. E.; Ata, A.; Yılmaz, F. *Eur. Polym. J.* **2011**, *47*, 2283-2294.

(36) Lowe, M. A.; Kiya, Y.; Henderson, J. C.; Abruña, H. D. *Electrochem. Commun.* **2011**, *13*, 462-465.

(37) Conte, S.; Rodríguez-Calero, G. G.; Burkhardt, S. E.; Lowe, M. A.; Abruña, H. D. *RSC Adv.* **2013**, *3*, 1957-1964.

(38) Xu, L.; Yang, F.; Su, C.; Ji, L.; Zhang, C. *Electrochim. Acta* **2014**, *130*, 148-155.

(39) Nyström, G.; Razaq, A.; Strømme, M.; Nyholm, L.; Mihranyan, A. *Nano Lett.* **2009**, *9*, 3635-3639.

(40) Rudge, A.; Davey, J.; Raistrick, I.; Gottesfeld, S.; Ferraris, J. P. *J. Power Sources* **1994**, *47*, 89-107.

(41) Snook, G. A.; Kao, P.; Best, A. S. *J. Power Sources* **2011**, *196*, 1-12.

(42) Visco, S. J.; DeJonghe, L. C. *J. Electrochem. Soc.* **1988**, *135*, 2905-2909.

(43) Visco, S. J.; Mailhe, C. C.; De Jonghe, L. C.; Armand, M. B. *J. Electrochem. Soc.* **1989**, *136*, 661-664.

(44) Visco, S. J.; Liu, M.; De Jonghe, L. C. *J. Electrochem. Soc.* **1990**, *137*, 1191-1192.

(45) Liu, M.; Visco, S. J.; De Jonghe, L. C. *J. Electrochem. Soc.* **1991**, *138*, 1891-1895.

(46) Sotomura, T.; Uemachi, H.; Takeyama, K.; Naoi, K.; Oyama, N. *Electrochim. Acta* **1992**, *37*, 1851-1854.

(47) Oyama, N.; Tatsuma, T.; Sato, T.; Sotomura, T. *Nature* **1995**, *373*, 598-600.

(48) Oyama, N.; Hatozaki, O. *Macromol. Symp.* **2000**, *156*, 171-178.

(49) Oyama, N.; Kiya, Y.; Hatozaki, O.; Morioka, S.; Abruña, H. D. *Electrochem. Solid-State Lett.* **2003**, *6*, A286-A289.

(50) Kiya, Y.; Hatozaki, O.; Oyama, N.; Abruña, H. D. *J. Phys. Chem. C* **2007**, *111*, 13129-13136.

(51) Rodríguez-Calero, G. G.; Lowe, M. A.; Kiya, Y.; Abruña, H. D. *J. Phys. Chem. C* **2010**, *114*, 6169-6176.

(52) Kiya, Y.; Hutchison, G. R.; Henderson, J. C.; Sarukawa, T.; Hatozaki, O.; Oyama, N.; Abruña, H. D. *Langmuir* **2006**, *22*, 10554-10563.

(53) Naoi, K.; Kawase, K. i.; Mori, M.; Komiyama, M. *J. Electrochem. Soc.* **1997**, *144*, L173-L175.

(54) Deng, S.-R.; Kong, L.-B.; Hu, G.-Q.; Wu, T.; Li, D.; Zhou, Y.-H.; Li, Z.-Y. *Electrochim. Acta* **2006**, *51*, 2589-2593.

(55) Williams, D. L.; Byrne, J. J.; Driscoll, J. S. *J. Electrochem. Soc.* **1969**, *116*, 2-4.

(56) Häringer, D.; Novák, P.; Haas, O.; Piro, B.; Pham, M. C. *J. Electrochem. Soc.* **1999**, *146*, 2393-2396.

(57) Han, X.; Chang, C.; Yuan, L.; Sun, T.; Sun, J. *Adv. Mater.* **2007**, *19*, 1616-1621.

(58) Song, Z.; Zhan, H.; Zhou, Y. *Chem. Commun.* **2009**, 448-450.

(59) Song, Z.; Zhan, H.; Zhou, Y. *Angew. Chem., Int. Ed.* **2010**, *49*, 8444-8448.

(60) Zhao, L.; Zhao, J.; Hu, Y.-S.; Li, H.; Zhou, Z.; Armand, M.; Chen, L. *Adv. Energy Mater.* **2012**, *2*, 962-965.

(61) Park, Y.; Shin, D.-S.; Woo, S. H.; Choi, N. S.; Shin, K. H.; Oh, S. M.; Lee, K. T.; Hong, S. Y. *Adv. Mater.* **2012**, *24*, 3562-3567.

(62) Nakahara, K.; Iwasa, S.; Satoh, M.; Morioka, Y.; Iriyama, J.; Suguro, M.; Hasegawa, E. *Chem. Phys. Lett.* **2002**, *359*, 351-354.

(63) Nakahara, K.; Iriyama, J.; Iwasa, S.; Suguro, M.; Satoh, M.; Cairns, E. J. *J. Power Sources* **2007**, *165*, 398-402.

(64) Nakahara, K.; Iriyama, J.; Iwasa, S.; Suguro, M.; Satoh, M.; Cairns, E. J. *J. Power Sources* **2007**, *165*, 870-873.

CHAPTER TWO

HIGH POWER ORGANIC CATHODES USING THIN FILMS OF ELECTROPOLYMERIZED BENZIDINE POLYMERS

2-1. Introduction

The demand for and integration of sustainable energy technologies and the intermittent nature of renewable energy sources, such as solar and wind, promotes the advancement of electrochemical energy storage (EES) systems.[1] Lithium ion batteries (LIBs) are employed in a wide range of applications, from portable electronics and electric vehicles to grid energy storage, due to their high energy and power densities. However, current LIBs do not meet the performance requirements for future applications, especially automotive and grid applications.[2-5] The disparity between conventional cathodes (e.g., $LiCoO_2$, $LiFePO_4$) and anodes (e.g., LiC_6) in terms of capacity, cost and abundance, motivates research on alternative cathode materials such as organic compounds.[1,6] Organic molecules are especially attractive for EES applications because they can be designed and tuned to be light weight and capable of multiple electron transfers at high potentials, thereby maximizing gravimetric capacity and energy density to potentially achieve values greater than commercial LIBs (>160 mA h g^{-1}, >250 W h kg^{-1}), although at lower volumetric energy densities.[7]

The pursuit of alternatives to inorganic cathode materials has identified several different types of promising organic molecules, such as conducting polymers, organosulfur compounds, carbonyl-based compounds, and free radical polymers.[7] In the field of organic electrodes, thin electroactive polymer films have attracted interest as electrodes in flexible batteries for wearable technologies and microbatteries for miniaturized electronic devices.[8,9] Thin films of redox-active, amorphous polymers are mechanically flexible and can have high power densities because of the short ion

transport lengths and the fact that (dis)charge processes do not involve metal ion insertion.[9,10] Conducting polymers (e.g., polypyrrole)[11,12] and radical polymers[13,14] have been employed as cathodes in paper-based batteries. The conductivity and insolubility of conducting polymers are attractive features but the low capacities, due to low doping levels and sloping charge/discharge curves, limit their practicality.[8] Nitroxide-based polymers are stable for hundreds of cycles, but they typically undergo only one electron transfer per repeat unit, and consequently, have limited specific capacity.[15-17] The practical use of organic materials requires the development of electrodes with better performance. We have been involved in the design (*in silico*), synthesis and characterization of organic-based cathode materials for EES applications.[18-20] We are especially interested in materials that can not only exchange multiple electrons per formula unit at high potentials, but that can also sustain high charge and discharge rates. Such a system would combine the energy density of a battery with the power density of a supercapacitor. Furthermore, if such a material could be generated via electropolymerization, thus yielding a conformal film on any conductive substrate serving as current collector, one could have a system with an arbitrary "form factor."

Herein we describe an electropolymerized benzidine polymer that can be reversibly oxidized in two one-electron steps at high potentials (>3.3 V vs. Li/Li^+) and at fast rates (1,000 C), with minimal capacity loss after one hundred cycles. In other words, we have developed a high performance pseudocapacitance material with the voltage plateaus and high capacities characteristic of batteries, but capable of the high cycling rates of supercapacitors.

2-2. Results and Discussion

A developing class of organic cathode materials is arylamine compounds that

can undergo two reversible oxidations to a quinoidal dication at high potentials. *N,N,N′,N′*-Tetramethyl-*p*-phenylenediamine (TMPD) is a promising molecule due to its high theoretical capacity, and two reversible one-electron transfers at high redox potentials.[21-23] The stable radical cation, commonly known as Wurster's Blue due to its color, can be further oxidized to the quinonediiminium dication (Figure 2-1). Similarly, *N,N,N′,N′*-tetramethylbenzidine (TMB) exhibits two reversible one-electron transfers and electrochromic behavior, turning yellow-green as the dication.[22] While the additional phenyl ring lowers the theoretical capacity for TMB, this effect can be offset in part by the increased stability of the oxidized species due to an extended delocalization system, and positive shifts in redox potentials. In addition, benzidines

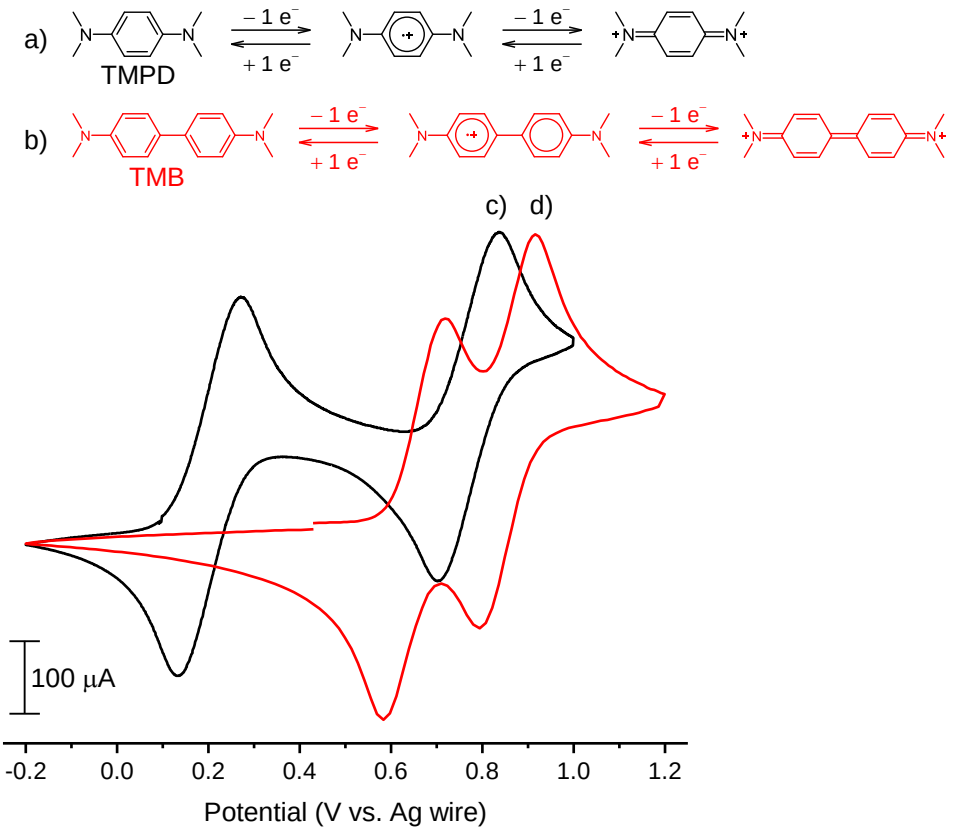

Figure 2-1. Redox reactions of (a) TMPD and (b) TMB and the corresponding cyclic voltammograms (CV) of 10 mM (c) TMPD and (d) TMB in $(^{n}Bu)_4N(ClO_4)/CH_3CN$ at 50 mV s^{-1}.

can be formed by oxidizing anilines; for example, TMB is the widely known coupling product of *N,N*-dimethylaniline (DMA).[24-26] However, the solubility of small molecules precludes their feasibility as electrode materials. Our strategy to overcome those issues was to incorporate TMB moieties into insoluble polymers through the oxidative coupling of anilines.

Figure 2-2 shows the mechanism for the oxidative coupling of *N,N*-dimethylaniline to yield TMB.[24-26] Initially, *N,N*-dimethylaniline oxidizes to the radical cation, which can form a C-C bond at the *para*-position with another *N,N*-dimethylaniline radical cation. Deprotonation of the coupled product affords TMB. This oxidative coupling has been exploited by other groups to form benzidine polymers using monomers with at least two aniline groups.[27-29] We studied the electropolymerization and electrochemical properties of benzidine films with varying

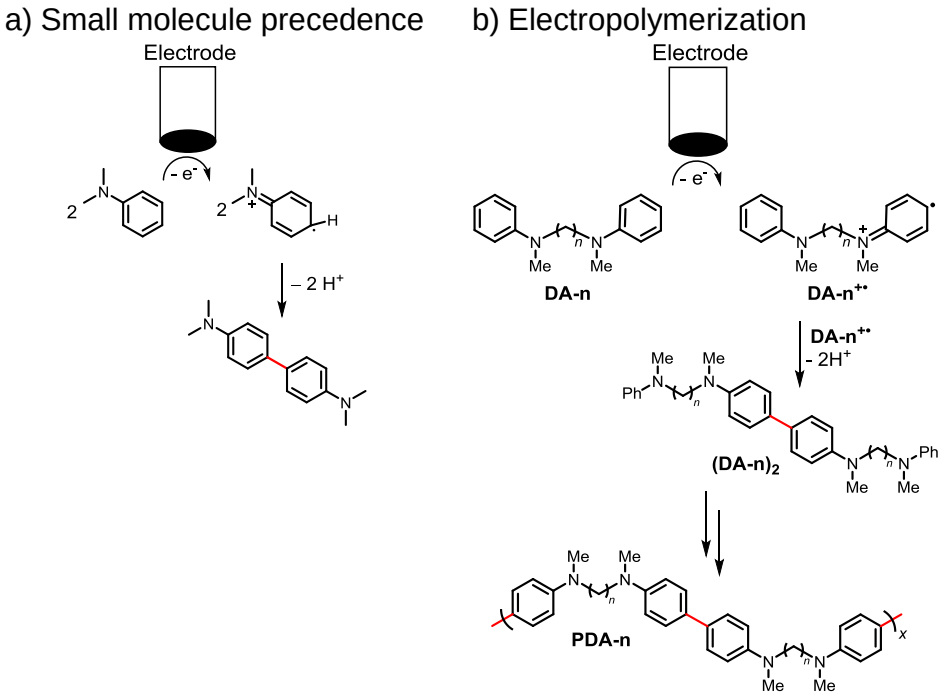

Figure 2-2. (a) The mechanism for the oxidative coupling of *N,N*-dimethylaniline to yield *N,N,N′,N′*-tetramethylbenzidine. (b) Using the analogous oxidative coupling to electropolymerize dianilinoalkanes, **DA-n**.

alkyl linkers between the polymerizable end groups to develop a redox-active polymer with excellent cycling stability and high capacities at fast rates.

A series of di- and trianilinoalkanes was synthesized with different alkyl lengths connecting the anilines (Figure 2-3a). Based on the oxidation of *N,N*-

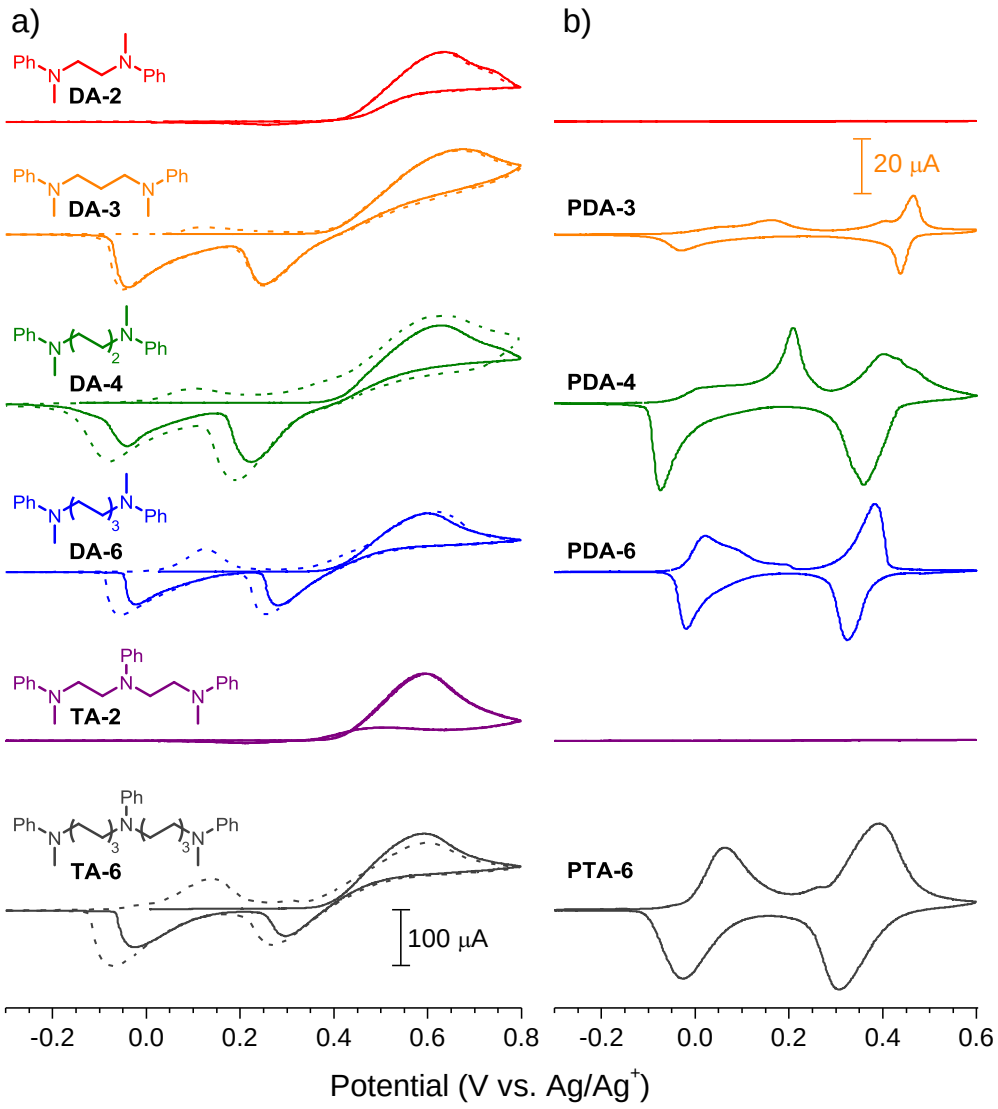

Figure 2-3. (a) Cyclic voltammograms (CV) of 10 mM monomer in 0.1 M $[NBu_4][PF_6]$ in CH_2Cl_2 on the 1st (solid line) and 2nd cycle (dashed line). (b) CVs of electrodes prepared from (a) cycled in 0.1 M $[NBu_4][PF_6]$ in CH_3CN. All CVs on 100 µA scale except as indicated. Scan rate: 20 mV s^{-1}.

dimethylaniline, these monomers should electropolymerize to form polymer films on the electrodes. Figure 2-2b shows the proposed mechanism for the electropolymerization of dianilines, analogous to the oxidation and dimerization of *N,N*-dimethylaniline to TMB. Initially, the dianiline (**DA-n**) oxidizes to the radical cation, **DA-n**$^{+\bullet}$, that can form a C-C bond at the *para*-position of the anilines with another **DA-n**$^{+\bullet}$. Deprotonation affords the neutral dimer that can continue the process of oxidation, coupling, and deprotonation. At sufficiently high molecular weight, the polymer precipitates and deposits on the electrode. Oxidation of benzidine in the repeat unit of the polymer (**PDA-n**) forms the radical cation (**PDA-n**$^{+\bullet}$) that can be further oxidized to the quinoidal dication, **PDA-n**$^{2+}$. The benzidine polymers have theoretical capacities of 170-224 mA h g^{-1}, which are greater than the practical capacity of $LiCoO_2$ (140 mA h g^{-1}).

Figure 2-3a shows the cyclic voltammograms (CV) of all monomers at 10 mM concentration in 0.1 M $[NBu_4][PF_6]$ in CH_2Cl_2 at glassy carbon electrodes (GCE). On the first cycle (solid lines), all of the monomers begin oxidizing at > +0.42 V vs. Ag/Ag^+. The appearance of two reduction peaks on the subsequent negative sweep corresponds to the newly formed benzidine, indicating that the oxidative coupling was successful. These assignments were based on similar observations in the coupling of DMA to TMB.[24-26] **DA-2** and **TA-2** were the only monomers that did not display two reduction peaks suggesting unwanted side reactions. On the second cycle (dashed lines), some of the monomers display a new oxidation peak between 0-0.2 V that also corresponds to benzidine. The increase in reduction peak currents on successive cycles is indicative of polymer deposition and film growth.

After electropolymerization, the electrodes were rinsed with CH_2Cl_2 to remove soluble oligomers and cycled in monomer-free 0.1 M $[NBu_4][PF_6]$ in CH_3CN (Figure 2-3b). As expected from Figure 2-3a, there was no Faradaic (redox) response for

electrodes cycled in **DA-2** or **TA-2**. All of the other modified electrodes exhibited two redox couples, corresponding to the **PD(T)A-n**/**PD(T)A-n**$^{+\bullet}$ and the **PD(T)A-n**$^{+\bullet}$/ **PD(T)A-n**$^{2+}$ couples, referred to in this dissertation as the first and second redox couples, respectively. As the alkyl linker size was increased from ethyl to butyl, the Faradaic response of the modified electrodes also increased which indicates that more polymer was deposited onto the electrode. This trend suggests that there are repulsive interactions between charged benzidine moieties that interfere with the electropolymerization and film deposition process. Alkyl linker size also has an effect on the electrochemistry of the polymer films. The first redox couples of **PDA-3** and **PDA-4** have a large peak to peak separation (ΔE_p > 190 mV) while **PDA-6** and **PTA-6** have ΔE_p < 90 mV. The ΔE_p is expected to be 0 V for kinetically facile surface-confined systems and the non-zero ΔE_p for the polymer films can be partially accounted for by the fast scan rate, since at slower scan rates, the ΔE_ps of **PDA-6** approached 0 V (*vide infra*). The second redox couple for all films had ΔE_p < 90 mV and the oxidation potentials shifted negative with increasing alkyl linker length in the transition from **PDA-n**$^{+\bullet}$ to **PDA-n**$^{2+}$. This negative shift indicates that the dication is more stable (i.e. it is easier to oxidize the radical cation) with longer alkyl chains between the charged benzidine moieties.

Along with the linker size of the monomers, we studied the effect of solvent polarity on the electropolymerization of **DA-6** (Figure 2-4). The onset of monomer oxidation shifts negative in more polar solvents, e.g., from +0.41 V in CH_2Cl_2 to +0.25 V in CH_3CN. The oxidation curve is more slanted in the lower dielectric solvents (e.g., CH_2Cl_2), and this is due to resistivity of the electrolyte during the electron transfer. The cathodic peak currents are larger in lower dielectric solvents and correspondingly, more polymer was deposited on the electrodes. Dichloromethane was found to be the best solvent for the electropolymerization, and a higher concentration of electrolyte

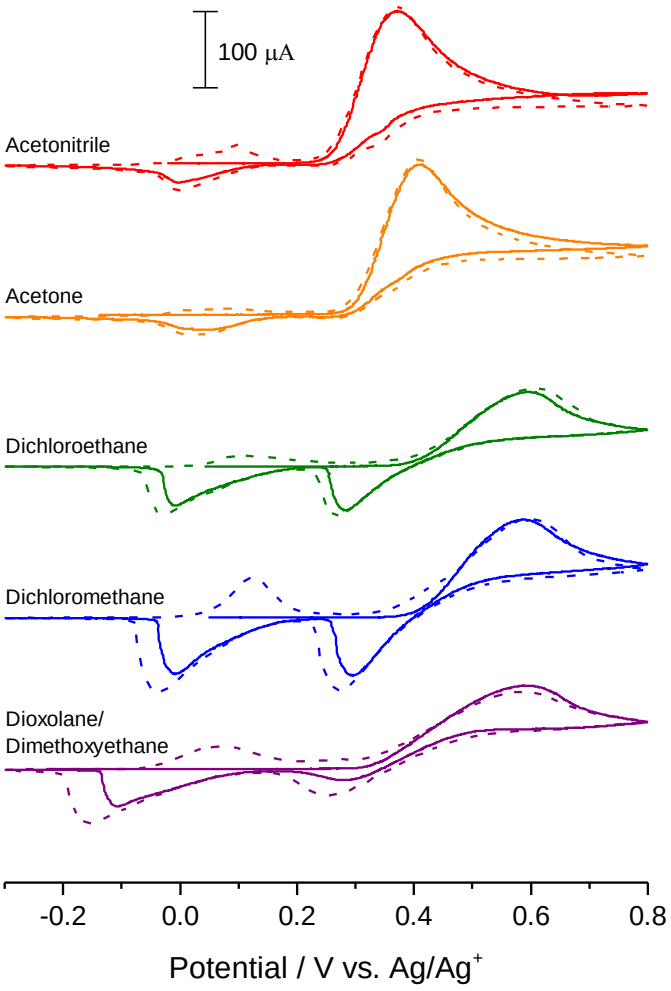

Figure 2-4. Cyclic voltammograms of 10 mM **DA-6** in 0.1 M $[NBu_4][PF_6]$/solvent on the 1st (solid line) and 2nd cycle (dashed line). All CVs on 100 µA scale. Scan rate: 20 mV s^{-1}.

(0.5 M) was used to lower the solution resistance.

The progress of **DA-6** electropolymerization and the charged state of **PDA-6** can be followed visually due to the electrochromic properties of benzidines. The indium tin oxide (ITO) electrode is colorless at potentials before the first redox couple, turns green during the first redox couple, and marigold during the second redox couple. The changes in absorbance of **PDA-6** deposited on ITO were monitored

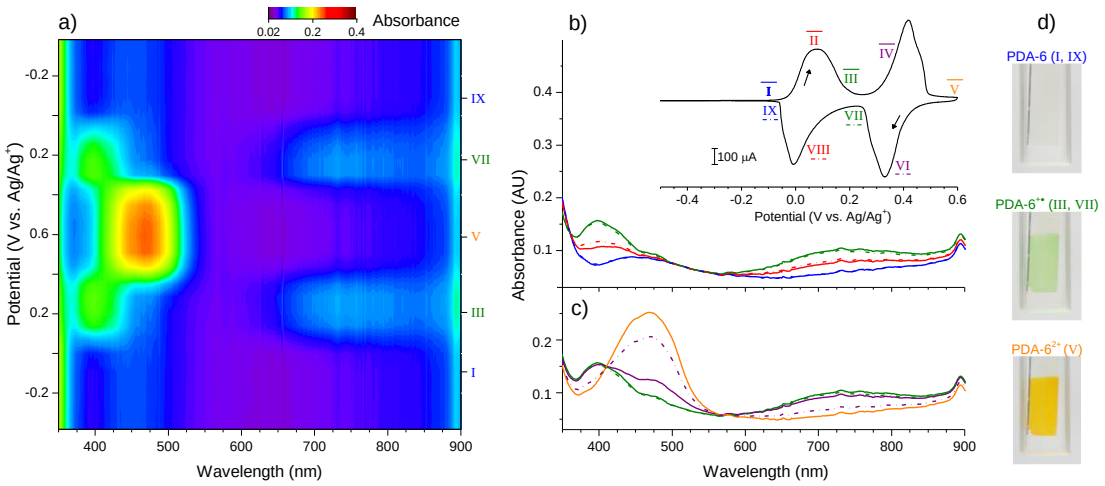

Figure 2-5. (a) Contour plot of the *in situ* UV-Vis spectroelectrochemistry of **PDA-6** deposited onto ITO electrode during one cycle. Inset: Corresponding CV of **PDA-6** film cycled in 0.1 M $[NBu_4][PF_6]$ in CH_3CN at 10 mV s^{-1} with Roman numeral markers relating designated potentials to UV-Vis spectra. UV-Vis spectra of **PDA-6** at designated potentials (b) between −0.10–0.22 V for the **PDA-6**/**PDA-6**$^{+\bullet}$ couple and (c) between +0.20–0.60 V for the **PDA-6**$^{+\bullet}$/**PDA-6**$^{2+}$ couple. (d) Pictures of **PDA-6** film on ITO in the neutral, cationic and dicationic states.

throughout one cycle by *in situ* spectroelectrochemistry. The contour plot of UV-Vis spectra (Figure 2-5) demonstrates that the spectroelectrochemistry of **PDA-6** is highly reversible and symmetric. There are five distinct regions that corresponds to the changes in oxidation state from neutral **PDA-6** to **PDA-6**$^{+\cdot}$ and **PDA-6**$^{2+}$, and back again to **PDA-6**$^{+\cdot}$ and finally neutral **PDA-6**. The UV-Vis spectra of the ITO electrode at potentials during the first redox couple contain several well-defined isosbestic points at 360, 498, and 565 nm (Figure 2-5b), while the UV-Vis spectra of the second redox couple contain two isosbestic points at 411 and 570 nm (Figure 2-5c). The isosbestic points indicate that the polymer cleanly and reversibly converts between the three redox states. The spectra of neutral **PDA-6** at potentials I and IX, before any oxidation and after complete reduction respectively, overlap entirely. Similarly, the spectra match at potentials III and VII when the polymer has been oxidized and reduced to **PDA-6**$^{+\cdot}$ respectively. The electrochromic nature of **PDA-6** means that the

state of charge can be determined visually in transparent EES devices, and the films displayed typical switching times for electrochromic polymer films on the order of 1-2 seconds.[30]

The applicability of this family of benzidine polymers, as cathode materials in thin-film electrochemical energy storage systems, was initially examined by cycling the electropolymerized films using CV in 0.1 M $[NBu_4][PF_6]$ in CH_3CN. Further studies focused on **PDA-6** because the polymer, with a theoretical capacity of 181 mA h g^{-1}, exhibits two well-behaved redox couples and great charge retention (Figure 2-6). **PDA-6** and **PTA-6** had comparable charge retention (>97%), while **PDA-4** retained 85% of its initial capacity after eight cycles, and **PDA-3** lost half of its initial capacity within five cycles. This trend clearly shows that polymers with longer alkyl linkers between benzidine groups have better cycling performance. This could be due in parts to electrochemical and chemical stability from lower electrostatic interactions

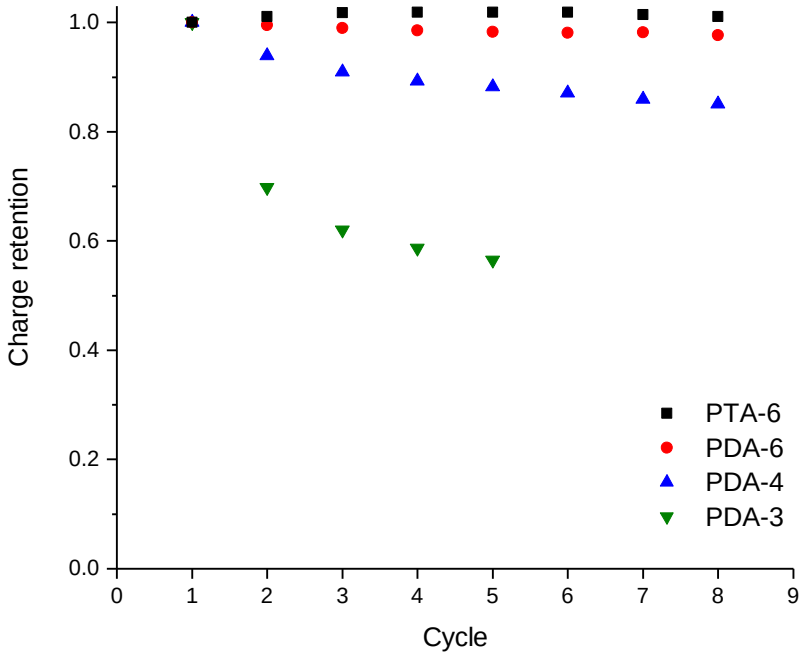

Figure 2-6. The performance of polymer films, deposited on GCE as in Figure 2-3a, cycled in 0.1 M $[NBu_4][PF_6]/CH_3CN$ at 20 mV s^{-1}.

between charged benzidine groups, better polymer film formation and morphology on GCEs, and higher insolubility for the polymer films.

Cycle-life performance testing was conducted using galvanostatic cycling experiments at different current densities. Thin films of **PDA-6** were electrodeposited

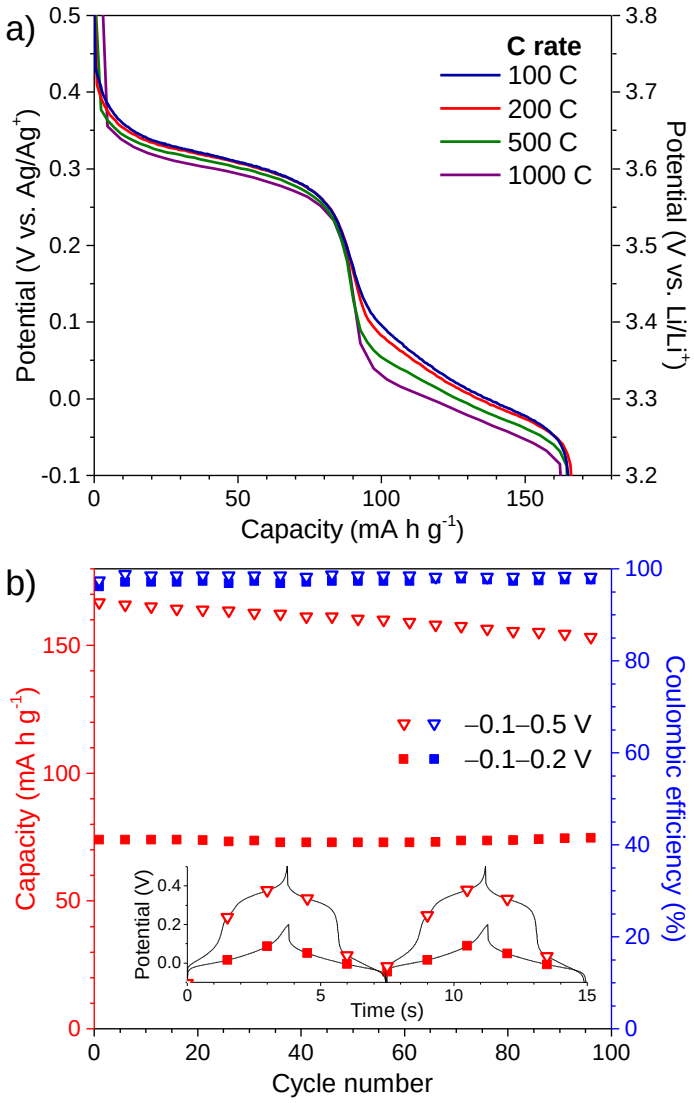

Figure 2-7. (a) Discharge curves for **PDA-6** at various C rates. (b) The capacity (red) and Coulombic efficiency (blue) of **PDA-6** with different positive cutoffs in 0.5 M $[NBu_4][PF_6]/CH_3CN$ at rate of 1,000 C. Inset: Representative charge and discharge curves for **PDA-6** with different potential ranges. The range was −0.1–0.2 V (square) and −0.1–0.5 V (triangle) vs. Ag/Ag^+.

onto GCE in 0.5 M $[NBu_4][PF_6]$ in CH_2Cl_2 and cycled in 0.5 M $[NBu_4][PF_6]$ in CH_3CN. The film thickness of **PDA-6** on GCE was measured to be 101 nm by contact profilometry. After **PDA-6** was charged to **PDA-6**$^{2+}$, the polymer was discharged at various rates, where a rate of 1 C takes 1 h for a full charge or discharge. The discharge curves in Figure 2-7 display two voltage plateaus at approximately +0.31 and 0 V vs. Ag/Ag^+ (3.6 and 3.3 V vs. Li/Li^+) that correspond closely to the two reductions from **PDA-6**$^{2+}$ to neutral **PDA-6**. Remarkably, at rates of 100–1,000 C, the thin film was discharged to ~165 mA h g^{-1} (or 5.09 mC cm^{-2}). At the cycle rate of 1,000 C, the polymer was fully discharged in less than four seconds. The higher current densities at high C rates lead to an increase in the *IR* voltage drop due to the internal cell resistance, lowering cell performance. Contrary to most systems, including 50 nm polymer films,[11,17] the capacity did not decrease considerably at high current rates for **PDA-6**. While the discharge plateaus shifted negative at faster rates, as expected, the *IR* drop was not significant, even at 1,000 C, to significantly impact the capacity (only a 2% decrease in capacity with a tenfold increase in C rate). The remarkable rate capability of **PDA-6** is a result of the rapid kinetics of the two electron transfer reactions (k_s = 0.4, 0.5 s^{-1}) and the efficient charge propagation within the 100 nm polymer film, which has diffusion coefficients on the order of 10^{-9} cm^2 s^{-1}.

The comparable capacities at high C rates prompted additional tests of thin films of **PDA-6** as a high power cathode material. Figure 2-7b shows the cycling performance of the **PDA-6** film charged and discharged at 1,000 C for 100 cycles at two different positive potential limits. If the polymer was only cycled between the **PDA-6**/**PDA-6**$^{+\cdot}$ couple in the range −0.1−0.2 V vs. Ag/Ag^+, the capacity was 74 mA h g^{-1} and the film displayed excellent cycle performance with >99% discharge retention after 100 cycles and >96% Coulombic efficiency. When the range was expanded to −0.1–0.5 V, **PDA-6**$^{+\cdot}$ can be further oxidized to **PDA-6**$^{2+}$, thereby

increasing the capacity to 165 mA h g^{-1}. We accessed 91% of the theoretical capacity of 181 mA h g^{-1} in the thin film. The polymer film exhibited good cycling stability with 92% discharge retention after 100 cycles and >98% Coulombic efficiency. Similar trends were seen in **PDA-6** films cycled at slower rates.

When the polymer film was cycled over both redox couples, the total capacity was expected to have equal contributions from each redox couple. However, the second redox couple had a higher capacity than the first (91 compared to 74 mA h g^{-1}). The additional capacity can be accounted for by the flatter discharge plateau at +0.31 V than at 0 V which enables more capacity from the **PDA-6**$^{+\bullet}$/**PDA-6**$^{2+}$ couple than the **PDA-6**/**PDA-6**$^{+\bullet}$ couple (Figure 2-7a). Also, the charge calculated from a CV of **PDA-6** film reveals that there is more charge from the second redox couple than the first couple. One possible reason for this imbalance is that the film contains fragments of **PDA-6**$^{+\bullet}$ that can be oxidized to **PDA-6**$^{2+}$ but not reduced to **PDA-6**. This charge trapping

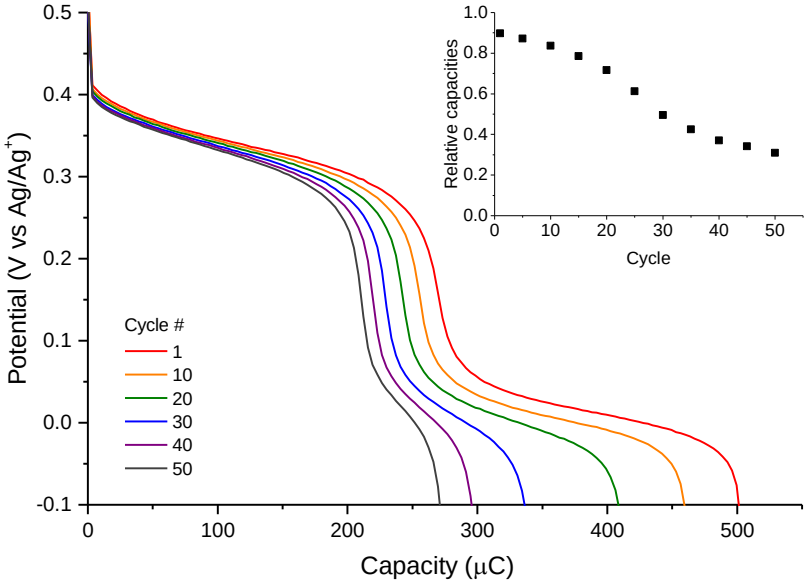

Figure 2-8. Discharge curves of **PTA-6** in 0.5 M [NBu_4][PF_6]/CH_3CN at an applied current of 36 μA. Inset: The relative capacities between the two couples with cycling, where the first reduction occurs between +0.2 and −0.1 V and the second reduction is between +0.5 and +0.2 V vs. Ag/Ag^+.

phenomenon was also seen in films of **PTA-6** where the capacity of the first redox couple decreased relative to the second couple during cycling (Figure 2-8). Attempts to improve charge retention by co-electropolymerizing the crosslinker **TA-6** with **DA-6** also gave rise to charge trapping and poorer cycling than **PDA-6** film alone.

2-3. Conclusions

In summary, we have developed a series of di- and trianilinoalkanes capable of forming thin electroactive films directly on electrodes, by electrochemical oxidative polymerization. Increasing the length of the alkyl linker between aniline groups facilitated the electropolymerization process and more polymer was deposited on the electrode. In comparison to shorter alkyl analogs, **PDA-6** and **PTA-6** exhibit two redox couples with small ΔE_ps. **PDA-6** displays reversible electrochromic behavior as the neutral, colorless polymer turns green as the radical cation (**PDA-6**$^{+\cdot}$) and marigold as the dication (**PDA-6**$^{2+}$) are generated. The ability to visually identify the state of charge of the cathode material could be useful in transparent EES devices. Due to the fast kinetics of the two electron transfers and the 100 nm thick film, **PDA-6** can be charged and discharged at rates up to 1,000 C without an appreciable loss in capacity or degradation of performance. The polymer displayed exceptional stability (>99% retention) when cycled only around the first couple. When the polymer is fully oxidized to **PDA-6**$^{2+}$, there are two distinct voltage plateaus and the film retains 92% of the initial capacity of 165 mA h g^{-1} after 100 cycles. These findings indicate the potential utility of **PDA-6** as a cathode material in thin-film batteries that combines the high capacity of batteries with the high power of supercapacitors. Investigation is currently underway to use the polymers on high surface area electrodes for 3D and flexible batteries.

2-4. General Considerations

All manipulations of air and water sensitive compounds were carried out under dry nitrogen using a Braun UniLab drybox or standard Schlenk line techniques. ^{1}H NMR spectra were recorded on a Varian INOVA 400 (^{1}H, 400 MHz) and referenced with residual non-deuterated solvent shift ($CHCl_3$ = 7.26 ppm). ^{13}C NMR spectra were recorded on Varian INOVA 500 (^{13}C, 125 MHz) spectrometer and referenced to chloroform (77.16 ppm). High resolution mass spectrometry (HRMS) analyses were carried out on a Thermo Scientific Exactive Orbitrap MS system equipped with an Ion Sense DART ion source. Flash column chromatography was performed using silica gel (particle size 40-64 μm, 230-400 mesh).

Electrochemistry experiments were performed at 22 °C using a Hokuto Denko HABF1510m or a Princeton Applied Research VersaSTAT 3 potentiostat. All cyclic voltammetry (CV) measurements were carried out in a fritted three compartment cell using a glassy carbon working electrode (GCE, 3 mm diameter), a large-area Pt counter electrode, and a Ag/Ag^+ (0.05 M $AgClO_4$ and 0.1 M $[NBu_4][ClO_4]$ in CH_3CN) reference electrode. The potential, 0 V, measured using a Ag/Ag^+ reference electrode is +3.3 V vs. Li/Li^+. UV-Vis absorption spectra were obtained using a HP 8453 diode array spectrophotometer using a fritted three compartment cell.

The thickness of the electropolymerized films on GCE were measured with a contact profilometer (Tencor Alpha Step 500) after scraping away a section of the polymer film with a razor blade. Line scans were performed at different points along the film edge. The thickness readings were then averaged to determine the mean film thickness.

2-5. Materials

Tris(dibenzylideneacetone)dipalladium(0) ($Pd_2(dba)_3$), DavePhos (2-(dicyclohexylphosphino)-2'-(*N,N*-dimethylamino))-1,1'-biphenyl), and sodium *tert*-butoxide (NaO^{t}Bu) were purchased from Strem and used as received. Bromobenzene and acetonitrile were purchased from Sigma-Aldrich and distilled after standing over CaH_2. *N,N′*-dimethylethylenediamine, *N,N′*-dimethyl-1,3-propanediamine, and *N,N′*-dimethyl-1,6-hexanediamine were purchased from Sigma-Aldrich and distilled from KOH. HPLC grade toluene and dichloromethane were purchased from Fischer Scientific and dried over an alumina column. Tetrabutylammonium hexafluorophosphate was purchased from TCI America and recrystallized twice from absolute ethanol and dried under vacuum. Indium-tin oxide (ITO) coated glass slides (10 Ω/sq. in.) were purchased from Nanocs and cleaned by sonicating in acetone, and then isopropanol. All other reagents were purchased from commercial sources and used as received.

Synthesis of Di- and Trianilinoalkane Monomers

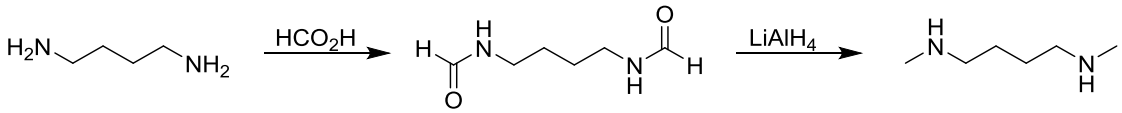

1a **2a** **3a**

N,N′-Dimethyl-1,4-butanediamine (3a)

N,N′-Dimethyl-1,4-butanediamine was prepared according to a literature procedure.[31] Formic acid (88% Macron, 35.2 mL, 0.821 mol) was added dropwise to 1,4-butanediamine (**1a**, Aldrich, 25 mL, 0.25 mol) at 0 °C. The solution was refluxed for 1 h, and then the pressure was lowered slowly until the reaction was refluxing under full vacuum for 4 h. White precipitate crashed out of the cooled reaction and was collected by filtration. The intermediate **2a** was recrystallized using isoamyl

alcohol and dried under reduced pressure to give a white powder (81% yield). The diamide (**2a**, 6.49 g, 45.0 mmol) was reduced using $LiAlH_4$ (7.25 g, 191 mmol) in 180 mL ether. After stirring overnight, the mixture was quenched with 20 mL water at 0 °C. The white mixture was filtered over Celite and washed with ether. The filtrate was dried over $MgSO_4$ and concentrated. Distillation under vacuum with KOH (b.p. 52 °C, 14 mmHg) afforded **3a** in 54 % isolated yield. ^{1}H NMR spectrum in ppm ($CDCl_3$, 400 MHz): δ 2.56 (m, 4H), 2.40 (s, 6H), 1.49 (m, 4H), 1.23 (br s, 2H) and was consistent with previous literature.[32]

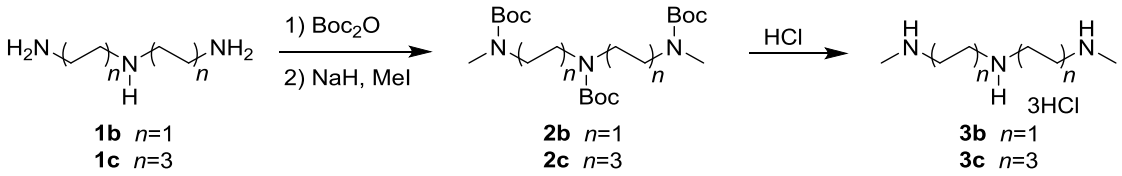

1b *n*=1
1c *n*=3

2b *n*=1
2c *n*=3

3b *n*=1
3c *n*=3

***N*-Methyl-*N′*-[2-(methylamino)ethyl]-1,2-ethanediamine trihydrochloride (3b)**

The triamine hydrochlorides were prepared by the method of Edwards.[33] Diethylenetriamine (**1b**, Aldrich, 1.02 g, 9.89 mmol) was dissolved in methanol (15 mL) and di-*tert*-butyl dicarbonate (TCI America, 7.3 g, 33 mmol) was added and the reaction stirred overnight (12 h). Water was added and the product was extracted with ether, washed with brine, dried with $MgSO_4$, and concentrated. The clear, colorless oil crystallized on standing at 25 °C resulting in a white powder (88% yield). In the glovebox, NaH (Aldrich 95%, 0.56 g, 23 mmol) was added to a Schlenk flask. The solution of tris-Boc-protected diethylenetriamine (2.98 g, 7.38 mmol) dissolved in dry DMF (4.5 mL) was injected in under N_2. After the mixture was stirred at 25 °C for 1 h, methyl iodide (Aldrich, 1.4 mL, 22 mmol) was added in dropwise. After 12 h, the reaction was quenched with water and the product was extracted into CH_2Cl_2 and washed with brine. The crude product was purified via flash column chromatography

using 30% ethyl acetate/hexanes as the eluent to give **2b** as a clear, viscous oil (42% isolated yield).

Compound **2b** (1.35 g, 3.13 mmol) was dissolved in absolute ethanol (8 mL) and 2 M HCl in ether (8 mL, 16 mmol) was added. After 5 h, the white precipitate was collected by filtration and dried under vacuum to give **3b** (89% isolated yield). ^{1}H NMR spectrum (D_2O, 400 MHz): δ 3.42-3.56 (m, 8H), 2.80 (s, 6H) and was consistent with previous literature.[34]

***N*-Methyl-*N′*-[6-(methylamino)hexyl]-1,6-hexanediamine trihydrochloride (3c)**

Bis(hexamethylene)triamine (**1c**, Aldrich, 0.50 g, 2.3 mmol) was dissolved in methanol (5 mL) and di-*tert*-butyl dicarbonate (TCI America, 1.68 g, 7.70 mmol) was added and the reaction stirred overnight (12 h). Water was added and the product was extracted with ether, washed with brine, dried with $MgSO_4$, and concentrated. The product was purified by column chromatography using 20% ethyl acetate/hexanes to obtain a clear, colorless oil (91% yield). In the glovebox, NaH (Aldrich 95%, 0.275 g, 11.4 mmol) was added to a Schlenk flask. The tris-Boc-protected bis(hexamethylene)triamine (1.47 g, 2.86 mmol) dissolved in dry DMF (6 mL) was injected in under N_2. After the mixture was stirred at 25 °C for 1 h, methyl iodide (Aldrich, 1.36 mL, 21.8 mmol) was added in dropwise. After 12 h, the reaction was quenched with water and the product was extracted into CH_2Cl_2 and washed with brine. The crude product was purified via flash column chromatography using 30% ethyl acetate/hexanes as the eluent to give **2c** as a clear, viscous oil (62% isolated yield).

Compound **2c** (0.82 g, 1.5 mmol) was dissolved in absolute ethanol (4 mL) and 2 M HCl in ether (10 mL, 20 mmol) was added. After 5 h, the white precipitate was collected by filtration and dried under vacuum to give **3c** (79% isolated yield). ^{1}H

NMR spectrum (D_2O, 400 MHz): δ 3.02 (t, 8H), 2.70 (s, 6H), 1.69 (br s, 8H), 1.41 (br s, 8H).

Representative Pd-Catalyzed Amination Procedure A

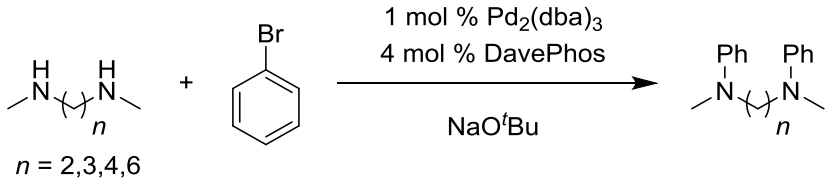

In the glovebox, $Pd_2(dba)_3$ (1 mol %), DavePhos (4 mol %) and NaO^{t}Bu (2.3 equiv) were added to an oven-dried Schlenk tube equipped with a magnetic stir bar. Then chlorobenzene (2.5 mL/mmol) was added, followed by bromobenzene (9 equiv) and the diamine (1 equiv). After sealing, the tube was heated in an oil bath set at 100 °C for 5 d. After cooling, the cooled mixture was filtered over Celite and washed with CH_2Cl_2. The filtrate was concentrated and evacuated under reduced pressured to remove excess bromobenzene and solvent. The crude product was purified by flash column chromatography.

Representative Pd-Catalyzed Amination Procedure B

In the glovebox, NaO^{t}Bu (2.8 equiv) and bromobenzene (9 equiv) were added to an oven-dried Schlenk tube equipped with a magnetic stir bar. Then the diamine (1 equiv) in 0.25 mL/mmol of toluene was added, followed by a mixture of $Pd_2(dba)_3$ (1 mol %) and DavePhos (4 mol %) in 0.5 mL/mmol toluene. After sealing, the tube was heated in an oil bath set at 50 °C overnight for 12 h, then at 100 °C for 12 h. After cooling, the cooled mixture was filtered over Celite and washed with CH_2Cl_2. The filtrate was concentrated and the crude product was purified by flash column chromatography.

Representative Pd-Catalyzed Amination Procedure C

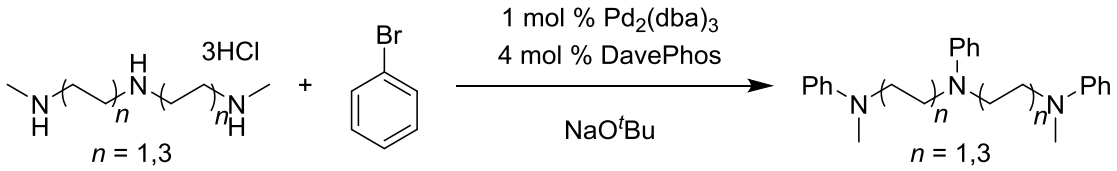

In the glovebox, $Pd_2(dba)_3$ (1 mol %), DavePhos (4 mol %) and NaO^{t}Bu (6 equiv) were added to an oven-dried Schlenk tube equipped with a magnetic stir bar. Then bromobenzene and the triamine (1 equiv) were added. After sealing, the tube was heated in an oil bath set at 100 °C for 3 d. After cooling, the cooled mixture was filtered over Celite and washed with CH_2Cl_2. The filtrate was concentrated and evacuated under reduced pressured to remove excess bromobenzene. The crude product was purified by flash column chromatography.

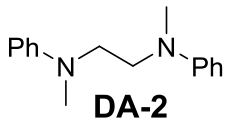

DA-2

***N,N′*-Dimethyl-*N,N′*-diphenylethylenediamine (DA-2)**

Following the general procedure B, a mixture of bromobenzene (1.5 g, 9.6 mmol), *N,N′*-dimethylethylenediamine (88 mg, 1.0 mmol), $Pd_2(dba)_3$ (9.5 mg, 10 μmol), DavePhos (16.7 mg, 42.4 μmol), NaO^{t}Bu (272 mg, 2.83 mmol), and toluene (0.75 mL) was heated to 50 °C for 12 h then 100 °C for 12 h. The crude product was purified by flash column chromatography using 5% ethyl acetate/hexanes as the eluent (R_f = 0.32) to give a yellow powder (97% isolated yield). Spectroscopic characterization was consistent with that reported in previous literature.[35] ^{1}H NMR spectrum ($CDCl_3$, 400 MHz): δ 7.22-7.29 (m, 4H), 6.69-6.75 (m, 6H), 3.55 (s, 4H), 2.95 (s, 6H). ^{13}C NMR ($CDCl_3$, 125 MHz): δ 148.98, 129.43, 116.36, 111.94, 49.85,

38.82. HRMS (DART-MS) m/z calculated for $C_{16}H_{20}N_2^+$ (M + H^+) 241.1621, found 241.1700.

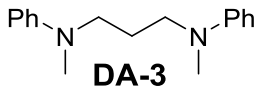

DA-3

***N,N′*-Dimethyl-*N,N′*-diphenyl-1,3-propanediamine (DA-3)**

Following the general procedure A, a mixture of bromobenzene (1.5 g, 9.6 mmol), *N,N′*-dimethyl-1,3-propanediamine (107 mg, 1.05 mmol), $Pd_2(dba)_3$ (9.5 mg, 10 μmol), DavePhos (20.7 mg, 52.6 μmol), NaO^{t}Bu (230 mg, 2.39 mmol), and chlorobenzene (2.5 mL) was heated to 100 °C for 5 d. The crude product was purified by flash column chromatography using 5% ethyl acetate/hexanes as the eluent (R_f = 0.24) to give a yellow oil (88% isolated yield). ^{1}H NMR spectrum ($CDCl_3$, 400 MHz): δ 7.18-7.25 (m, 4H), 6.66-6.73 (m, 6H), 3.37 (t, 4H), 2.92 (s, 6H), 1.83-1.93 (m, 2H). ^{13}C NMR ($CDCl_3$, 125 MHz): δ 129.28, 116.43, 112.57, 50.61, 38.50, 24.28. HRMS (DART-MS) m/z calculated for $C_{17}H_{22}N_2^+$ (M + H^+) 255.1778, found 255.1854.

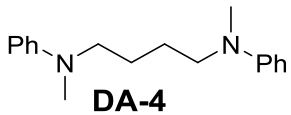

DA-4

***N,N′*-Dimethyl-*N,N′*-diphenyl-1,4-butanediamine (DA-4)**

Following the general procedure A, a mixture of bromobenzene (1.5 g, 9.6 mmol), **3a** (122 mg, 1.05 mmol), $Pd_2(dba)_3$ (9.2 mg, 10 μmol), DavePhos (22.7 mg, 57.7 μmol), NaO^{t}Bu (235 mg, 2.44 mmol), and chlorobenzene (2.5 mL) was heated to 100 °C for 5 d. The crude product was purified by flash column chromatography using 5% ethyl acetate/hexanes as the eluent (R_f = 0.23) to give a yellow powder (78% isolated yield). ^{1}H NMR spectrum ($CDCl_3$, 400 MHz): δ 7.20-7.26 (m, 4H), 6.66-6.72

(m, 6H), 3.34 (m, 4H), 2.92 (s, 6H), 1.59-1.64 (m, 4H). ^{13}C NMR ($CDCl_3$, 125 MHz): δ 149.37, 129.30, 116.14, 112.28, 52.80, 38.43, 24.56. HRMS (DART-MS) m/z calculated for $C_{18}H_{25}N_2^+$ (M + H^+) 269.2012, found 269.2012.

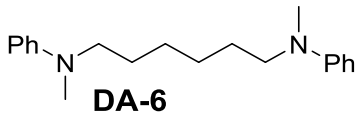

DA-6

***N,N′*-Dimethyl-*N,N′*-diphenyl-1,6-hexanediamine (DA-6)**

Following the general procedure B, a mixture of bromobenzene (1.5 g, 9.6 mmol), *N,N′*-dimethyl-1,6-hexanediamine (146 mg, 1.01 mmol), $Pd_2(dba)_3$ (9.4 mg, 10 μmol), DavePhos (17 mg, 43 μmol), NaO^{t}Bu (270 mg, 2.81 mmol), and toluene (0.75 mL) was heated to 50 °C for 12 h then 100 °C for 12 h. The crude product was purified by flash column chromatography using 5% ethyl acetate/hexanes as the eluent (R_f = 0.26) to give a yellow oil (82% isolated yield). Spectroscopic characterization was consistent with that reported in previous literature.[36] ^{1}H NMR spectrum ($CDCl_3$, 400 MHz): δ 7.19-7.25 (m, 4H), 6.66-.6.71 (m, 6H), 3.30 (t, 4H), 2.91 (s, 6H), 1.54-1.63 (m, 4H), 1.33-1.40 (m, 4H). ^{13}C NMR ($CDCl_3$, 125 MHz): δ 149.38, 129.23, 115.95, 112.17, 52.79, 38.38, 27.20, 26.75. HRMS (DART-MS) m/z calculated for $C_{20}H_{28}N_2^+$ (M + H^+) 297.2247, found 297.2325.

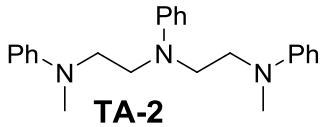

TA-2

***N*-Methyl-*N′*-[2-(methylphenylamino)ethyl]-*N,N′*-diphenyl-1,2-ethanediamine (TA-2)**

Following the general procedure C, a mixture of bromobenzene (2.5 g, 16 mmol), **3b** (128 mg, 0.532 mmol), $Pd_2(dba)_3$ (16 mg, 17 μmol), DavePhos (38 mg, 96 μmol), NaO^{t}Bu (360 mg, 3.75 mmol) was heated to 100 °C for 3 d. The crude product was purified by flash column chromatography using 4% ethyl acetate/hexanes as the eluent (R_f = 0.15) to give a yellow powder (74% isolated yield). ^{1}H NMR spectrum ($CDCl_3$, 400 MHz): δ 7.18-7.29 (m, 5H), 6.63-6.76 (m, 9H), 3.50 (s, 8H), 2.90 (s, 6H). ^{13}C NMR ($CDCl_3$, 125 MHz): δ 148.95, 147.57, 129.72, 129.47, 116.51, 116.37, 112.02, 111.58, 50.08, 48.24, 38.87. HRMS (DART-MS) m/z calculated for $C_{24}H_{30}N_3^+$ (M + H$^+$) 360.2434, found 360.2434.

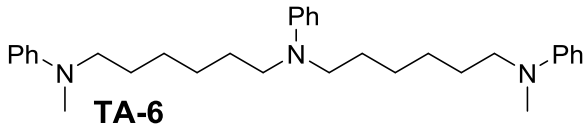

TA-6

***N*-Methyl-*N′*-[6-(methylphenylamino)hexyl]-*N*,*N′*-diphenyl-1,6-hexanediamine (TA-6)**

Following the general procedure C, a mixture of bromobenzene (2.5 g, 16 mmol), **3c** (470 mg, 1.33 mmol), $Pd_2(dba)_3$ (29 mg, 32 μmol), DavePhos (54 mg, 0.14 mmol), NaO^{t}Bu (813 mg, 8.46 mmol) was heated to 100 °C for 3 d. The crude product was purified by flash column chromatography using 5% ethyl acetate/hexanes as the eluent (R_f = 0.18) to give a yellow oil (47% isolated yield). ^{1}H NMR spectrum ($CDCl_3$, 400 MHz): δ 7.17-7.24 (m, 6H), 6.61-6.70 (m, 9H), 3.30 (t, 4H), 3.23 (t, 4H), 2.91 (s, 6H), 1.54-1.62 (m, 8H), 1.33-1.37 (m, 8H). ^{13}C NMR ($CDCl_3$, 125 MHz): δ 149.41, 148.14, 129.33, 129.26, 115.98, 115.35, 112.19, 111.83, 52.83, 51.10, 38.42, 27.35, 27.23, 26.79. The γ-carbon to aniline groups (27.23 ppm) exhibit chemical shift equivalence. HRMS (DART-MS) m/z calculated for $C_{32}H_{45}N_3^+$ (M + H$^+$) 471.3608, found 471.3686.

2-6. Electrochemical Measurements

Cyclic Voltammetry (CV) & Chronoamperometry

CV and chronoamperometry measurements were taken in a three-electrode cell configuration using a 3 mm diameter GCE working electrode, a Ag/Ag^+ reference electrode and a coiled Pt wire counter electrode in separate compartments connected by medium porosity glass frits. The GCE were polished with 1.0 μm, 0.3 μm, and 0.05 μm alumina (EXTEC) mixtures, rinsed with distilled water and acetone, sonicated in acetone for 1 min, and dried prior to use. The Pt counter electrode was flame annealed prior to use.

Films of **PDA-6** were prepared on GCEs by anodic electrochemical polymerization of 5 mM **DA-6** in 0.5 M $[NBu_4][PF_6]/CH_2Cl_2$ at 20 mV s^{-1} between −0.5–0.8 V for two cycles, unless specified otherwise. After the polymerization, the modified electrodes were rinsed gently with CH_2Cl_2 and CH_3CN. After air-drying, the electrodes were dried under vacuum for at least 4 h. Throughout this dissertation, the first couple refers to the electron transfer between the neutral and radical cation species, while the second couple refers to the electron transfer between the radical cation and dicationic species.

Table 2-1. The electrochemical values for polymer films from Figure 2-3b.

Name	$E^{0\prime}{}_1$ (V)	ΔE_{p1} (V)	$E^{0\prime}{}_2$ (V)	ΔE_{p2} (V)	Theoretical capacity (mA h g^{-1})
PDA-2	-	-	-	-	223
PDA-3	0.067	0.192	0.452	0.029	211
PDA-4	0.068	0.285	0.381	0.044	200
PDA-6	0.002	0.041	0.354	0.058	181
PTA-2	-	-	-	-	224
PTA-6	0.019	0.089	0.350	0.083	170

As a control, the electrochemical activity of TMB was examined using CV in acetonitrile (Figure 2-9). As expected for the soluble TMB, there are linear

correlations between the peak currents and the square root of the scan rate for both redox processes.[37] This linear fit is indicative of systems that have reversible electron transfers in solution and are under diffusional transport.

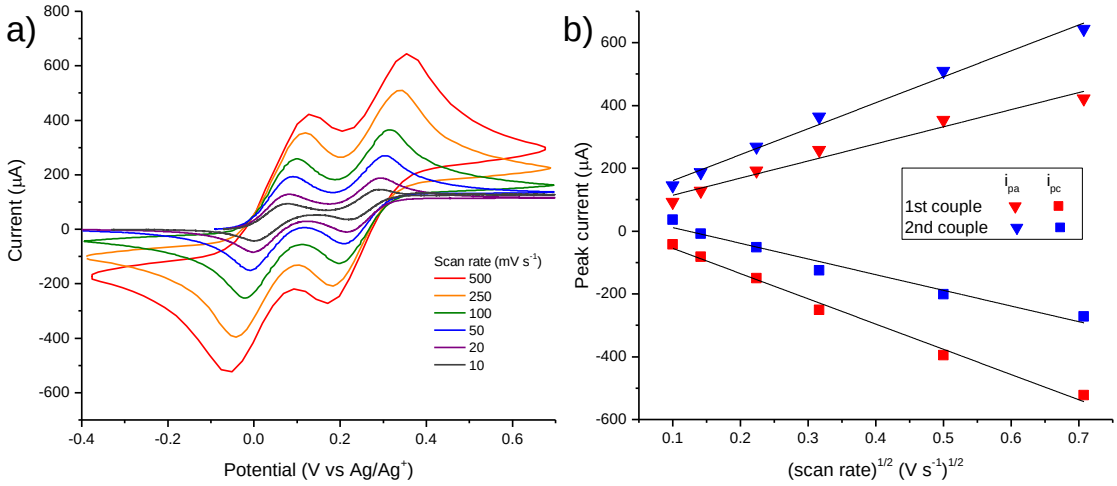

Figure 2-9. (a) Sweep rate dependent CVs of 10 mM *N,N,N′,N′*-tetramethylbenzidine (TMB, Aldrich) in 0.1 M $[NBu_4][PF_6]/CH_3CN$. (b) The dependence of the peak currents of the two redox couples of TMB on the square root of the scan rate.

In contrast, surface-confined systems with fast electron transfer processes exhibit linear correlations between the current peaks and the scan rate. The scan rate dependence studies were performed on a thin film of **PDA-6** deposited on GCE and cycled in 0.5 M $[NBu_4][PF_6]/CH_3CN$ between −0.3–0.6 V (Figure 2-10). First, the peak to peak separation, ΔE_p, is expected to be lower at slower sweep rates since the electrolyte ions have more time to diffuse into the polymer film. The ΔE_p is predicted to be 0 V for ideal, kinetically facile surface-confined systems. This was observed in PDA-6 where the ΔE_p approached 0 V at slower scan rates. Second, the polymer films exhibited linear correlations between the peak currents and the scan rate. These findings indicate the polymer films undergo fast electron transfer processes.

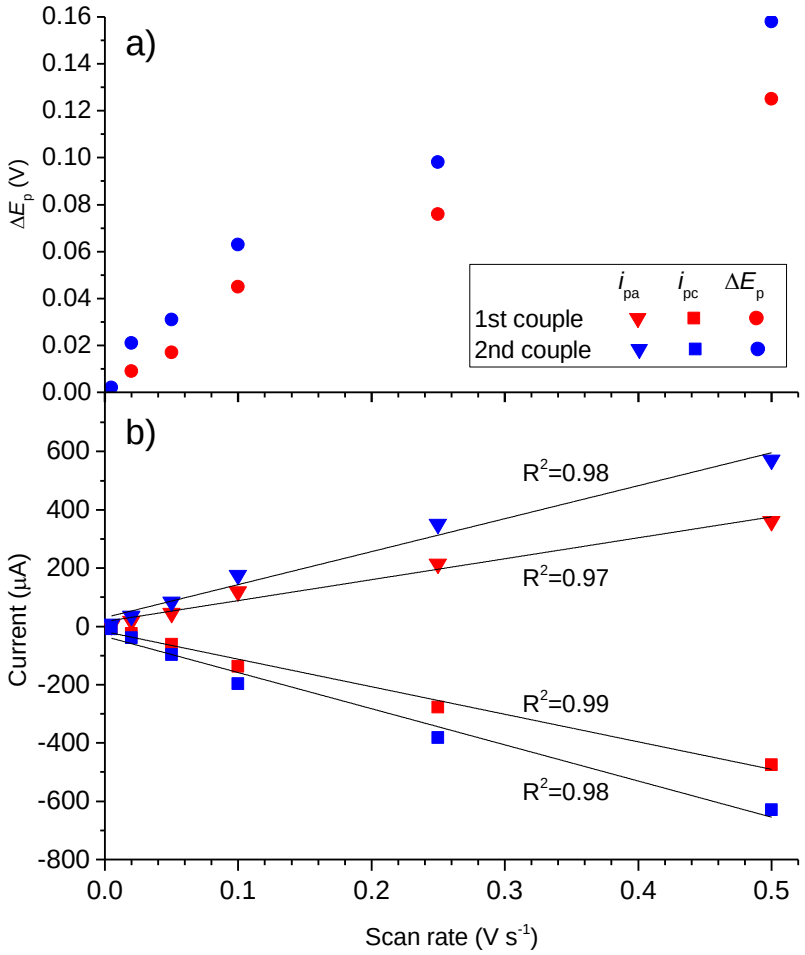

Figure 2-10. (a) The difference in peak potentials (ΔE_p) of the two redox couples of **PDA-6** at various scan rates. (b) The dependence of the anodic and cathodic peak currents (i_{pa} and i_{pc}, respectively) of the first and second couples of **PDA-6** on scan rates.

Next, the growth of the polymer films by electropolymerization was examined (Figure 2-11). During electropolymerization of **DA-6**, the peak currents increased in steady increments on successive cycles, suggesting linear polymer deposition and film growth. This hypothesis was tested by examining the peak currents of modified electrodes that were prepared by different deposition cycles. These plots indicate that the polymer film growth follows a linear correlation with the number of electropolymerization cycles. This suggests that film thickness can be controlled by either the monomer concentration or the number of deposition cycles.

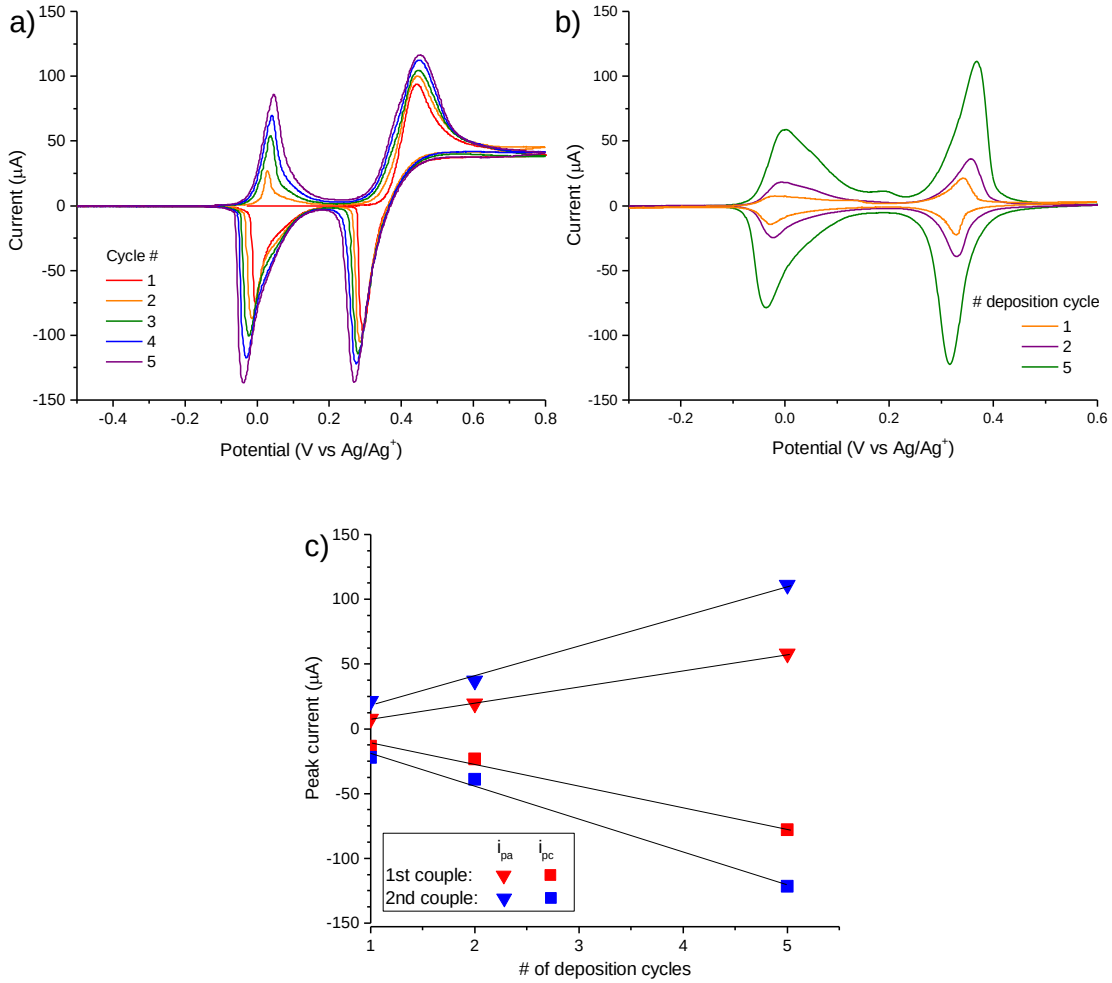

Figure 2-11. (a) Successive CVs of 5 mM **DA-6** in 0.5 M $[NBu_4][PF_6]/CH_2Cl_2$ during electropolymerization at 20 mV s^{-1}. (b) CVs of **PDA-6** films that were prepared by different deposition cycles, cycled in 0.5 M $[NBu_4][PF_6]/CH_3CN$ at 20 mV s^{-1}. (c) Dependence of the anodic and cathodic peak currents (i_{pa} and i_{pc}, respectively) of **PDA-6** on the number of deposition cycles during film preparation.

The charge was calculated using a CV of **PDA-6** to understand the differences in the capacity between the first and second redox couples during galvanostatic cycling. The charge (Q) of each peak was calculated by integrating the current under the peaks after subtraction of the contribution from the double layer (shown in blue lines in Figure 2-12). The plot also shows the differences in the peak potentials (ΔE_p) of the two redox couples, which were both under 25 mV.

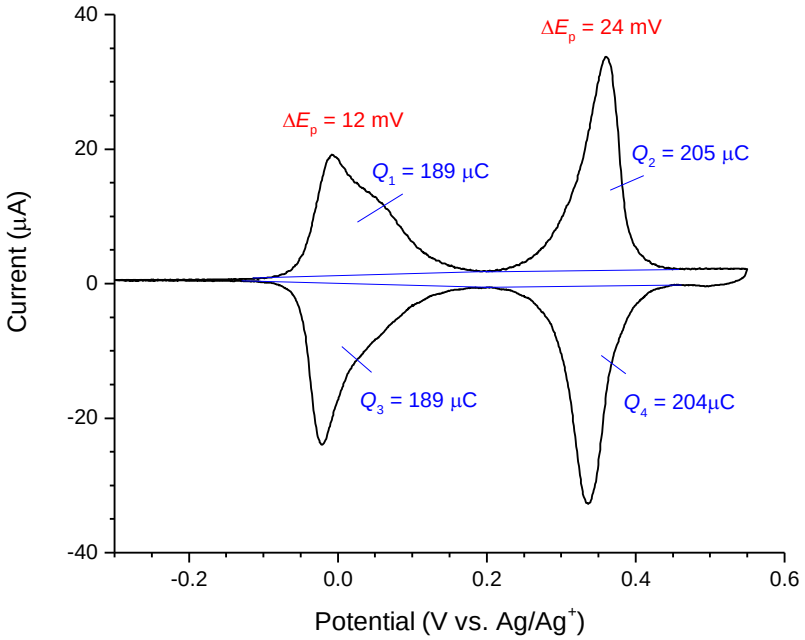

Figure 2-12. The cyclic voltammogram of **PDA-6** cycled in 0.5 M $[NBu_4][PF_6]/CH_3CN$ at 10 mV s^{-1}.

The charge for the first redox couple is smaller than the charge for the second redox couple (189 μC compared to 204 μC). The polymer film is expected to have equal contributions from both redox couples, and the fact that there is more charge from the second redox couple implies that there are **PDA-6**$^{+\cdot}$ trapped in the radical cation state that can be oxidized to **PDA-6**$^{2+}$ but not reduced to **PDA-6**. Both redox couples have high Coulombic efficiency of >99%.

Laviron Analysis

The Laviron method[38] was used for the determination of the charge transfer rate constants of adsorbed species. The same CVs used for Figure 2-10 (scan rate dependence of **PDA-6**) were used for the analysis. The dependence of the difference between peak potentials (E_p) and the formal redox potential ($E^{0\prime}$) was plotted vs. the logarithm of the scan rate (log(ν)) (Figure 2-13). The plot yields two straight lines per redox couples when log(scan rate) > −1.0. The electron transfer coefficient, α, and the

electron transfer rate constant, k_s, were calculated using Equation 2 and the straight lines from Figure 2-12.[39]

$$E_p = E^{0'} - \frac{RT}{\alpha n F}\ln\left(\frac{\alpha n F}{RTk_s}\right) - \frac{RT}{\alpha n F}\ln(\nu) \qquad (2)$$

where R is the gas constant (8.314 J K^{-1} mol^{-1}), T is the temperature (293 K), n is the number of electrons, and F is the Faraday constant (96,485 C mol^{-1}). The constants were determined to be α=0.42 and k_s = 0.4 s^{-1} for the first redox couple, and α=0.46 and k_s = 0.5 s^{-1} for the second redox couple.

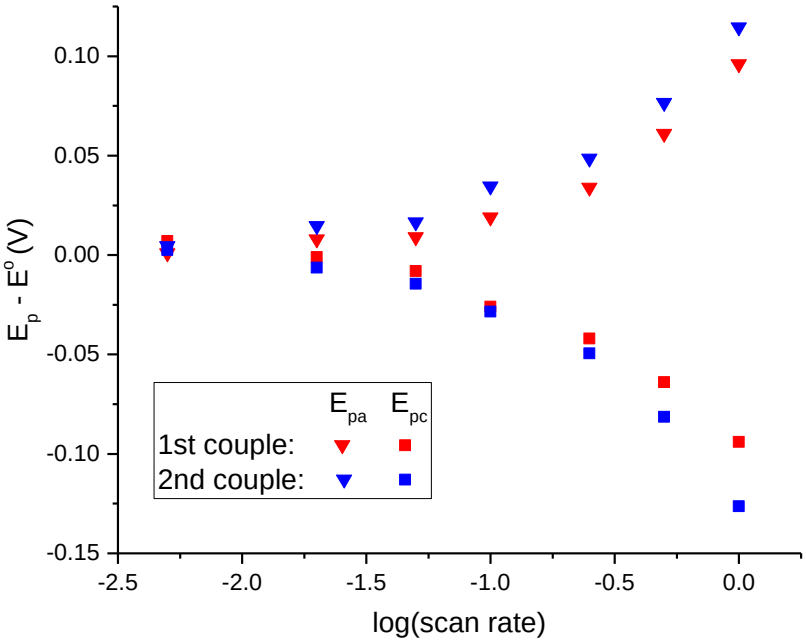

Figure 2-13. Dependence of the difference between peak potentials (E_p) and the formal redox potential ($E^{0\prime}$) on the logarithm of the scan rate (log(ν)).

Determination of Diffusion Coefficient

Chronoamperometry was performed by holding the potential at 0.8 V for several seconds, and measuring the current with time. The graph, known as a Cottrell plot, of the current vs. the reciprocal square root of time was plotted (Figure 2-14). The slope of the linear portion of the plot and Equation 3 was used to determine the diffusion coefficient of **PDA-6** film as 2.4 x 10^{-9} cm^2 s^{-1}.

$$i = \frac{nFACD^{1/2}}{(\pi t)^{1/2}} \quad (3)$$

where i is the current (A), A is the area (cm^2), C is the concentration (mol cm^{-3}), D is the diffusion constant (cm^2 s^{-1}), and t is the time (s).

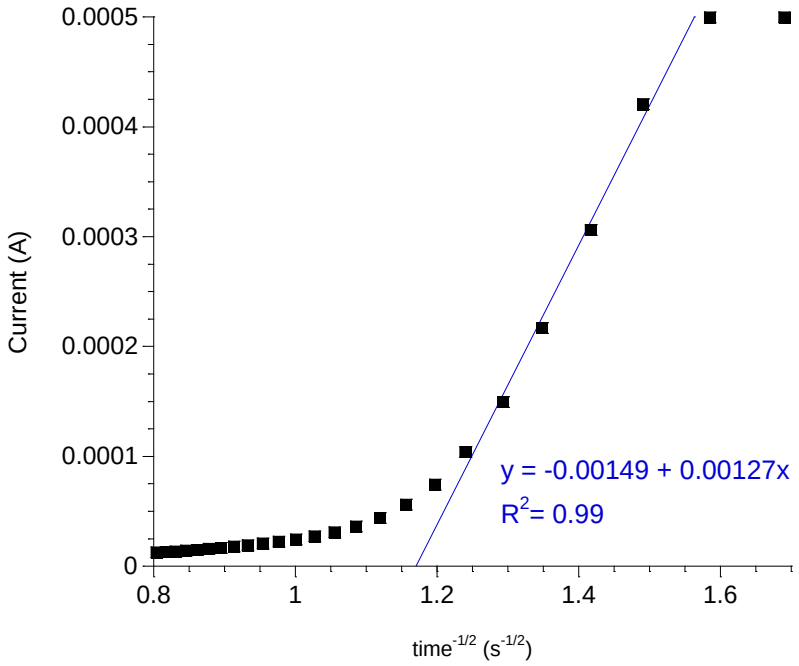

Figure 2-14. Cottrell plot of **PDA-6** in 0.1 M $[NBu_4][PF_6]/CH_3CN$.

Spectroelectrochemical Experiments

ITO coated glass slides were cut to ~5x75 mm sized electrodes and copper tape was wrapped around the top of the electrode to facilitate electrical contact. For the *in situ* spectroelectrochemical studies, **PDA-6** was deposited on an ITO electrode by electropolymerization of 0.5 mM **DA-6** in 0.1 M $[NBu_4][PF_6]/CH_2Cl_2$ at 20 mV s^{-1} between −0.5–0.8 V. After the polymerization, the modified electrodes were rinsed gently with CH_2Cl_2 and CH_3CN. The modified ITO electrode was placed facing the light path in a fritted three compartment glass cell, along with the Ag/Ag^+ reference electrode and a coiled Pt wire counter electrode. The modified electrode was cycled in 0.1 M $[NBu_4][PF_6]/CH_3CN$ at 10 mV s^{-1} between −0.5–0.6 V and UV-Vis spectra were collected every 8 seconds.

For the switching time experiments, the ITO electrodes were deposited as described above. The switching time is a measurement of the time required for an electrochromic material to fully switch colors. For measuring the switching time for the dication from the neutral polymer, the potential was held at -0.2 V and 0.5 V for 3 cycles of 5, 2, 1, 0.5 seconds, and the absorbance was measured at 469 nm (Figure 2-15). For measuring the switching time for the radical cation, the potential was held at -0.2 V and 0.3 V for 3 cycles of 5, 2, 1, 0.5 seconds, and the absorbance was measured at 400 nm (Figure 2-16). The switching time between the neutral, colorless polymer film and the dicationic, marigold-colored **PDA-6**$^{2+}$ is 1.8 seconds. The switching time between the neutral, colorless polymer film and the green-colored **PDA-6**$^{+\bullet}$ is 0.9 seconds. These are typical values for fast, electrochromic polymers. The slower switching time to the marigold-colored **PDA-6**$^{2+}$ is likely due to the time it takes to form the **PDA-6**$^{+\bullet}$ before oxidizing further to the dicationic polymer.

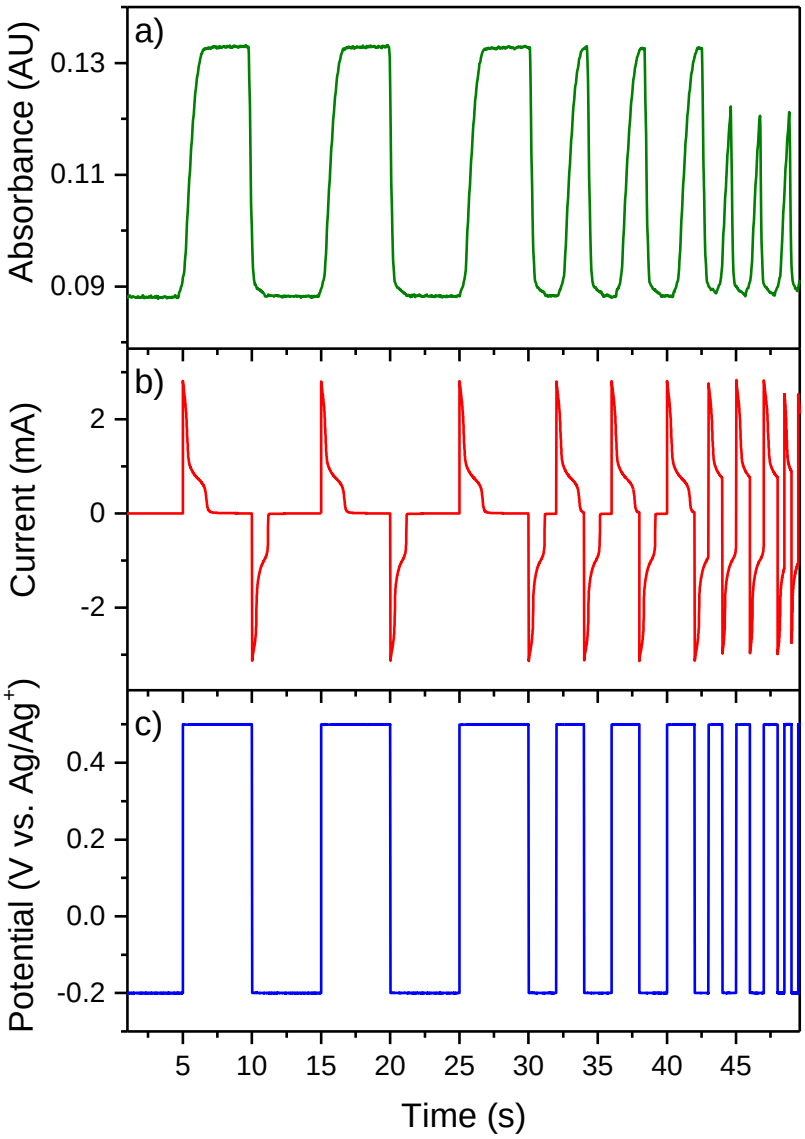

Figure 2-15. Simultaneously acquired (a) absorbance at 469 nm and (b) current measurements at set (c) applied potentials of **PDA-6** deposited onto an ITO electrode in 0.5 M $[NBu_4][PF_6]/CH_3CN$. The switching time between the neutral, colorless polymer film and the dicationic, marigold-colored **PDA-6**$^{2+}$ is 1.8 seconds.

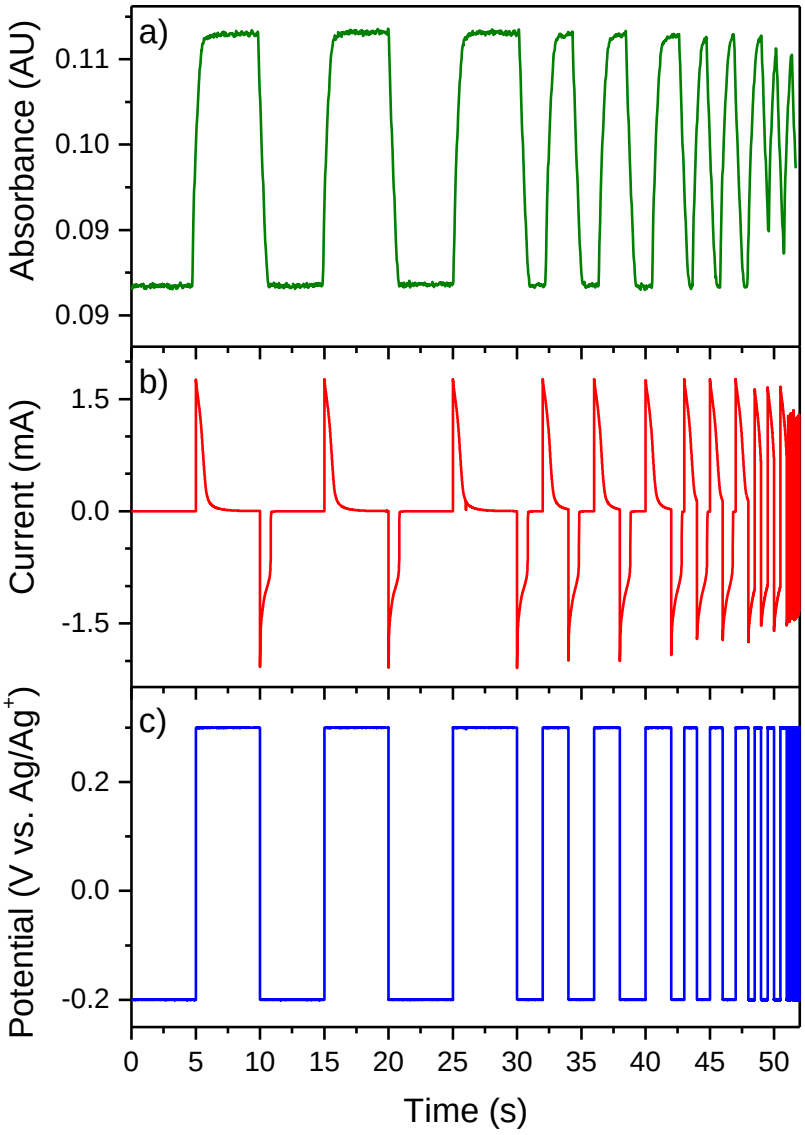

Figure 2-16. Simultaneously acquired (a) absorbance at 400 nm and (b) current measurements at set (c) applied potentials of **PDA-6** deposited onto an ITO electrode in 0.5 M $[NBu_4][PF_6]/CH_3CN$. The switching time between the neutral, colorless polymer film and the green-colored **PDA-6**$^{+\bullet}$ is 0.9 seconds.

Galvanostatic Cycling

Galvanostatic charge-discharge measurements were taken in a three-electrode cell configuration using the modified GCE, a Ag/Ag^+ reference electrode and a Pt wire counter electrode in 0.5 M $[NBu_4][PF_6]/CH_3CN$. Initially, a CV at 10 mV s^{-1} of the electrode was taken between −0.3–0.2 V to determine the amount of charge (capacity) stored for the initial one-electron process (charge of reduction peak). Then, the applied current was calculated to obtain the desired C-rate. The |applied current| was the same for charging and discharging, unless specified otherwise. The polymer was charged and discharged in 0.5 M $[NBu_4][PF_6]/CH_3CN$ between −0.1–0.5 V.

$$\text{C rate } (h^{-1}) = \frac{\text{applied current } (\mu A)}{\text{capacity } (\mu C)} \quad (3)$$

$$\text{applied current} = \frac{\text{C rate}}{3600} \times \text{capacity} \quad (4)$$

The capacities (mA h g^{-1}) were calculated from galvanostatic cycling experiments using the total charge (mA h) passed during charge/discharge and the approximate mass of the polymer film (w). The mass, w, of the film was calculated by the following equation: $w = h\rho A$. The film thickness, h, was determined by profilometry, the density, ρ, was estimated to be 1.0 g cm^{-3}, and the area, A, of the GCE was 0.0707 cm^2. The Coulombic efficiency (%) was calculated from the capacity of the film after discharging divided by the capacity from charging.

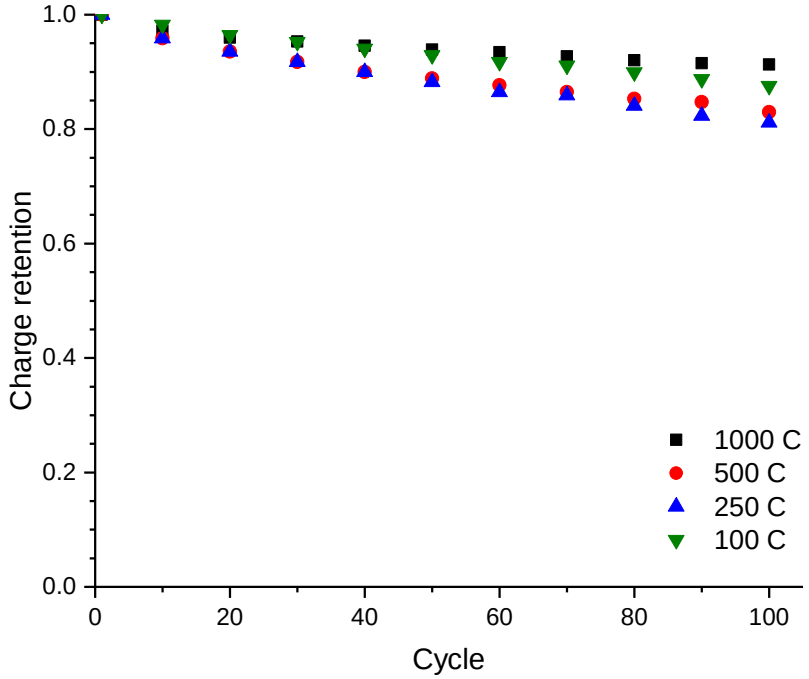

Figure 2-17. Performance of **PDA-6** films cycled at various C rates over 100 cycles. The polymer films on GCE were galvanostatically charged and discharged in 0.5 M $[NBu_4][PF_6]/CH_3CN$ between −0.1–0.5 V. The |applied current| was the same for the charge and discharge except for 100 C which was charged at 1000 C and discharged at 100 C.

The cycling rate performance of **PDA-6** was examined using galvanostatic cycling at four different C rates over 100 cycles (Figure 2-17). The film retained over 80% of its initial capacity after 100 cycles at all four cycling rates. The best charge retention (92%) is at the highest cycling rate of 1,000 C, which takes 3.6 seconds to complete a charging or discharging cycle. Figure 2-17 shows that **PDA-6** has good cycling performance at various high C rates.

2-7. ^{1}H and ^{13}C NMR Spectra
N,N′-Dimethyl-*N,N′*-diphenylethylenediamine (DA-2)

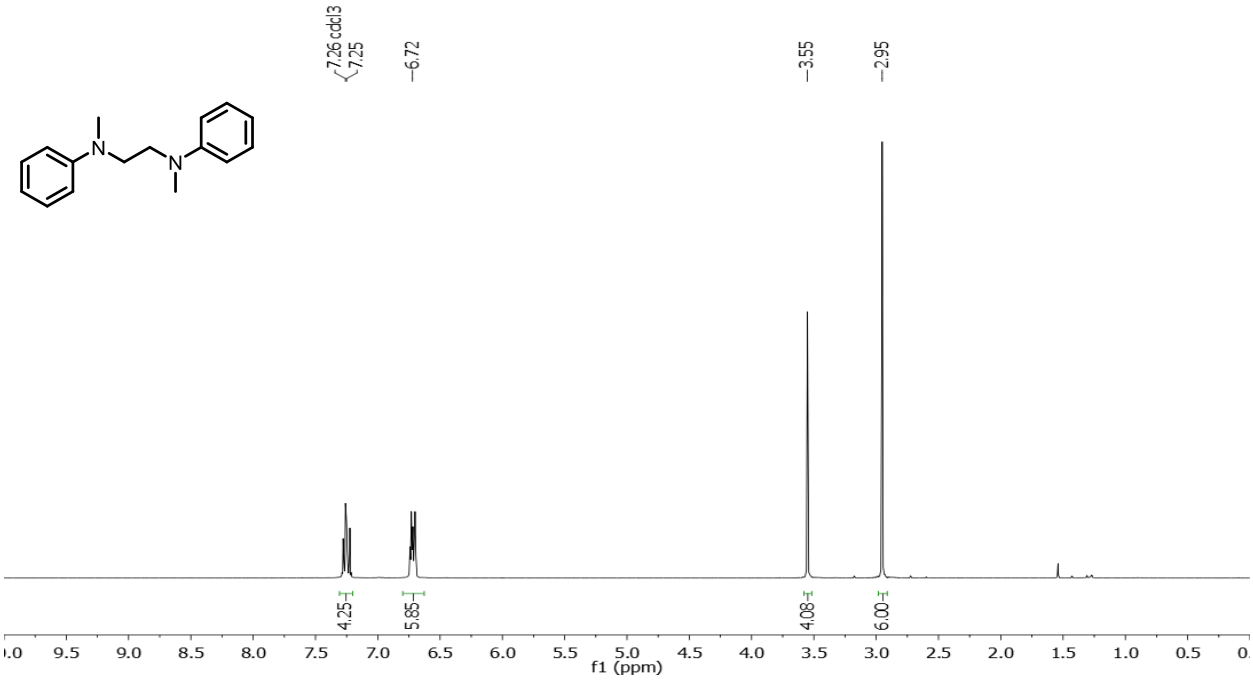

Figure 2-18. ^{1}H NMR spectrum (400 MHz, $CDCl_3$) of *N,N′*-dimethyl-*N,N′*-diphenylethylenediamine (**DA-2**).

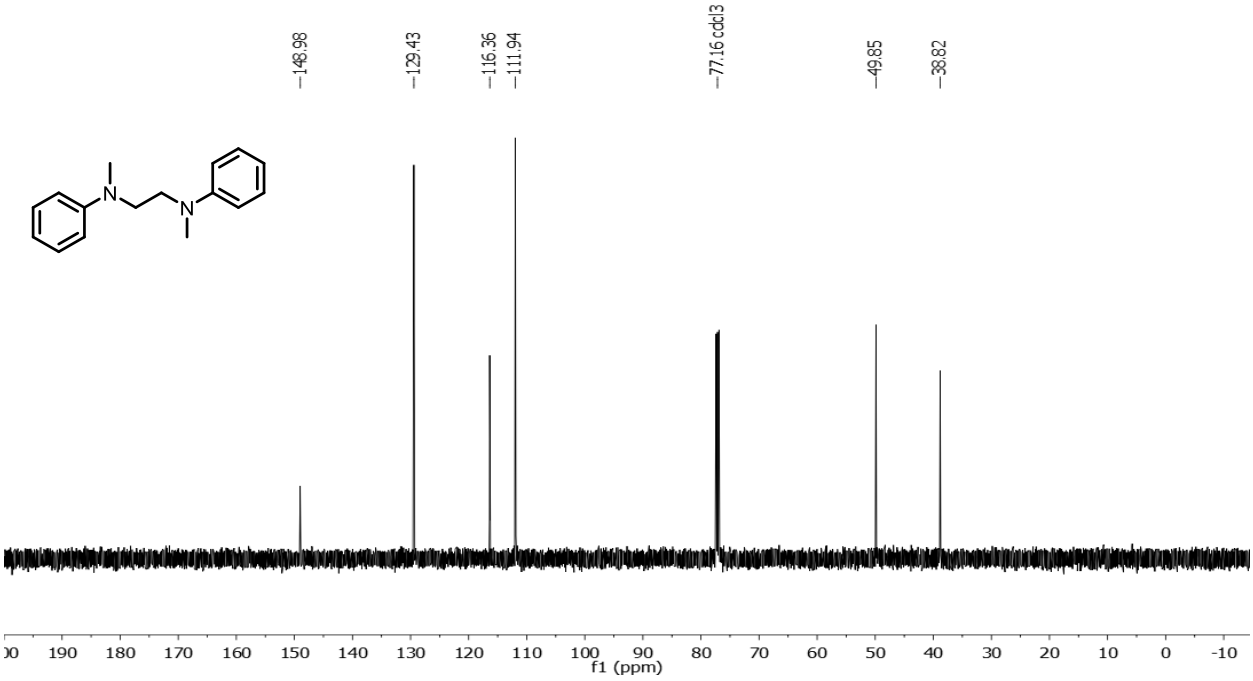

Figure 2-19. ^{13}C NMR spectrum (125 MHz, $CDCl_3$) of *N,N′*-dimethyl-*N,N′*-diphenylethylenediamine (**DA-2**).

***N,N′*-Dimethyl-*N,N′*-diphenyl-1,3-propanediamine (DA-3)**

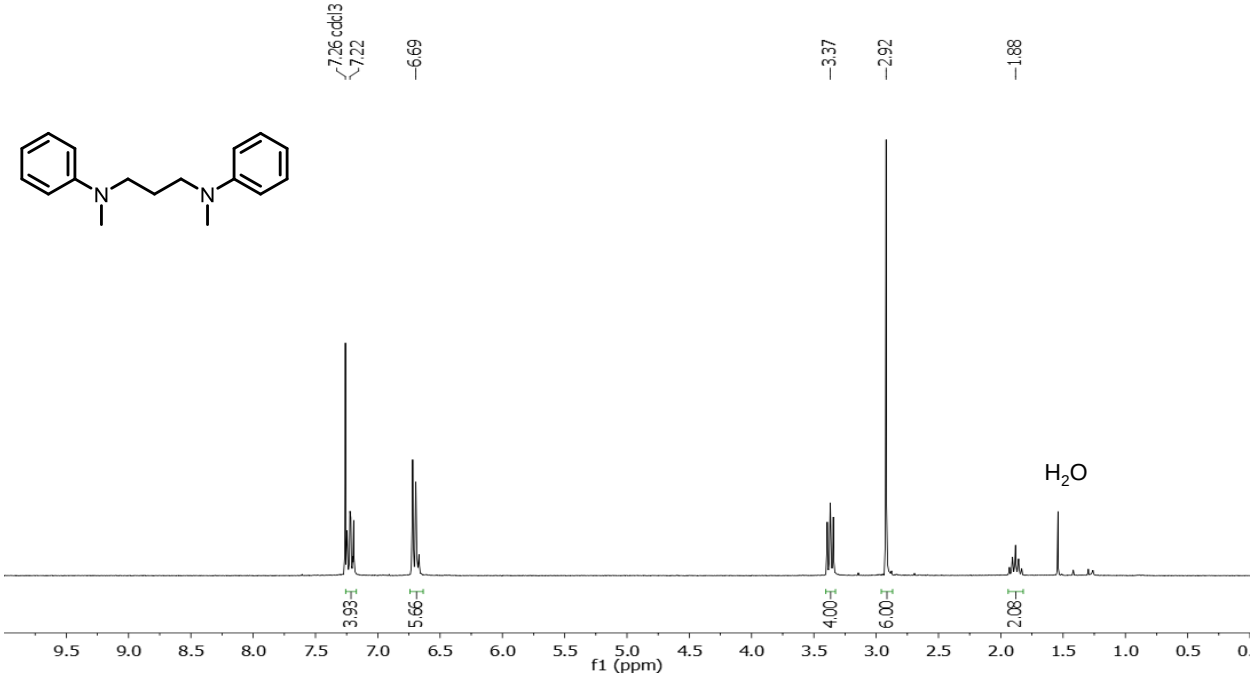

Figure 2-20. ^{1}H NMR spectrum (400 MHz, $CDCl_3$) of *N,N′*-dimethyl-*N,N′*-diphenyl-1,3-propanediamine (**DA-3**).

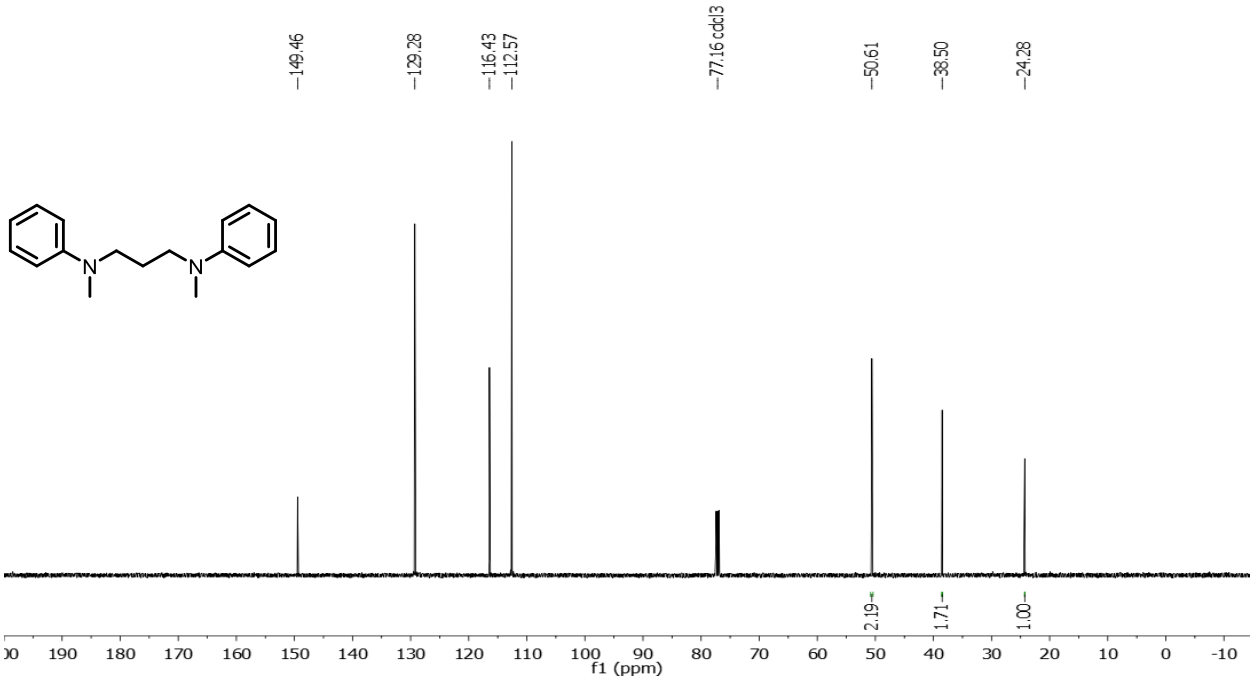

Figure 2-21. ^{13}C NMR spectrum (125 MHz, $CDCl_3$) of *N,N′*-dimethyl-*N,N′*-diphenyl-1,3-propanediamine (**DA-3**).

***N,N′*-Dimethyl-*N,N′*-diphenyl-1,4-butanediamine (DA-4)**

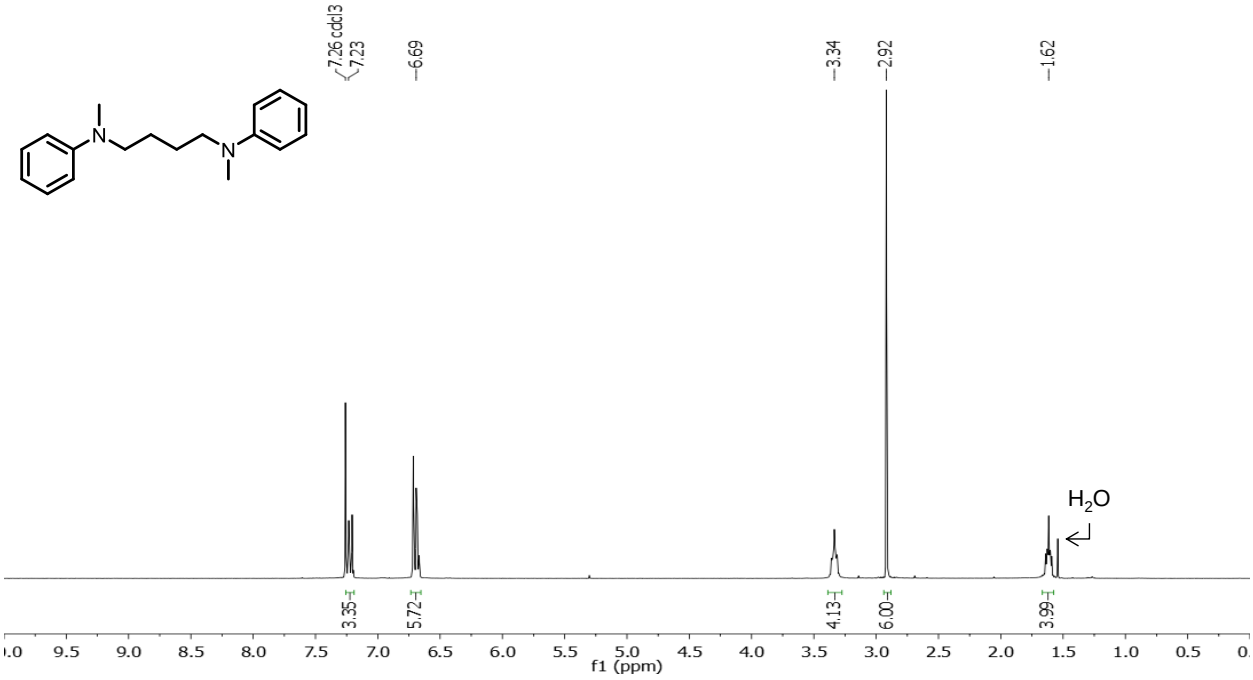

Figure 2-22. ^{1}H NMR spectrum (400 MHz, $CDCl_3$) of *N,N′*-dimethyl-*N,N′*-diphenyl-1,4-butanediamine (**DA-4**).

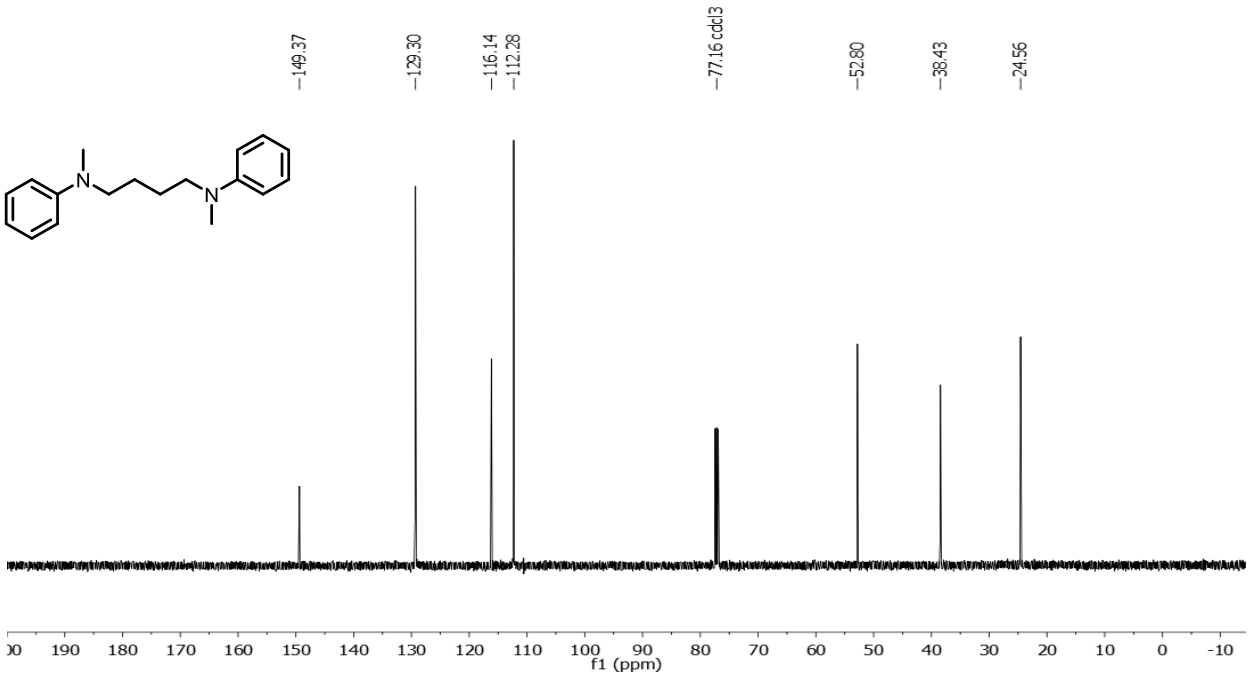

Figure 2-23. ^{13}C NMR spectrum (125 MHz, $CDCl_3$) of *N,N′*-dimethyl-*N,N′*-diphenyl-1,4-butanediamine (**DA-4**).

***N,N′*-Dimethyl-*N,N′*-diphenyl-1,6-hexanediamine (DA-6)**

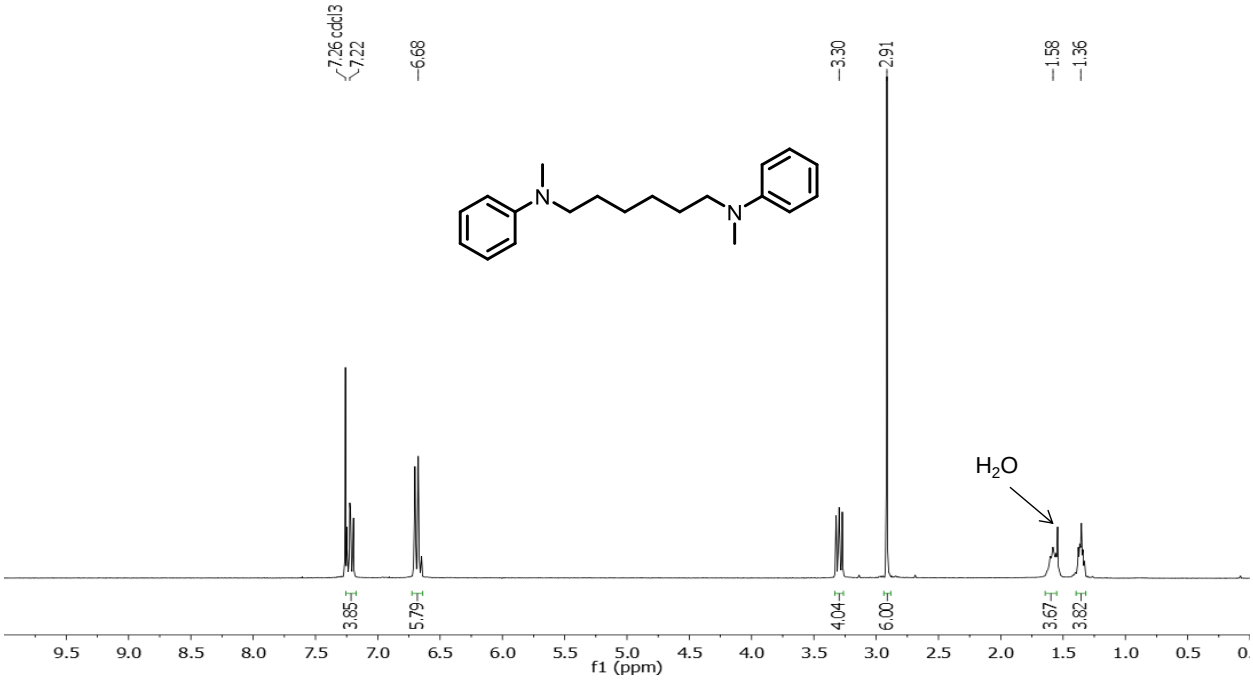

Figure 2-24. ^{1}H NMR spectrum (400 MHz, $CDCl_3$) of *N,N′*-dimethyl-*N,N′*-diphenyl-1,6-hexanediamine (**DA-6**).

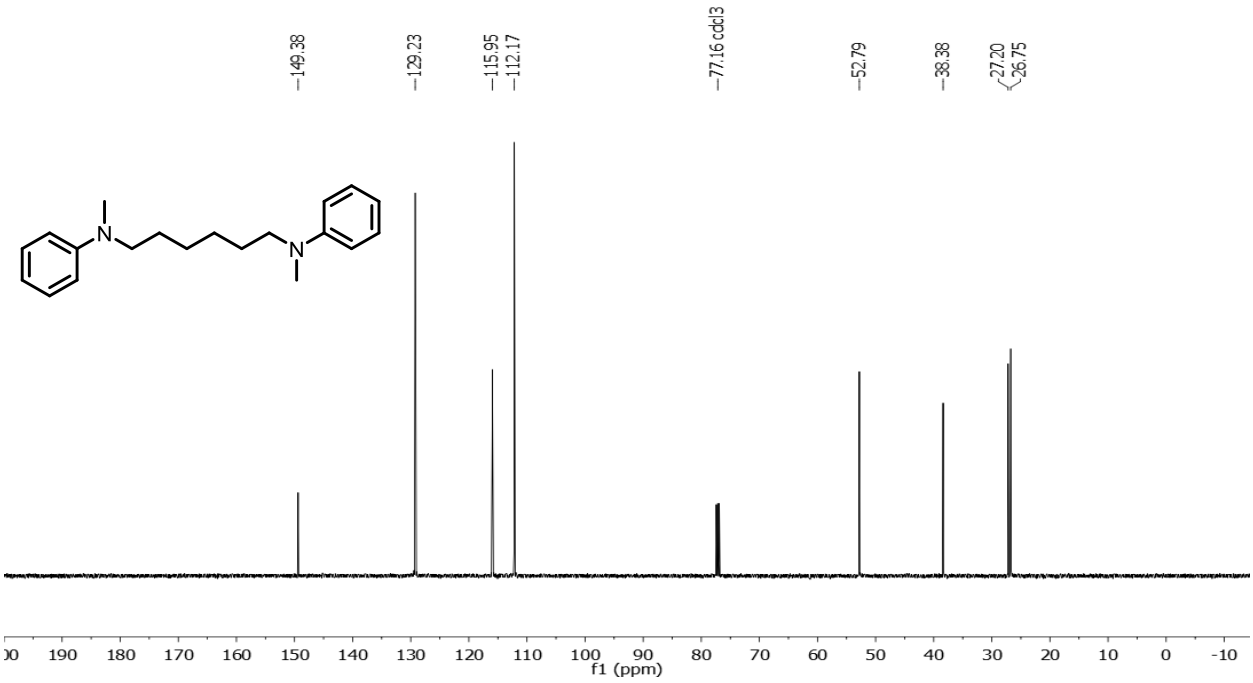

Figure 2-25. ^{13}C NMR spectrum (125 MHz, $CDCl_3$) of *N,N′*-dimethyl-*N,N′*-diphenyl-1,6-hexanediamine (**DA-6**).

***N*-Methyl-*N′*-[2-(methylphenylamino)ethyl]-*N*,*N′*-diphenyl-1,2-ethanediamine (TA-2)**

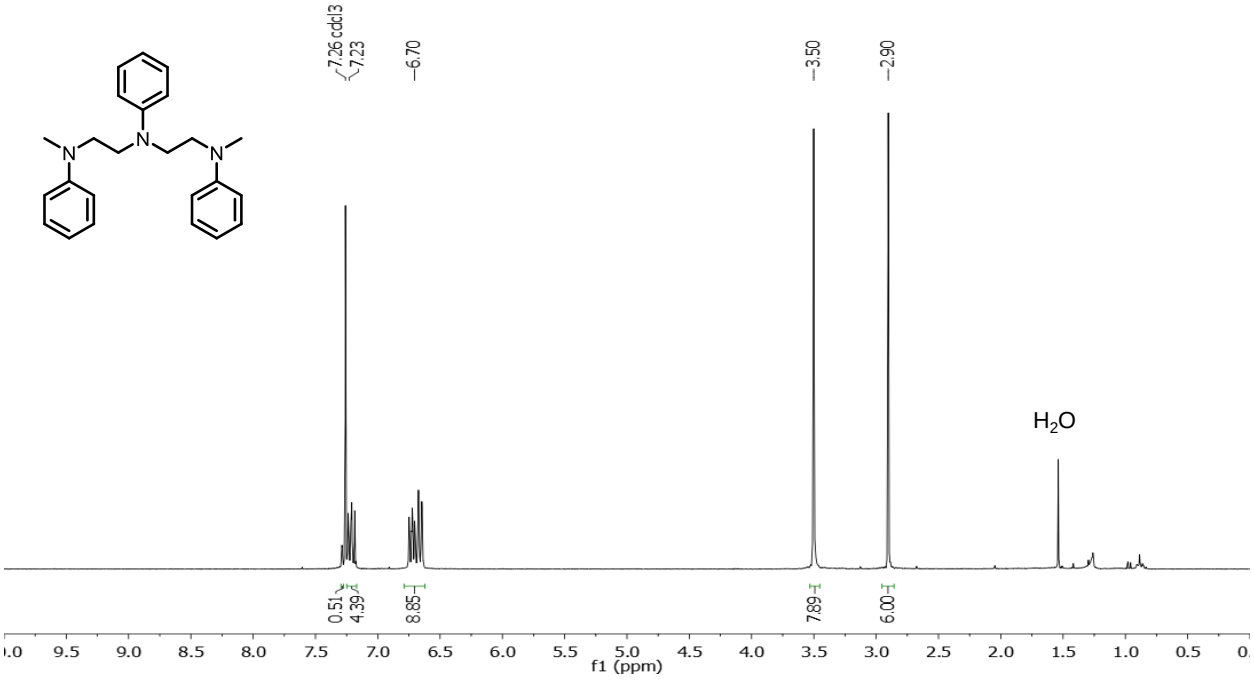

Figure 2-26. ^{1}H NMR spectrum (400 MHz, $CDCl_3$) of *N*-methyl-*N′*-[2-(methylphenylamino)ethyl]-*N*,*N′*-diphenyl-1,2-ethanediamine (**TA-2**).

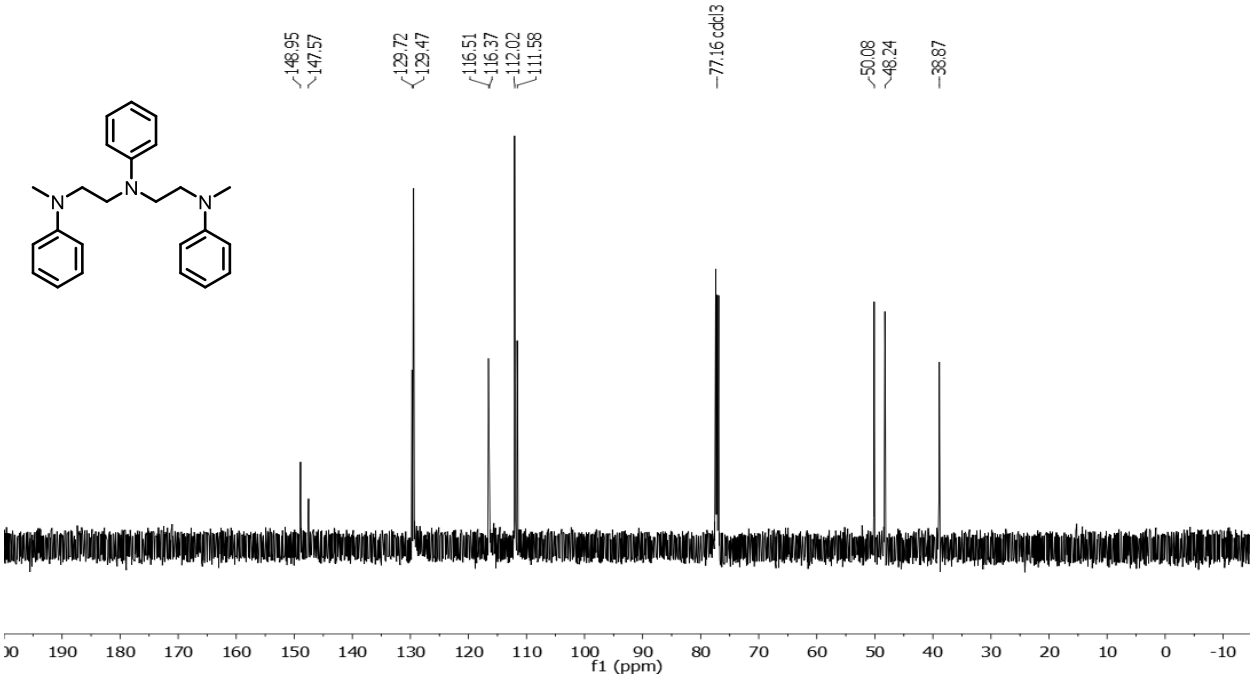

Figure 2-27. ^{13}C NMR spectrum (125 MHz, $CDCl_3$) of *N*-methyl-*N′*-[2-(methylphenylamino)ethyl]-*N*,*N′*-diphenyl-1,2-ethanediamine (**TA-2**).

***N*-Methyl-*N′*-[6-(methylphenylamino)hexyl]-*N*,*N′*-diphenyl-1,6-hexanediamine (TA-6)**

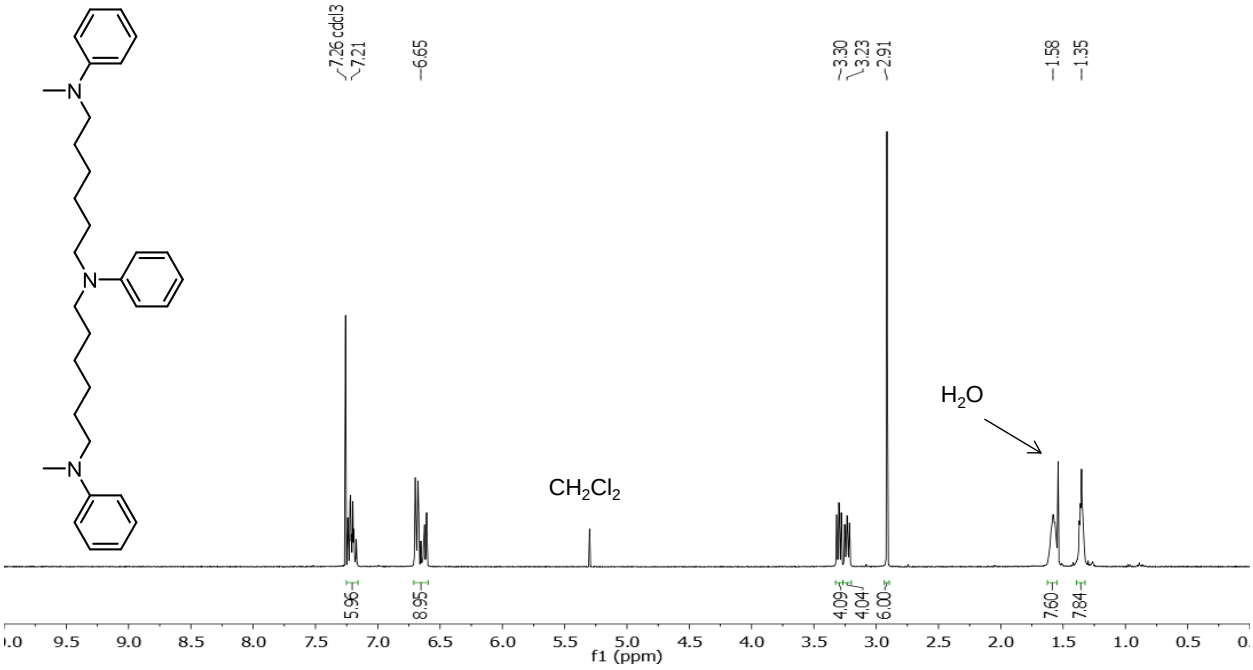

Figure 2-28. ^{1}H NMR spectrum (400 MHz, $CDCl_3$) of *N*-Methyl-*N′*-[6-(methylphenylamino)hexyl]-*N*,*N′*-diphenyl-1,6-hexanediamine (**TA-6**).

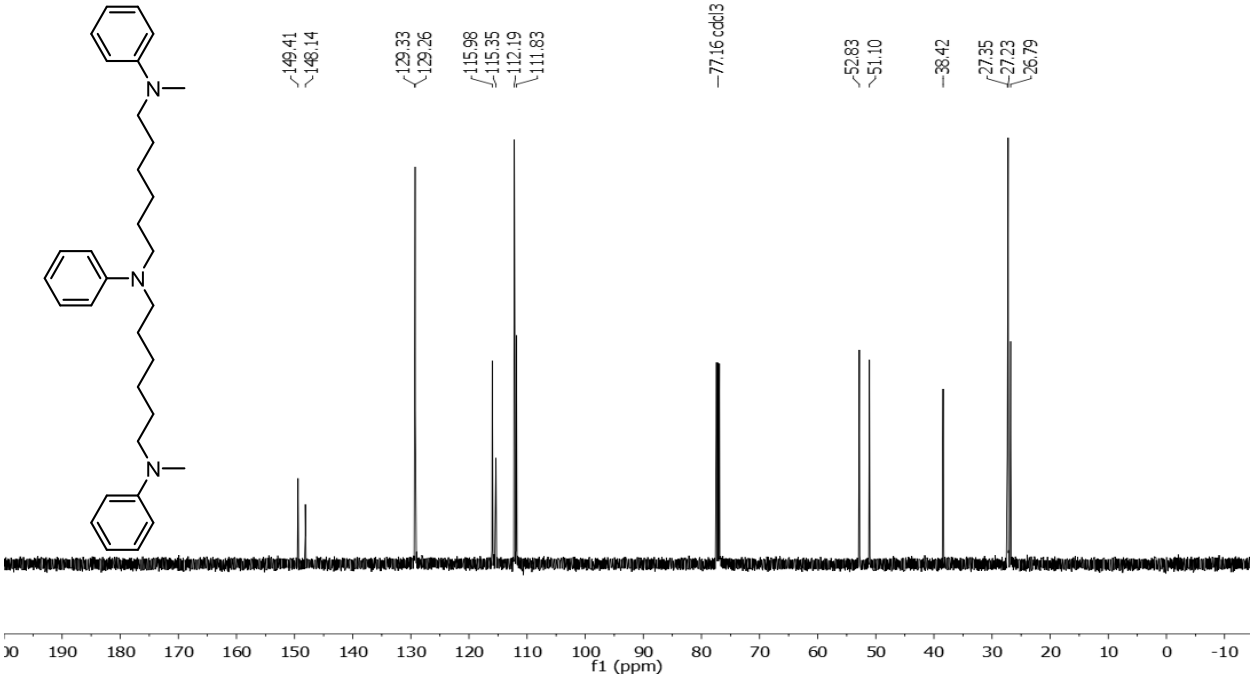

Figure 2-29. ^{13}C NMR spectrum (125 MHz, $CDCl_3$) of *N*-Methyl-*N′*-[6-(methylphenylamino)hexyl]-*N*,*N′*-diphenyl-1,6-hexanediamine (**TA-6**).

REFERENCES

(1) Armand, M.; Tarascon, J. M. *Nature* **2008**, *451*, 652-657.

(2) Goodenough, J. B.; Abruña, H. D.; Buchanan, M. V. *Basic Research Needs for Electrical Energy Storage. Report of the Basic Energy Sciences Workshop on Electrical Energy Storage*, 2007.

(3) Goodenough, J. B.; Kim, Y. *Chem. Mater.* **2009**, *22*, 587-603.

(4) Scrosati, B.; Garche, J. *J. Power Sources* **2010**, *195*, 2419-2430.

(5) Tarascon, J. M.; Armand, M. *Nature* **2001**, *414*, 359-367.

(6) Larcher, D.; Tarascon, J. M. *Nat. Chem.* **2015**, *7*, 19-29.

(7) Liang, Y.; Tao, Z.; Chen, J. *Adv. Energy Mater.* **2012**, *2*, 742-769.

(8) Nyholm, L.; Nyström, G.; Mihranyan, A.; Strømme, M. *Adv. Mater.* **2011**, *23*, 3751-3769.

(9) Nishide, H.; Oyaizu, K. *Science* **2008**, *319*, 737-738.

(10) Arico, A. S.; Bruce, P.; Scrosati, B.; Tarascon, J.-M.; van Schalkwijk, W. *Nat. Mater.* **2005**, *4*, 366-377.

(11) Nyström, G.; Razaq, A.; Strømme, M.; Nyholm, L.; Mihranyan, A. *Nano Lett.* **2009**, *9*, 3635-3639.

(12) Wang, J.-Z.; Chou, S.-L.; Chen, J.; Chew, S.-Y.; Wang, G.-X.; Konstantinov, K.; Wu, J.; Dou, S.-X.; Liu, H. K. *Electrochem. Commun.* **2008**, *10*, 1781-1784.

(13) Suga, T.; Konishi, H.; Nishide, H. *Chem. Commun.* **2007**, *17*, 1730-1732.

(14) Kim, J.-K.; Scheers, J.; Ahn, J.-H.; Johansson, P.; Matic, A.; Jacobsson, P. *J. Mater. Chem. A* **2013**, *1*, 2426-2430.

(15) Janoschka, T.; Hager, M. D.; Schubert, U. S. *Adv. Mater.* **2012**, *24*, 6397-6409.

(16) Hung, M.-K.; Wang, Y.-H.; Lin, C.-H.; Lin, H.-C.; Lee, J.-T. *J. Mater. Chem.* **2011**, *22*, 1570-1577.

(17) Wang, Y.-H.; Hung, M.-K.; Lin, C.-H.; Lin, H.-C.; Lee, J.-T. *Chem. Commun.* **2011**, *47*, 1249-1251.

(18) Burkhardt, S. E.; Lowe, M. A.; Conte, S.; Zhou, W.; Qian, H.; Rodríguez-Calero, G. G.; Gao, J.; Hennig, R. G.; Abruña, H. D. *Energy Environ. Sci.* **2012**, *5*, 7176-7187.

(19) Conte, S.; Rodríguez-Calero, G. G.; Burkhardt, S. E.; Lowe, M. A.; Abruña, H. D. *RSC Adv.* **2013**, *3*, 1957-1964.

(20) Lowe, M. A.; Kiya, Y.; Henderson, J. C.; Abruña, H. D. *Electrochem. Commun.* **2011**, *13*, 462-465.

(21) Michaelis, L.; Schubert, M. P.; Granick, S. *J. Am. Chem. Soc.* **1939**, *61*, 1981-1992.

(22) Dvořák, V.; Němec, I.; Zýka, J. *Microchem. J.* **1967**, *12*, 324-349.

(23) Ito, A.; Sakamaki, D.; Ino, H.; Taniguchi, A.; Hirao, Y.; Tanaka, K.; Kanemoto, K.; Kato, T. *Eur. J. Org. Chem.* **2009**, *2009*, 4441-4450.

(24) Mizoguchi, T.; Adams, R. N. *J. Am. Chem. Soc.* **1962**, *84*, 2058-2061.

(25) Yang, H.; Wipf, D. O.; Bard, A. J. *J. Electroanal. Chem.* **1992**, *331*, 913-924.

(26) Larumbe, D.; Gallardo, I.; Andrieux, C. P. *J. Electroanal. Chem. Interfacial Electrochem.* **1991**, *304*, 241-247.

(27) Wang, L.; Wang, Q. Q.; Cammarata, V. *J. Electrochem. Soc.* **1998**, *145*, 2648-2654.

(28) Leung, M.-K.; Chou, M.-Y.; Su, Y. O.; Chiang, C. L.; Chen, H.-L.; Yang, C. F.; Yang, C.-C.; Lin, C.-C.; Chen, H.-T. *Org. Lett.* **2003**, *5*, 839-842.

(29) Chandrasekhar, P.; Gumbs, R. W. *J. Electrochem. Soc.* **1991**, *138*, 1337-1346.

(30) Choi, K.; Yoo, S. J.; Sung, Y.-E.; Zentel, R. *Chem. Mater.* **2006**, *18*, 5823-5825.

(31) Denmark, S. E.; Pham, S. M. *J. Org. Chem.* **2003**, *68*, 5045-5055.

(32) Deviínsky, F.; Lacko, I.; Krasnec, L. *Synthesis* **1980**, *1980*, 303-305.

(33) Edwards, M. L.; Prakash, N. J.; Stemerick, D. M.; Sunkara, S. P.; Bitonti, A. J.; Davis, G. F.; Dumont, J. A.; Bey, P. *J. Med. Chem.* **1990**, *33*, 1369-1375.

(34) Larsson, P.-F.; Astvik, P.; Norrby, P.-O. *Beilstein J. Org. Chem.* **2012**, *8*, 1909-1915.

(35) Lennartson, A.; Kokoli, T.; Hakansson, M. *Acta Crystallogr., Sect. E: Struct. Rep. Online* **2005**, *61*, o2904-o2906.

(36) Neigenfink, J.; Martin, A.; Wendel, V.; Abraham, W. *J. Prakt. Chem.* **1998**, *340*, 632-641.

(37) Bard, A. J.; Faulkner, L. R.; 2nd ed.; Wiley: New York, 2001.

(38) Laviron, E. *J. Electroanal. Chem. Interfacial Electrochem.* **1979**, *101*, 19-28.

(39) Paulo, T. d. F.; Diógenes, I. C. N.; Abruña, H. D. *Langmuir* **2011**, *27*, 2052-2057.

CHAPTER THREE

POLYARYLAMINES: ORGANIC CATHODE MATERIALS FOR ELECTROCHEMICAL ENERGY STORAGE

3-1. Introduction

The demand for higher performing electrochemical energy storage (EES) systems for portable electronics, electric vehicles, and grid energy storage has motivated researchers to investigate materials with higher energy and power densities. Organic compounds are a promising class of materials for EES devices, such as batteries and supercapacitors, due to their abundance, light weight, and diverse and tuneable structures.[1,2] Their charge/discharge rates are not kinetically limited by metal ion insertion reactions like many inorganic materials (e.g. $LiCoO_2$), and can thus be used in high power applications. Furthermore, they are sustainable and if derived from biomass, potentially renewable, alternatives to inorganic cathode materials.[3] A strategy to improve the performance of EES devices is to develop better cathode materials since current anode materials have much higher capacities than cathode materials.[4] Low molar mass organic compounds that undergo multiple electron transfer processes at high redox potentials have higher theoretical capacities (>160 mA h g^{-1}) and energy densities (>450 W h kg^{-1}) than commercial inorganic cathode materials, although they have lower volumetric energy densities.[5] Due to the diversity of organic redox-active compounds, there are a variety of types of organic electrode materials that can be applied to EES devices, including conducting polymers, organosulfur compounds, stable radicals, and carbonyl-based compounds.[5-9]

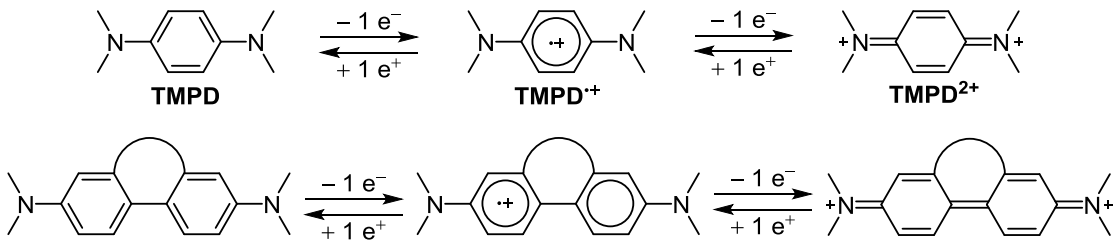

Figure 3-1. Mechanism of redox processes of TMPD and arylamine analogs.

Our group has investigated and tested materials as candidates for cathodes in EES devices.[10-12] We were especially interested in *N,N,N′,N′*-tetramethyl-*p*-phenylenediamine (TMPD) due to its two reversible electron transfers at high redox potentials and low molecular weight.[13,14] The oxidation of TMPD yields the well-known stable radical cation, Wurster's Blue, which can be further oxidized to the quinoidal dication, $TMPD^{2+}$ (Fig. 3-1). We previously anchored TMPD to conductive polymer backbones to mitigate the dissolution of active material into the electrolyte, and to increase the conductivity of the electrode material.[11] This approach yielded electroactive polymer films directly on conductive substrates but involved optimization of the monomer and multistep synthesis. In the present case, the intent was to develop a modular and simpler process to synthesize polyarylamines in order to study the electrochemical activity of various arylamines for EES applications. The Pd-catalyzed amination reaction couples aryl halides with primary or secondary amines to form arylamines.[15,16] The cross-coupling reaction can also be used to synthesize polymers, such as polytriarylamines and polyanilines.[17-21] This polymerization method allows for facile, modular synthesis of an array of polyarylamines by varying the structure of the aryl halide and amine monomers (Fig. 3-2).

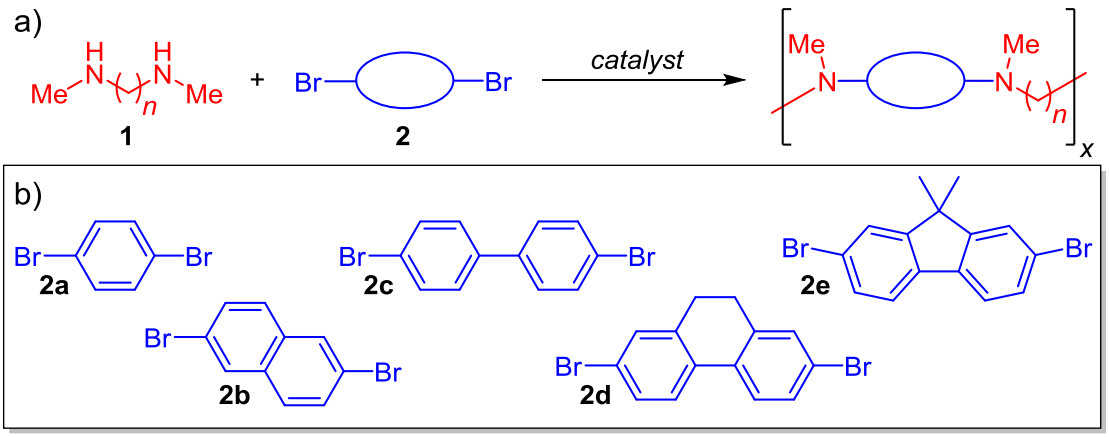

Figure 3-2. a) Pd-catalyzed polycondensation of diamines with dibromoarenes. b) Dibromoarenes investigated in this work.

Four factors must be taken into account when designing organic cathode materials. First, the capacity of a material is inversely proportional to its molar mass (of the repeat unit for polymers). Second, the electron transfer processes should be at high redox potentials (>3.0 V vs. Li/Li^+) to maximize energy densities. Third, the materials should exhibit fast charge transfer kinetics thus enabling high C-rate operation. Finally, the material should have high charge retention and Coulombic efficiency with cycling. With these parameters in mind, we were interested in developing polyarylamines with good cycling performance, and theoretical capacities and energy densities competitive with commercial EES devices. Polytriphenylamine and its derivatives have been explored as electrode materials due to their reversible redox processes at ~3.6 V (vs. Li) but these polymers have low theoretical capacities (<130 mA h g^{-1}).[22-24] Herein we report a Pd-catalyzed polycondensation of dibromoarenes with secondary acyclic, aliphatic diamines to synthesize redox-active polyarylamines with theoretical capacities between 160-330 mA h g^{-1}. To the best of our knowledge, these are the first reported Pd-catalyzed cross-coupled polymers using acyclic, aliphatic amines.

3-2. Results and Discussion

Initially, we focused on optimizing the synthesis and electrochemical activity of the polymers by varying the alkyl length of diamines **1** (Table 3-1). Using dibromobenzene, **2a**, we obtained four polymers with different alkyl spacers between the redox-active phenylenediamine groups. As the alkyl length increased from ethylene to hexamethylene, the theoretical capacity decreased from 330 to 245 mA h g^{-1} for the phenylenediamine polymers. The $Pd_2(dba)_3$/ 2-dicyclohexylphosphino-2′-(*N,N*-dimethylamino)biphenyl (DavePhos) catalytic system afforded low molecular weight polymers in good yield. It was challenging to obtain high molecular weight polymers because of the step-growth nature of the polycondensation reaction, and the propensity for acyclic secondary amines to *β*-hydride eliminate and terminate the growing polymer chain.[15] Higher molecular weight polymers have been reported using aromatic amines,[18-20] or cyclic amines.[17] Kanbara and co-workers were unsuccessful in their attempts to synthesize polymers using acyclic amines.[17] By using the biaryl phosphine ligand, DavePhos, we were able to obtain polymers, which are, to the best

Table 3-1. Pd-catalyzed polycondensation of alkyldiamines with dibromobenzene.

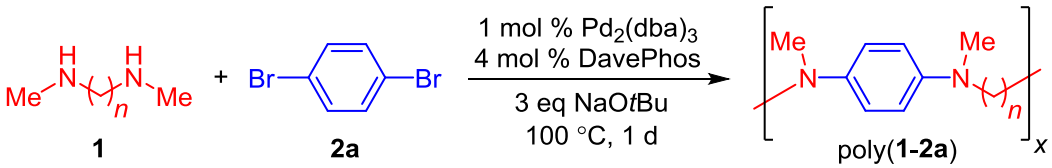

1 **2a** poly(**1-2a**)

Entry[a]	**1**	Theoretical Capacity (mA h g^{-1})	Isolated yield[b] (%)	M_n[c] (kDa)	M_w/M_n[c]
1	**1a** (n = 2)	330	61	n.d.[d]	n.d.[d]
2	**1b** (n = 3)	304	73	1.3	1.2
3	**1c** (n = 4)	282	76	1.1	1.1
4	**1d** (n = 6)	245	81	2.3	1.5

[a] Polymerizations were run at 0.27 M concentration in toluene. [b] Determined after precipitating the polymer in MeOH. [c] Determined by gel permeation chromatography in THF at 30 °C, calibrated with polystyrene standards. [d] Not determined due to low solubility in THF.

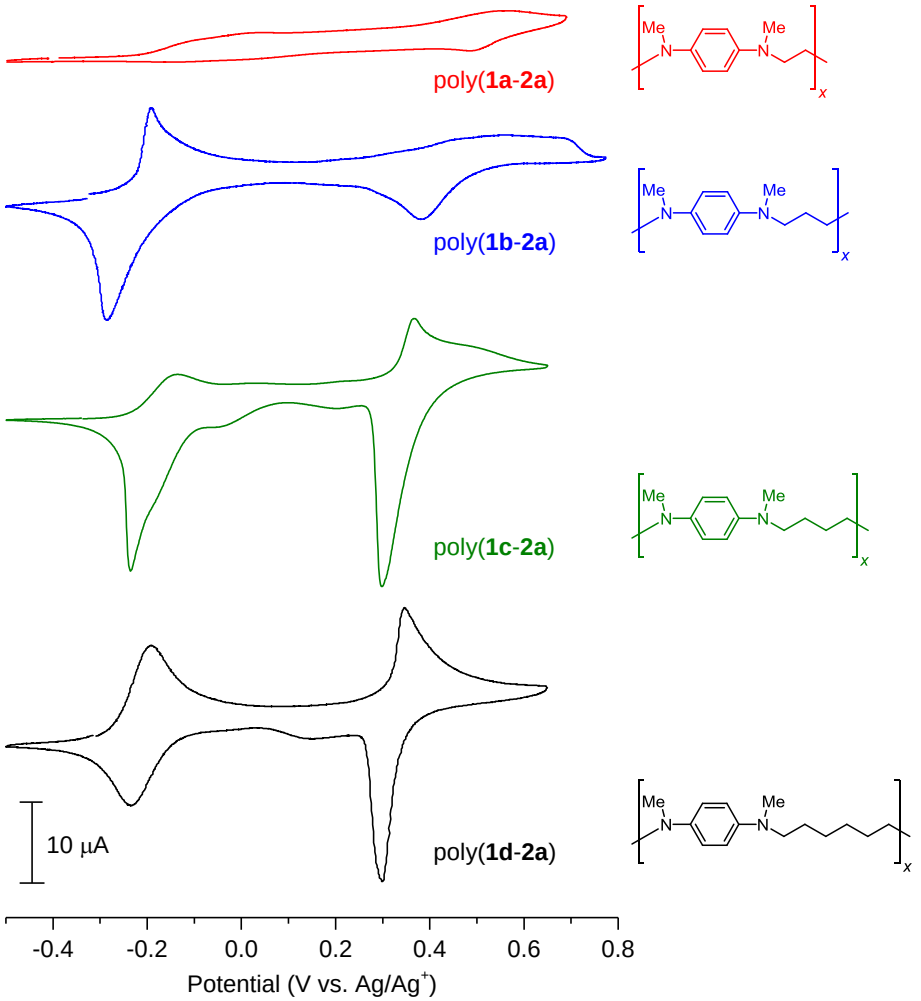

Figure 3-3. Cyclic voltammograms (CV) of poly(**1-2a**) in 0.1 M $[NBu_4][ClO_4]$ in CH_2Cl_2 at 20 mV s^{-1}. All CVs on 10 μA scale.

of our knowledge, the first reported Pd-catalyzed polycondensation products using acyclic, aliphatic amines.

Fig. 3-3 shows the cyclic voltammograms (CV) of the phenylenediamine polymers, poly(**1-2a**), at 2 mM concentration in repeat unit, in 0.1 M $[NBu_4][ClO_4]/CH_2Cl_2$. The length of the alkyl spacer between arylamine groups significantly affected the electrochemical response of the polymers. The polymer with an 1,2-ethylene linker, poly(**1a-2a**), did not display the two well-defined and reversible redox waves expected for a TMPD-containing polymer. Instead, it exhibited

two small irreversible processes at −75 mV and 524 mV, respectively. Fig. 3-3 shows that as the alkyl linker increased from ethylene to hexamethylene, the corresponding polymer displayed better resolved redox processes. The first redox couple for poly(**1b-2a**) is reversible at −142 mV, and the second redox couple exhibited a broad oxidation peak that is indicative of more complex processes than a simple one-electron transfer. The reductive sweep exhibited two well-resolved peaks at peak potential values of 381 mV and −284 mV, respectively. The morphology of these peaks is typical of a "stripping-type" response, suggesting that the oxidation of the polymer to charged species resulted in the precipitation of a polymer film on the electrode surface, in a way reminiscent of the behavior of poly(vinylferrocene).[25,26] Both the tetramethylene- and hexamethylene-linked phenylenediamine polymers displayed two redox couples with sharp reduction peaks, again reminiscent of poly(vinylferrocene) behavior. The formal potentials for both processes shifted negative as the alkyl linker increased in length, indicating that the phenylenediamine polymers are more stable when the redox-active TMPD groups are separated by a longer distance. This trend suggests that the irreversible response for poly(**1a-2a**) is likely due to repulsive interactions between TMPD moieties in the polymer. These findings agree with the electrochemical responses of electropolymerized benzidine polymer films with different spacers.[12] Poly(**1d-2a**) displayed the most reversible redox processes with the smallest peak to peak separations (ΔE_p). From these studies, we determined that arylamines should be separated by hexamethylene linkers to obtain the best well-defined and reversible redox responses.

Previous studies by Michaelis[13] on Wurster's salts, and Roberts[27] on polycyclic aromatics established that resonance delocalization and coplanarity of the molecules are important factors in stabilizing arylamine radical cations. The cycling performance of the electrode material is critical for EES applications, and better capacity retention

can often offset a lower capacity. We investigated the electrochemical performance of extended aryl systems that can undergo analogous redox processes to the TMPD-containing polymers (Fig. 3-1). Four polycyclic arylamine polymers were synthesized in good yield (Table 3-2). As expected, the theoretical capacities of the polymers decreased for these polymers (160-200 mA h g^{-1}) relative to those described above for the dibromobenzene derivatives. However, some of the redox processes shifted to higher potentials (*vide infra*).

Fig. 3-4 shows the CVs of poly(**1d-2**), at 4 mM concentration in repeat unit, in 0.1 M $[NBu_4][ClO_4]/CH_2Cl_2$. All of the polymers exhibited the anticipated two reversible, one-electron redox couples. As was the case for poly(**1-2a**), the voltammetric profiles were typical of processes that involve polymer deposition upon oxidation and stripping upon subsequent reduction. The two waves were spaced at least 450 mV apart for the phenylenediamine and naphthalenediamine polymers, poly(**1d-2a**) and poly(**1d-2b**), respectively. The difference between the formal

Table 3-2. Pd-catalyzed polycondensation of hexamethylenediamine with dibromoarenes.

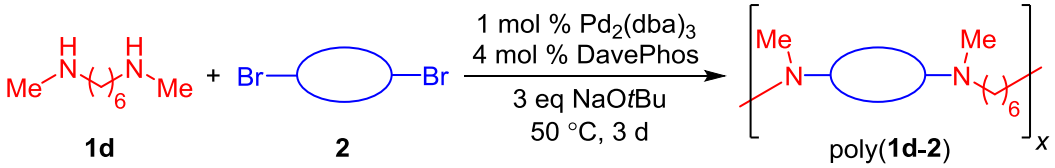

1d **2** poly(**1d-2**)

Entry[a]	**2**	Theoretical Capacity (mA h g^{-1})	Isolated yield[b] (%)	M_n[c] (kDa)	M_w/M_n[c]
1	**2a**	245	89	3.1	3.6
2	**2b**	200	96	2.2	2.0
3	**2c**	182	90	3.1	3.6
4	**2d**	167	96	4.8	6.0
5	**2e**	160	85	11.1	4.8

[a] Polymerizations were run at 0.25 M concentration in toluene. [b] Determined after precipitating the polymer in MeOH. [c] Determined by gel permeation chromatography in 1,1,1,3,3,3-hexafluoro-2-propanol containing 0.01 M tetraethylammonium nitrate, calibrated with poly(methyl methacrylate)standards.

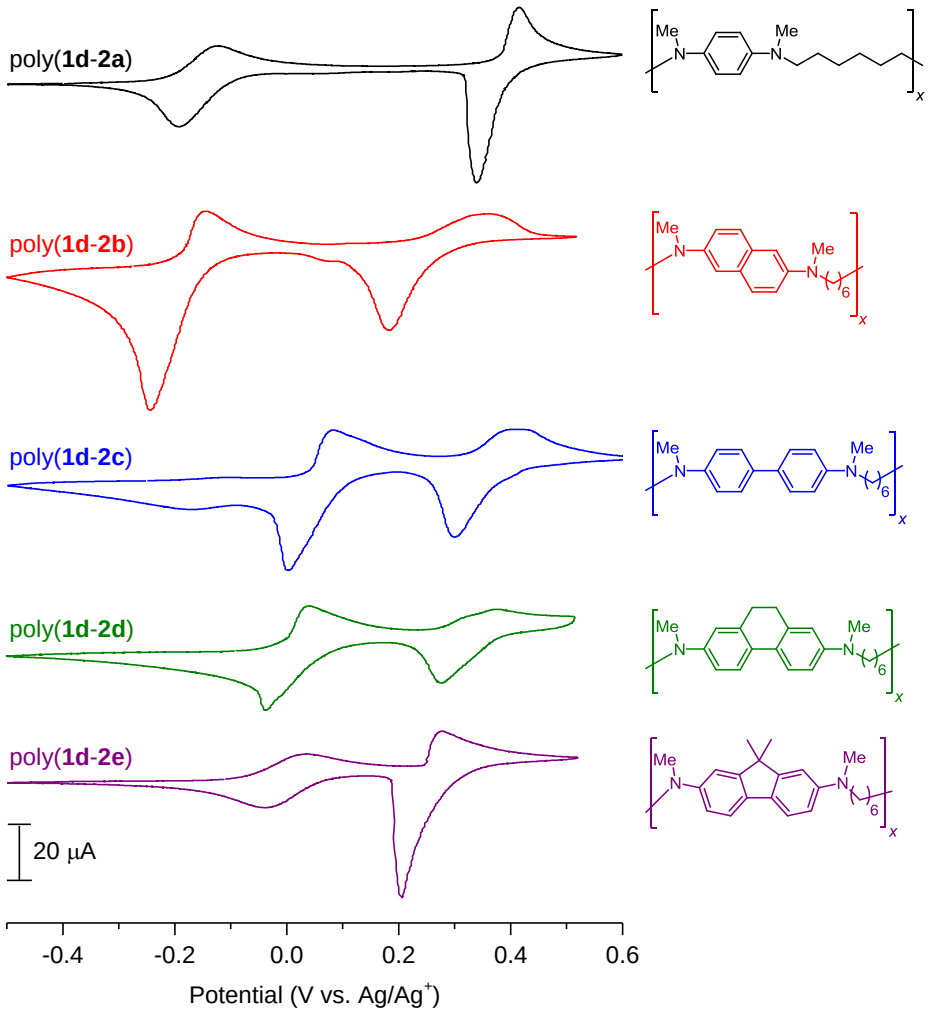

Figure 3-4. Cyclic voltammograms (CV) of poly(**1d-2**) in 0.1 M $[NBu_4][ClO_4]$ in CH_2Cl_2 at 20 mV s^{-1}. All CVs on 10 μA scale.

potentials was smaller, <325 mV, for the other polycyclic arylamine polymers, poly(**1d-2c**/**2d**/**2e**). The formal potentials for the first redox couple shifted positive from −194 mV for the naphthalenediamine-based poly(**1d-2b**) to >−4 mV for these polycyclic arylamine polymers. Positive potential shifts improve the theoretical energy density of the electrode materials as they increase the cell voltage. Recall that for batteries, energy density is the product of capacity and cell voltage. For these polymers, the potentials for both redox couples shifted negative as the aryl group changed from biphenyl to dihydrophenanthrene and to dimethylfluorene. This

negative shift indicates that the latter polymers, with higher molar mass and more constrained structures, are easier to oxidize to the radical cation and dication species.

All of the polymers with two well-defined redox processes generated an electroactive film on the electrode as indicated by sharp reduction peaks. After polymer films were deposited onto electrodes, the electrode was gently rinsed with CH_2Cl_2 to remove electrolyte and soluble polymers. The modified electrodes were subsequently cycled in monomer-free electrolyte to examine their electrochemical cycling performance (Figs. 3-6 – 3-14). Films of poly(**1d-2c**), poly(**1d-2d**), and poly(**1d-2e**) showed good cycling performance, while the rest of the polymers quickly lost half of their initial charge. These results suggested that larger arylamine groups deposited stable, insoluble films onto GCEs. The polycyclic arylamine polymers have lower theoretical capacities than the phenylenediamine polymers, but this effect is offset, at least in part, by the higher redox potentials. In addition, the larger arylamine polymers are more stable with cycling due to the larger delocalization systems for the cation radical and dication species. Based upon those results and the theoretical energy densities of the polymers, we focused on further characterizing the capacity retention of poly(**1d-2c**).

The performance of poly(**1d-2c**) was tested by cycling the polymer film in solvents typically used in practical EES applications. The modified electrode was cycled in 0.5 M $LiBF_4$/solvent. Fig. 3-5b shows that the charge retention of poly(**1d-2c**) is highly dependent on the solvent employed. When cycled in tetraglyme or ethylene carbonate:diethyl carbonate (EC:DEC, v/v = 1:1), the polymer film lost half of its initial capacity after only 5 cycles. However, in 1,3-dioxolane: dimethoxyethane (DOL:DME, v/v = 1:1), the polymer film exhibited a charge retention of 90% after 20 cycles. Initially, the charge increased for the first few cycles. This is likely due to improved polymer-electrolyte interactions which allowed more polymer to be

accessible to undergo electron transfer reactions. After the first few cycles, the charge retention of the polymer film leveled off and the CVs overlapped very well with each other (Fig. 3-5a). The second redox couple exhibited the symmetrical shape and small ΔE_p expected for surface-confined materials.[28]

However, the first oxidation peak was broader and flatter. This response was likely due to the polymer film reorganizing to accommodate for the incorporation of electrolyte and counterions, as well as shifting to a more thermodynamically stable conformation to optimize the delocalization of charge.[29-31] The shape of the first

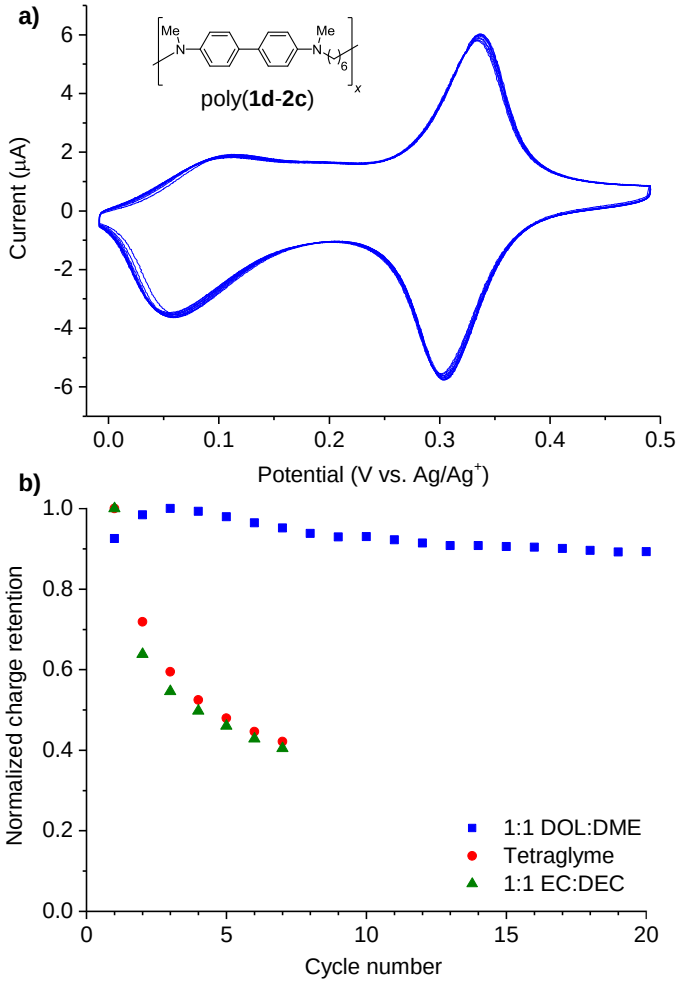

Figure 3-5. a) Ten CV cycles of poly(**1d-2c**) in 0.5 M $LiBF_4$ in 1,3-dioxolane:dimethoxyethane (DOL:DME) at 20 mV s^{-1}. b) The electrochemical cycling of poly(**1d-2c**) in 0.5 M $LiBF_4$ in various solvents at 20 mV s^{-1}.

oxidation peak varied in different solvents, once again emphasizing the importance of electrolyte-polymer interactions on electrochemical performance. In acetonitrile, the first oxidation peak shifted negative by 220 mV in the first few cycles, demonstrating a distinct reorganization/equilibration of the polymer film (Fig. 3-11). While in tetraglyme, the first oxidation peak was a symmetrical wave, matching the second oxidation peak (Fig. 3-12).

3-3. Conclusions

The Pd-catalyzed coupling reaction is a valuable technique to synthesize arylamine polymers. We were able to use acyclic, aliphatic amines to form various redox-active poly(arylamines). The alkyl spacer between arylamine groups had a large effect on the electrochemistry of the polymers, and two redox processes were observed for compounds with propyl or longer linkers. The hexyl-linked phenylenediamine polymers exhibited the most reversible redox processes, and other arylamine polymers were synthesized with this alkyl spacer. Poly(**1d**-**2c**) exhibited two reversible redox reactions at high potentials (>3.3 V vs. Li/Li^+), high theoretical capacity (182 mA h g^{-1}), and good cycling performance in practical EES electrolytes. These polymers are promising candidates for EES, and ongoing work is focused on synthesizing insoluble, redox-active polyarylamines. These initial cycling performance studies demonstrated the promise of arylamine polymers as cathode materials for electrochemical energy storage applications.

3-4. General Considerations

All manipulations of air and water sensitive compounds were carried out under dry nitrogen using a Braun UniLab drybox or standard Schlenk line techniques. ^{1}H NMR spectra were recorded on a Varian INOVA 400 (^{1}H, 400 MHz) and referenced with residual non-deuterated solvent shift ($CHCl_3$ = 7.26 ppm, C_6D_6 = 7.16 ppm). ^{13}C NMR spectra were recorded on Varian INOVA 500 (^{13}C, 125 MHz) spectrometer and referenced to chloroform (77.16 ppm) or benzene (128.06 ppm).

Gel permeation chromatography (GPC) analyses were carried out using an Agilent Technologies PL-GPC 50 Integrated GPC equipped with a UV detector and a refractive index detector as well as a Polymer Laboratories PL-AS RT GPC autosampler. The GPC used two PL gel Mini-MIX C columns (5 micron, 4.6 mm ID). The GPC columns were eluted with tetrahydrofuran at 30 °C at 0.3 mL/min and were calibrated using monodisperse polystyrene standards.

Polymer samples that were partially soluble in tetrahydrofuran were analyzed by Eastman Kodak Company. The polymers were examined using size-exclusion chromatography (SEC) at 40.0 °C in 1,1,1,3,3,3-hexafluoro-2-propanol (HFIP) containing 0.01 M tetraethylammonium nitrate. The GPC used three 8 mm x 300 mm KF-806L column from Shodex calibrated with narrow-molecular-weight distribution poly(methyl methacrylate) (PMMA) standards. The results provided are from a spectrophotometric detector operating at 270 and 320 nm.

Differential scanning calorimetry (DSC) measurements of polymer samples were performed on a Mettler-Toledo Polymer DSC instrument equipped with a chiller and an autosampler. Standard DSC experiments were made in aluminum pans using the following heating program: −70 °C to 200 °C at 10 °C/min, 200 to −70 °C at 10 °C/min, and then −70 °C to 200 °C at 10 °C/min, except as noted. Data was processed

using StarE software. All reported glass and melting temperatures were observed on the second heating cycle.

Electrochemistry experiments were performed at 22 °C using a Hokuto Denko HABF1510m or a Princeton Applied Research VersaSTAT 3 potentiostat. All cyclic voltammetry (CV) measurements were taken in a fritted three compartment cell using glassy carbon electrode (GCE, 3 mm diameter), a large-area Pt counter electrode, and a Ag/Ag^+ (0.05 M $AgClO_4$ and 0.1 M $[NBu_4][ClO_4]$ in CH_3CN) reference electrode. The potential, 0 V, measured using Ag/Ag^+ reference electrode is +3.3 V vs. Li/Li^+.

3-5. Materials

Tris(dibenzylideneacetone)dipalladium(0) ($Pd_2(dba)_3$), DavePhos (2-(dicyclohexylphosphino)-2'-(*N,N*-dimethylamino))-1,1'-biphenyl), and sodium tert-butoxide (NaO*t*Bu) were purchased from Strem and used as received. *N,N′*-Dimethylethylenediamine, *N,N′*-dimethyl-1,3-propanediamine, and *N,N′*-dimethyl-1,6-hexanediamine were purchased from Sigma-Aldrich and distilled from KOH. 1,4-Dibromobenzene was purchased from Sigma-Aldrich and sublimed under vacuum at 50 °C. 2,6-Dibromonaphthalene was purchased from Alfa Aesar and used as received. 4,4′-Dibromobiphenyl was purchased from Aldrich and recrystallized from toluene, and dried under vacuum. 2,7-Dibromo-9,9-dimethyl-9H-fluorene was purchased from TCI America and recrystallized from 5% ethyl acetate in hexanes, and dried under vacuum. 2,7-Dibromo-9,10-dihydrophenanthrene (**2d**)[32] and *N,N′*-Dimethyl-1,4-butanediamine (**1c**)[12] were prepared according to literature procedures.

HPLC grade toluene was purchased from Fischer Scientific and dried over an alumina column. Tetrabutylammonium perchlorate was purchased from TCI America and recrystallized twice from ethyl acetate and dried under vacuum. All other reagents were purchased from commercial sources and used as received.

Representative Polycondensation Procedure A (Table 3-1)

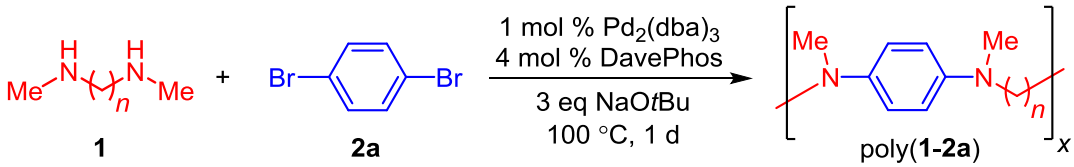

In the glovebox, $Pd_2(dba)_3$ (1 mol %), DavePhos (4 mol %), NaO*t*Bu (3 equiv), and dibromobenzene **2a** (1.1 equiv) were added to a 20-mL vial equipped with a magnetic stir bar. Then toluene (0.27 M in diamine) was added, followed by diamine **1** (1.0 equiv). The vial was sealed with a Teflon-lined cap, removed from the glovebox, and heated in an oil bath set at 100 °C for 1 day. After removal from the oil bath, the cooled mixture was added dropwise to MeOH. The precipitate was isolated by filtration and the polymer was dried under vacuum.

Table 3-3. Polymerization of alkyldiamines with dibromobenzene.

Entry	1	Theoretical Capacity (mA h g^{-1})	Isolated yield[a] (%)	M_n[b] (kDa)	M_w/M_n[b]
1	**1a** (n = 2)	330	61	n.d.[c]	n.d.[c]
2	**1b** (n = 3)	304	73	1.3	1.2
3	**1c** (n = 4)	282	76	1.1	1.1
4	**1d** (n = 6)	245	81	2.3	1.5

[a] Determined after precipitating the polymer in MeOH. [b] Determined by gel permeation chromatography in THF at 30 °C, calibrated with polystyrene standards. [c] Not determined due to low solubility in THF.

Optimization of Polymerization

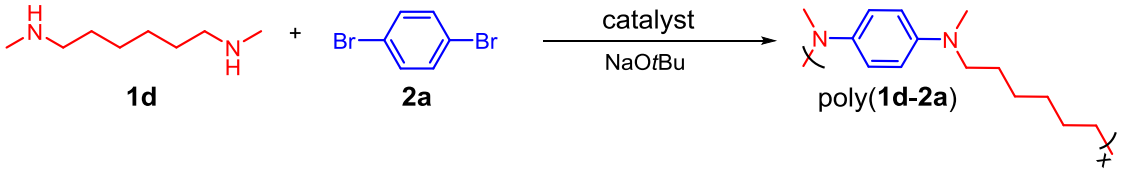

Table 3-4. Optimization of the polycondensation of poly(**1d-2a**).

Entry[a]	Catalyst	Temperature (° C)	Time (d)	Solvent	Isolated Yield[b] (%)	M_n[c] (kDa)	M_w/M_n[c]
1	**A**	100	1	toluene	0	-	-
2	**B**	100	1	toluene	70	2.3	1.5
3	**B**	50	1	toluene	0	-	-
4	**B**	50	3	toluene	89	2.9	1.7
5	**B**	50	6	toluene	93	4.2	2.0
6[d]	**B**	50	6	toluene	86	2.2	1.9
7[e]	**B**	50	6	toluene	67	1.2	1.5
8	**C**	50	10	toluene	0	-	-
9	**C**	50	4	THF	0	-	-
10	**C**	80	4	THF	77	1.5	1.8
11	**D**	80	4	THF	78	1.6	2.0

[a] Polymerization conditions: 1.1 eq dibromobenzene, 1.0 eq diamines, 2.8 eq NaO*t*Bu, solvent (0.27 M in diamine). [b] Determined after precipitating the polymer in MeOH. [c] Determined by gel permeation chromatography in THF at 30 ° C, calibrated with polystyrene standards. [d] 0.17 M in diamine. [e] 0.09 M in diamine.

A: 1 mol % $Pd[P(o\text{-tolyl})_3]_2Cl_2$, 4 mol % $P(o\text{-tolyl})_3$

B: 1 mol % $Pd_2(dba)_3$, 4 mol % DavePhos

C: 1 mol % DavePhos Pd G3, 1 mol % DavePhos

D: 1 mol % RuPhos Pd G3, 1 mol % RuPhos

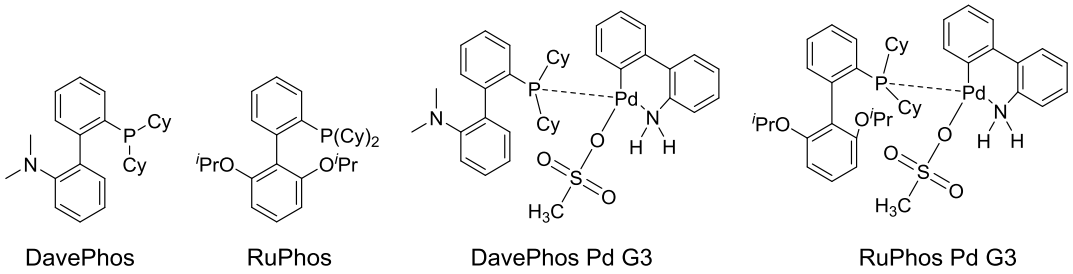

After the initial electrochemical studies on poly(**1-2a**), optimization of the polycondensation of poly(**1d-2a**) was performed to obtain higher molecular weight polymers (Table 3-4). Entry 4 gave the best results for the polycondensation of poly(**1d-2a**) but due to the lower solubility of poly(**1d-2**), they were ran under the conditions of entry 3.

Representative Polycondensation Procedure B (Table 3-2)

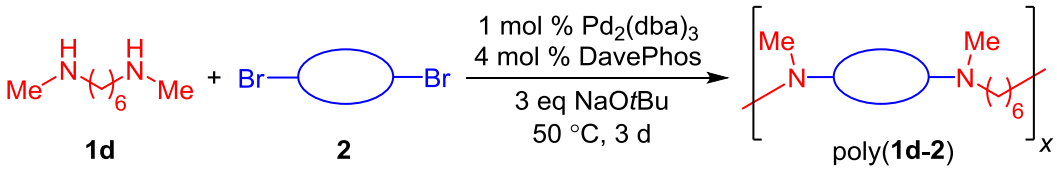

1d **2** poly(**1d-2**)

In the glovebox, $Pd_2(dba)_3$ (1 mol %), DavePhos (4 mol %), NaO*t*Bu (3 equiv.), and dibromoarene **2** (1.1 equiv.) were added to a 20-mL vial equipped with a magnetic stir bar. Then toluene (0.27 M in diamine) was added and the mixture was stirred for at least 2 minutes. Finally, diamine **1d** (1.0 equiv.) was added in. The vial was sealed with a Teflon-lined cap, removed from the glovebox, and heated in an oil bath set at 50 °C for 3 days. After removal from the oil bath, the cooled mixture was added dropwise to MeOH. The precipitate was isolated by filtration and the polymer was dried under vacuum.

Molecular weight was not determined for poly(**1d-2**) due to their poor solubility in THF.

3-6. Electrochemical Measurements

Cyclic Voltammetry (CV) & Chronoamperometry

CV and chronoamperometry measurements were taken in a three-electrode cell configuration using 3 mm diameter GCE working electrode, Ag/Ag^+ reference electrode and coiled Pt wire counter electrode in separate compartments connected by medium porosity glass frits. The GCE were polished with 1.0 μm, 0.3 μm, and 0.05 μm alumina (EXTEC) mixtures, rinsed with distilled water and acetone, sonicated in acetone for 1 min, and dried prior to use. The Pt counter electrode was flame annealed prior to use.

Films of poly(**1d**-**2c**) were prepared on GCEs by chronoamperometry of 4 mM in repeat unit of poly(**1d**-**2c**) in 0.5 M $[NBu_4][BF_4]/CH_2Cl_2$ at 275 mV vs. Ag/Ag^+ for 10 seconds. After the polymer films were adsorbed onto the GCEs, the modified electrodes were rinsed gently with CH_2Cl_2. After air-drying, the electrodes were dried under vacuum for at least 4 h. Throughout this report, the first couple refers to the electron transfer between the neutral and radical cation species, while the second couple refers to the electron transfer between the radical cation and dicationic species.

Table 3-5. The electrochemical values for polymer films from Figure 3-1.

Name	$E°'_1$ (mV)	$\Delta E_{p,1}$ (mV)	$E°'_2$ (mV)	$\Delta E_{p,2}$ (mV)	Theoretical capacity (mA h g^{-1})	Theoretical energy density (W h kg^{-1})
poly(**1a-2a**)	−75	-	524	72	330	1163
poly(**1b-2a**)	−237	93	469	177	304	1038
poly(**1c-2a**)	−185	98	335	66	282	952
poly(**1d-2a**)	−213	41	321	49	245	822

Table 3-6. The electrochemical values for polymer films from Figure 3-2.

Name	$E°'_1$ (mV)	$\Delta E_{p,1}$ (mV)	$E°'_2$ (mV)	$\Delta E_{p,2}$ (mV)	Theoretical capacity (mA h g^{-1})	Theoretical energy density (W h kg^{-1})
poly(**1d-2b**)	−194	99	270	175	200	668
poly(**1d-2c**)	43	78	356	107	182	637
poly(**1d-2d**)	1	77	326	99	167	578
poly(**1d-2e**)	−4	63	240	71	160	547

All of the polymers that show two reversible redox processes adsorb onto the electrodes during electrochemical experiments (Fig. 3-3, 3-4). Deposition by cyclic voltammetry or chronoamperometry produced films that had similar electrochemical responses, and both methods were used to form polymer films on GCEs. The modified electrodes were rinsed in CH_2Cl_2 and then cycled in polymer-free electrolyte (acetonitrile or tetraglyme) to examine the electrochemical performance of the deposited polymer films.

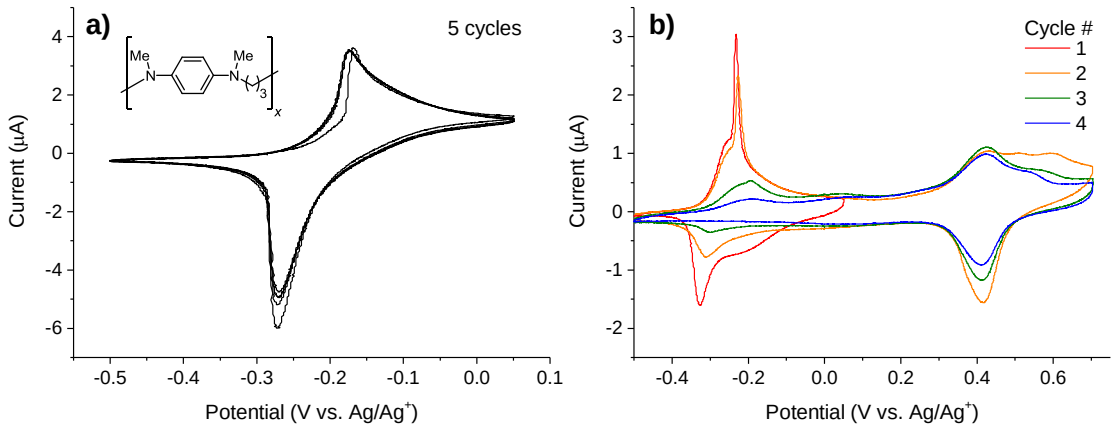

Figure 3-6. (a) A polymer film of poly(**1b-2a**) was adsorbed onto GCE by five CV cycles of 2 mM concentration in repeat unit of poly(**1b-2a**) in 0.1 M $[NBu_4][ClO_4]/CH_2Cl_2$ at 10 mV s^{-1}. (b) The CV of the modified electrode from a) cycled in 0.1 M $[NBu_4][ClO_4]/CH_3CN$ at 10 mV s^{-1}.

The CV of poly(**1b-2a**) shows a slightly sharp reduction peak, indicating that the polymer is adsorbed onto the electrode (Fig. 3-6a). This assumption is proven by cycling the modified electrode in polymer-free electrolyte (Fig. 3-6b). On the first cycle around the first redox couple, sharp oxidation and reduction peaks are observed. These sharp peaks are suggestive of charge trapping.[33] The subsequent cycles show two redox couples, as expected of *N,N,N′,N′*-tetramethyl-*p*-phenylenediamine (TMPD) containing polymers. However, with successive cycles, the current decreased, indicating a loss of poly(**1b-2a**), either from dissolution of the polymer into the electrolyte or irreversible reactions. The first redox couple lost most of its Faradaic current by the fourth cycle, while the second redox couple exhibited oxidation and reduction peaks, although at lower currents. The loss of Faradaic response for the first redox couple is another indicator that the polymer has trapped charges. Poly(**1b-2a**) should thermodynamically be reduced or oxidized at ~ −275 mV, but the polymer is trapped in the monocationic state. The retention of the second redox couple shows that the polymer can readily be oxidized to the dicationic polymer, and reduced to the

monocationic polymer. However, further reduction to the neutral polymer was impeded by charge trapping.

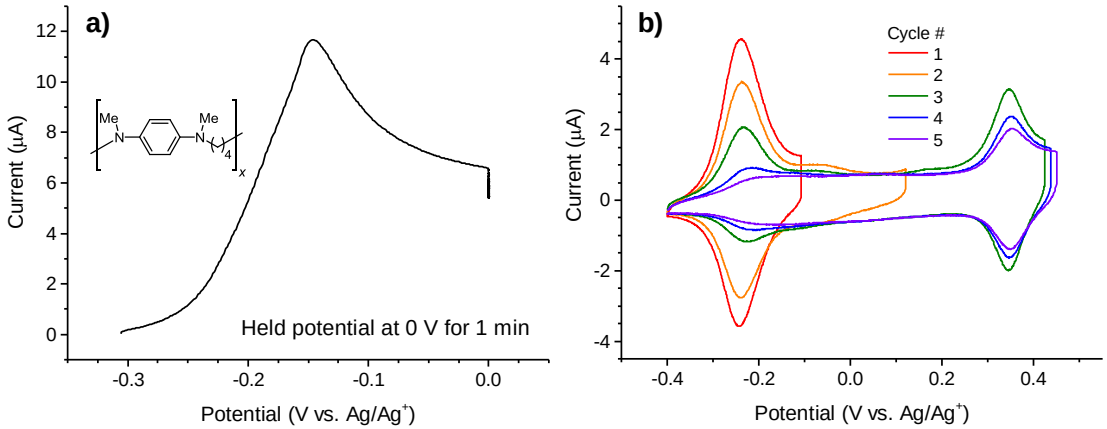

Figure 3-7. (a) A polymer film of poly(**1c**-**2a**) was adsorbed onto GCE by holding the potential at 0 V for 1 minute in 4 mM concentration in repeat unit of poly(**1c**-**2a**) in 0.1 M $[NBu_4][ClO_4]$/ CH_2Cl_2, after cycling to 0 V at 10 mV s^{-1}. (b) The CV of the modified electrode from a) cycled in 0.1 M $[NBu_4][ClO_4]/CH_3CN$ at 10 mV s^{-1}.

The CV of poly(**1c**-**2a**) shows two sharp reduction peaks, indicating that the polymer is adsorbed onto the electrode (Fig. 3-3). The potential was held at 0 V, past the first oxidation peak, for one minute to deposit a polymer film onto GCE. The modified electrode was in 0.1 M $[NBu_4][ClO_4]/CH_3CN$ at 10 mV s^{-1} (Fig. 3-7b). The CVs show two symmetrical redox couples, as expected for a surface-confined system. However, the current for both processes decreased with cycling, indicating a loss of active material, likely from dissolution of the polymer film into the electrolyte. The first redox couple lost most of its initial Faradaic current by the fifth cycle, while the second redox couple still exhibited oxidation and reduction peaks, although at lower currents. Similar to poly(**1b**-**2a**), this polymer system had trapped charges, wherein the polymer should thermodynamically be oxidized or reduced but did not undergo electron transfers for the first redox couple. The second redox couple is not affected as

the polymer can be oxidized to the dicationic state and reduced to the monocationic state.

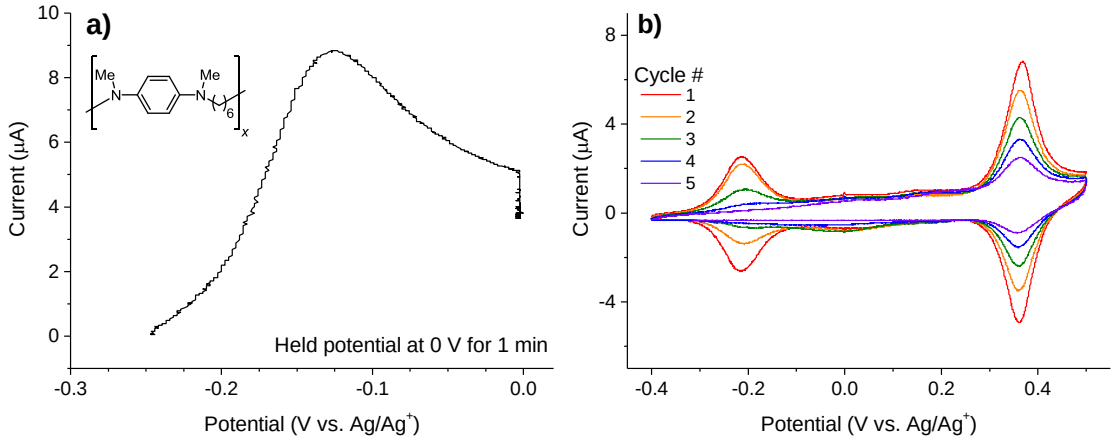

Figure 3-8. (a) A polymer film of poly(**1d-2a**) was adsorbed onto GCE by holding the potential at 0 V for 1 minute in 4 mM concentration in repeat unit of poly(**1d-2a**) in 0.1 M $[NBu_4][ClO_4]$/ CH_2Cl_2, after cycling to 0 V at 10 mV s^{-1}. (b) The CV of the modified electrode from a) cycled in 0.1 M $[NBu_4][ClO_4]/CH_3CN$ at 10 mV s^{-1}.

The CV of poly(**1d-2a**) shows two sharp reduction peaks, indicating that the polymer is adsorbed onto the electrode (Fig. 3-3). The potential was held at 0 V, past the first oxidation peak, for one minute to deposit a polymer film onto GCE. The modified electrode was cycled around both redox couples in 0.1 M $[NBu_4][ClO_4]/CH_3CN$ at 10 mV s^{-1} (Fig. 3-8b). The CVs show two symmetrical redox couples, as expected for a surface-confined system. However, the current for both processes decreased with cycling, indicating a loss of active material, likely from dissolution of the polymer film into the electrolyte. The first redox couple lost all Faradaic current by the fifth cycle, while the second redox couple still exhibited oxidation and reduction peaks, although at lower currents. Similar to poly(**1b-2a**), this polymer system had trapped charges, wherein the polymer should thermodynamically be oxidized or reduced but did not undergo electron transfers for the first redox

couple. The second redox couple is not affected as the polymer can be oxidized to the dicationic state and reduced to the monocationic state.

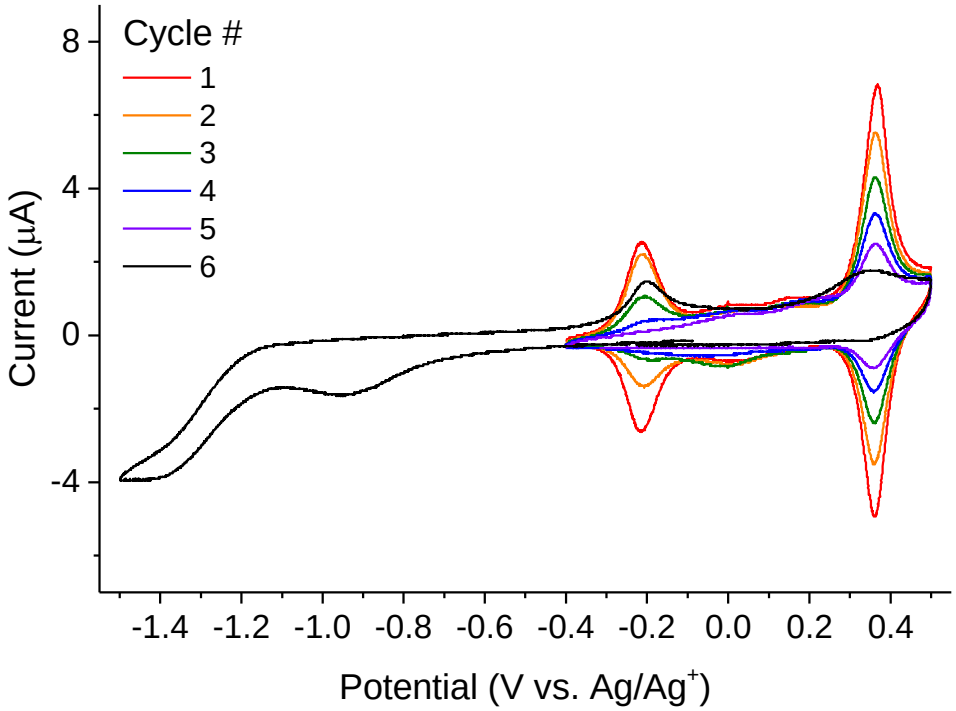

Figure 3-9. The CV of the modified electrode from Fig. 3-8b cycled in 0.1 M $[NBu_4][ClO_4]/CH_3CN$ at 10 mV s^{-1} to more negative potentials.

To investigate the charge trapping of poly(**1d-2a**), the modified electrode was swept more negative to −1.5 V, thereby increasing the driving force to reduce the polymer (Fig. 3-9). A reduction peak could be seen at approximately −950 mV, and an oxidation peak at −202 V was observed on the positive sweep. This experiment demonstrated that the charges trapped in the polymer can be reduced if there is a high enough driving force, amounting to an overpotential of 735 mV. The peak to peak separation (ΔE_p) for the first redox couple is ~750 mV due to charge trapping compared to 4 mV before the polymer film became charge trapped. Charge trapping decreased the available species that can undergo electron transfers (charge or discharge a device), and the method of releasing the trapped charges lowered the

energy output and the Coulombic efficiency. The poly(arylamine) must not trap charges to be a viable cathode material.

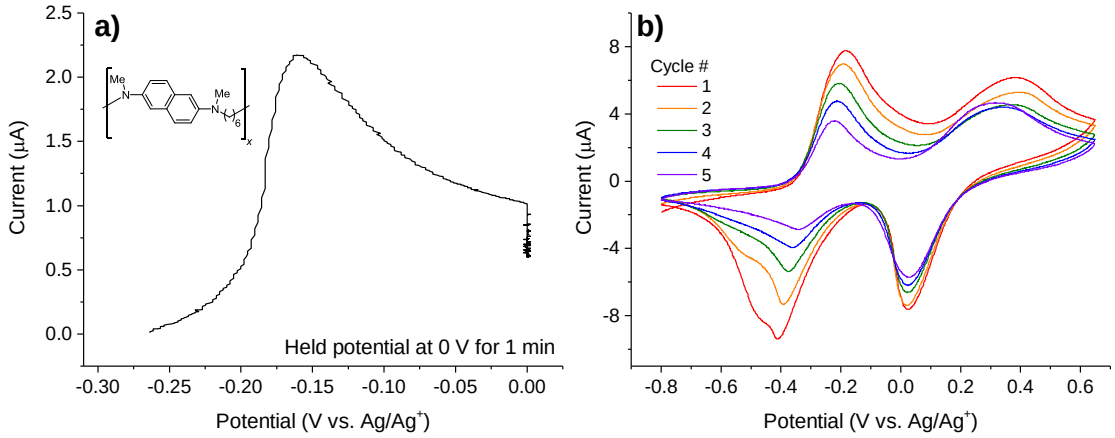

Figure 3-10. (a) A polymer film of poly(**1d-2b**) was adsorbed onto GCE by holding the potential at 0 V for 1 minute in 4 mM concentration in repeat unit of poly(**1d-2b**) in 0.1 M $[NBu_4][ClO_4]$/ CH_2Cl_2, after cycling to 0 V at 10 mV s^{-1}. (b) The CV of the modified electrode from a) cycled in 0.1 M $LiClO_4$/tetraglyme at 20 mV s^{-1}.

The CV of poly(**1d-2b**) shows two reduction peaks with non-diffusional looking tails, indicating that the polymer adsorbed onto the electrode (Fig. 3-4). The potential was held at 0 V, past the first oxidation peak, for one minute to deposit a polymer film onto GCE. The modified electrode was cycled around both redox couples in 0.1 M $LiClO_4$/tetraglyme at 20 mV s^{-1} (Fig. 3-10b). The CVs show two redox couples. However, the current for both processes decreased with cycling, indicating a loss of active material, likely from dissolution of the polymer film into the electrolyte. Also, similar to poly(**1b-2a**), the first redox couple lost Faradaic current faster than the second redox couple. As we conjectured above, this phenomenon is likely due to charge trapping, where the polymer is trapped in the monocationic state and cannot be reduced without a large driving force.

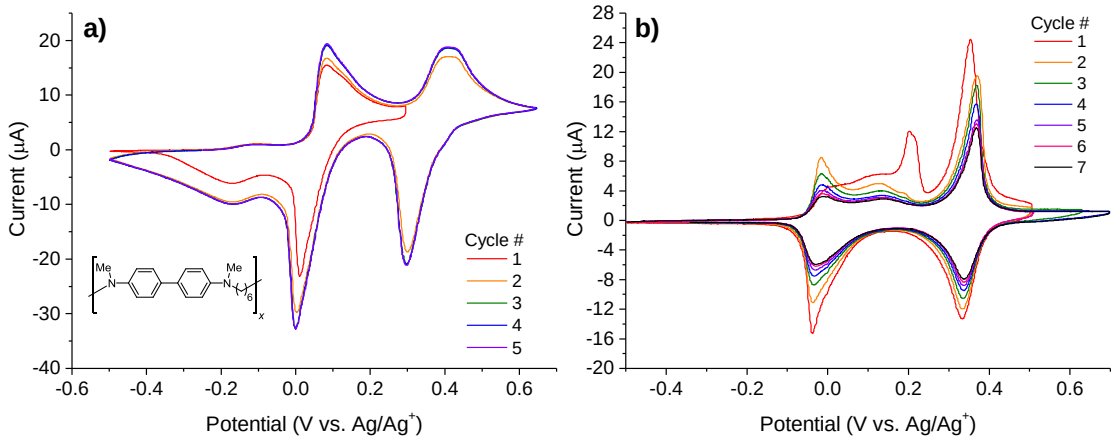

Figure 3-11. (a) A polymer film of poly(**1d-2c**) was adsorbed onto GCE by 5 CV cycles in 4 mM concentration in repeat unit of poly(**1d-2c**) in 0.1 M $[NBu_4][ClO_4]/CH_2Cl_2$. (b) The CV of the modified electrode from a) cycled in 0.1 M $[NBu_4][ClO_4]/CH_3CN$ at 20 mV s^{-1}.

The CV of poly(**1d-2c**) shows two reduction peaks with non-diffusional looking tails, indicating that the polymer adsorbed onto the electrode (Fig. 3-4). The polymer film was deposited onto GCE by cycling in the polymer solution for 5 CV cycles. The modified electrode was cycled around both redox couples in 0.1 M $[NBu_4][ClO_4]/CH_3CN$ at 20 mV s^{-1} (Fig. 3-11b). The CVs show two redox couples. The first oxidation peak was at 205 mV while the corresponding reduction peak was at −37 mV, resulting in a large ΔE_p of 242 mV. The second redox couple exhibited an ΔE_p of 21 mV, as expected of surface-confined systems. The large splitting in potentials for the first redox couple suggested that there was significant reorganization of the film as it transitioned from a neutral film to an oxidized polymer film. This trend has been observed in substituted cinnolines[29], tetrathiafulvalene in a Nafion matrix,[30] and oligomers of *p*-phenylenes.[31] On subsequent cycles, the first oxidation peak was at −15 mV and the ΔE_p decreased to 21 mV. This negative shift in potentials for the first oxidation peak is indicative of the polymer film having been reorganized to a more thermodynamically stable phase on the first cycle. We believe this

reorganization stems from the phenyl rings rotating to optimize the conjugation between the rings.

Initially, the current for both processes decreased with cycling, indicating a loss of active material, likely from dissolution of the polymer film into the electrolyte. After five cycles, the current stabilizes and subsequent cycles overlap with each other very well.

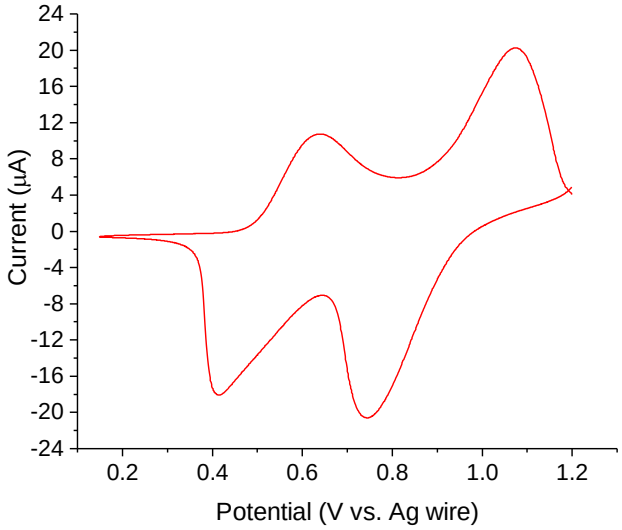

Figure 3-12. A polymer film of poly(**1d-2c**) cycled in 0.1 M $LiPF_6$/tetraglyme at 50 mV s^{-1}.

The electrochemical response of polymer films of poly(**1d-2c**) on GCE are dependent upon the electrolyte. As shown above, there is a clear potential shift for the first oxidation peak in acetonitrile upon initial cycling, and the first oxidation peak is broadened and flatter in 1,3-dioxolane:dimethoxyethane (DOL:DME, 1:1 v/v) (Fig. 3-5a). However, when the polymer film was cycled in 0.1 M $LiPF_6$/tetraglyme (Fig. 3-12), the first oxidation wave is symmetrical and resembles the second oxidation peak. Optimizing the polymer-electrolyte interactions is critical to form a conformal film during deposition, and to have good cycling performance.

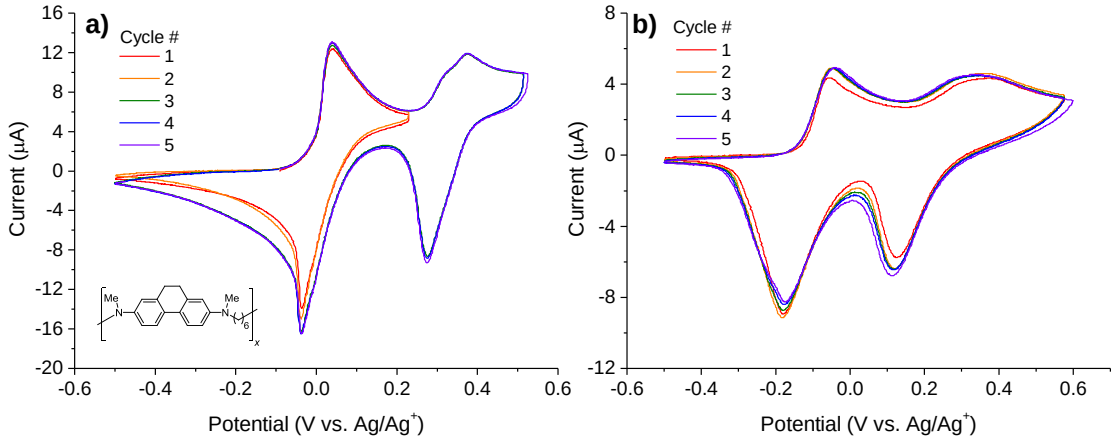

Figure 3-13. 85

The CV of poly(**1d-2d**) shows two sharp reduction peaks, indicating that the polymer is adsorbed onto the electrode (Fig. 3-4). The polymer film was deposited onto GCE by cycling in the polymer solution for 5 CV cycles. The modified electrode was cycled around both redox couples in 0.1 M $LiClO_4$/tetraglyme at 20 mV s^{-1} (Fig. 3-13b). The CVs show two redox couples. Unlike previous systems, the current for both redox processes did not diminish significantly with cycling. Furthermore, the polymer film did not trap charges after 5 cycles. The dihydrophenanthrene polymer is a potential cathode material due to its two redox processes and stable cycling.

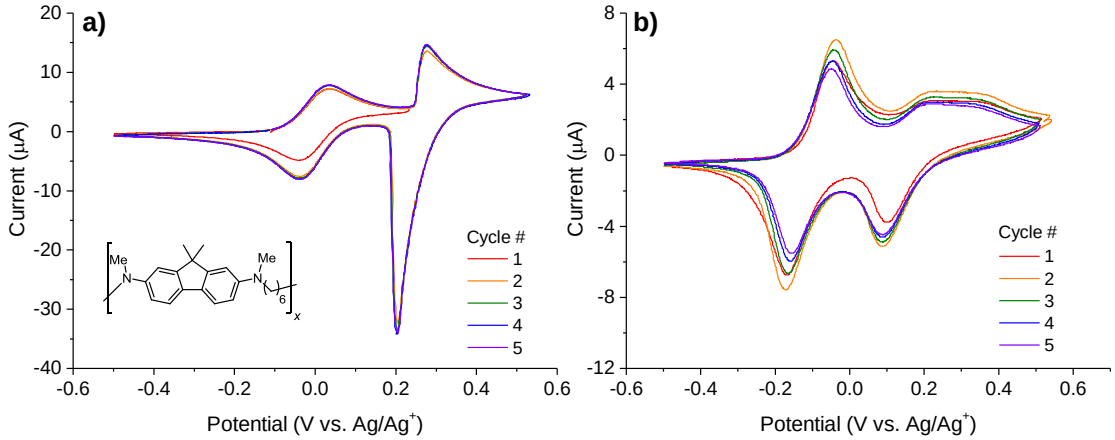

Figure 3-14. (a) A polymer film of poly(**1d-2e**) was adsorbed onto GCE by 5 CV cycles in 4 mM concentration in repeat unit of poly(**1d-2e**) in 0.1 M $[NBu_4][ClO_4]/CH_2Cl_2$. (b) The CV of the modified electrode from a) cycled in 0.1 M $LiClO_4$/tetraglyme at 20 mV s^{-1}.

The CV of poly(**1d-2e**) shows two sharp reduction peaks, indicating that the polymer is adsorbed onto the electrode (Fig. 3-3). The polymer film was deposited onto GCE by cycling in the polymer solution for 5 CV cycles. The modified electrode was cycled around both redox couples in 0.1 M $LiClO_4$/tetraglyme at 20 mV s^{-1} (Fig. 3-14b). The CVs show two redox couples. Unlike previous systems, the current for both redox processes did not diminish significantly with cycling. Furthermore, the polymer film did not trap charges after 5 cycles. The dihydrophenanthrene polymer is a potential cathode material due to its two redox processes and stable cycling.

3-7. Differential Scanning Calorimetry (DSC) Thermograms

Table 3-7. The polymer properties of poly(arylamines).

Entry	T_g[a] (°C)	T_m[a] (°C)
Poly(**1a-2a**)	45	179
Poly(**1b-2a**)	10	n.a.[b]
Poly(**1c-2a**)	42	110
Poly(**1d-2a**)	41	89
Poly(**1d-2b**)	43	137
Poly(**1d-2c**)	50	168
Poly(**1d-2d**)	78	n.a.[b]
Poly(**1d-2e**)	78	n.a.[b]

[a] Determined by DSC. [b] Not applicable; no melting transition observed.

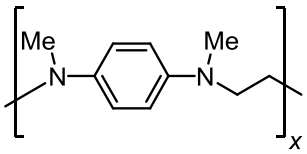

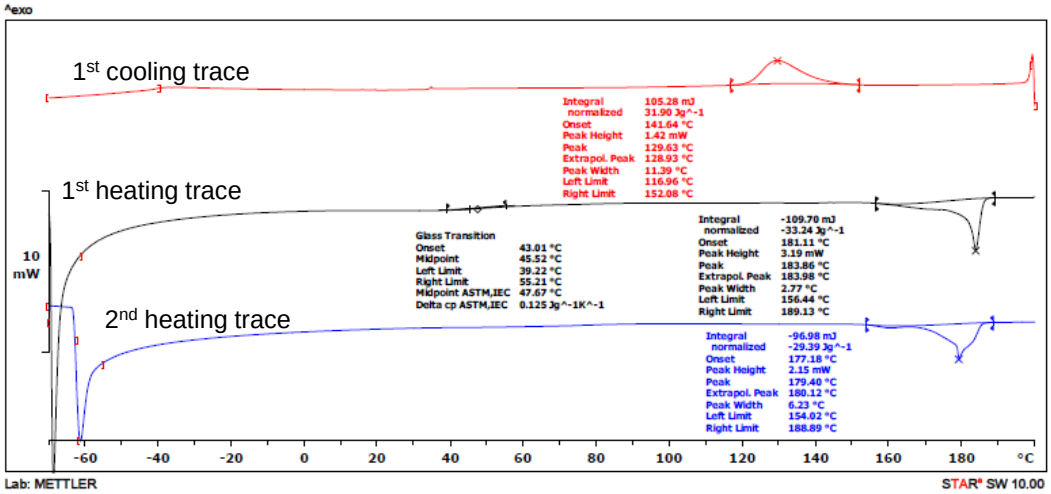

Figure 3-15. DSC traces of poly(**1a**-**2a**) (Table 3-1, entry 1).

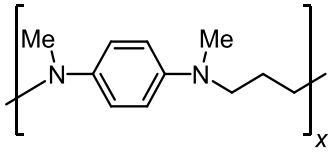

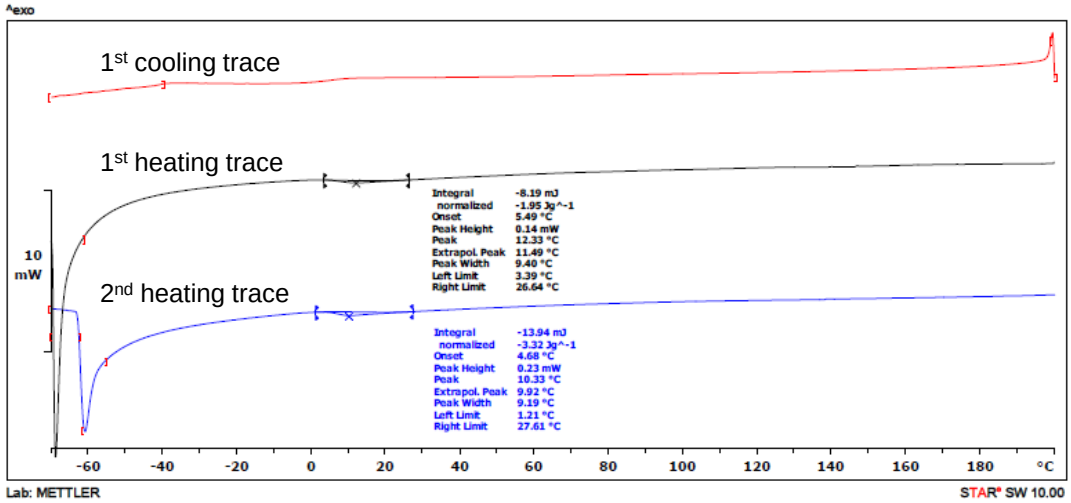

Figure 3-16. DSC traces of poly(**1b**-**2a**) (Table 3-1, entry 2).

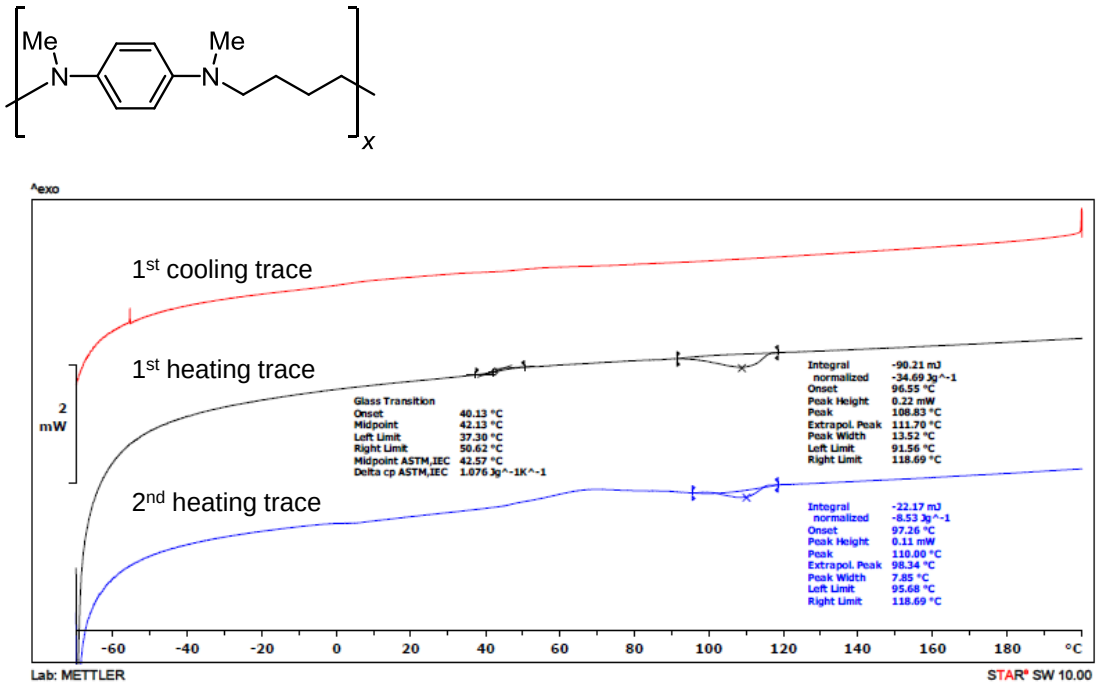

Figure 3-17. DSC traces of poly(**1c-2a**) (Table 3-1, entry 3).

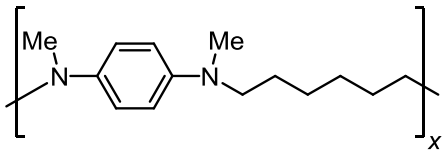

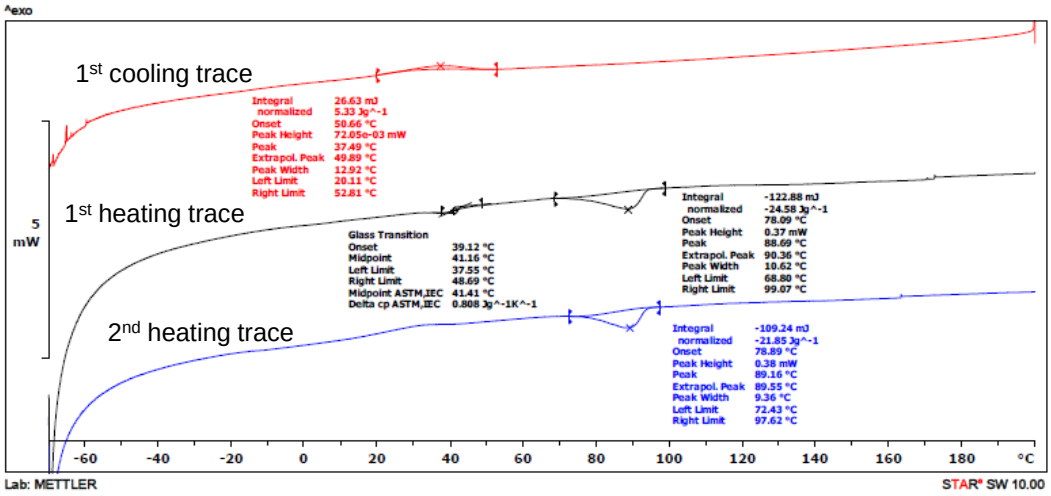

Figure 3-18. DSC traces of poly(**1d-2a**) (Table 3-1, entry 4).

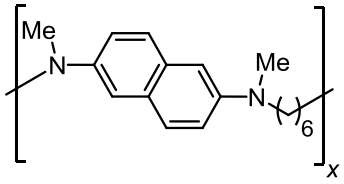

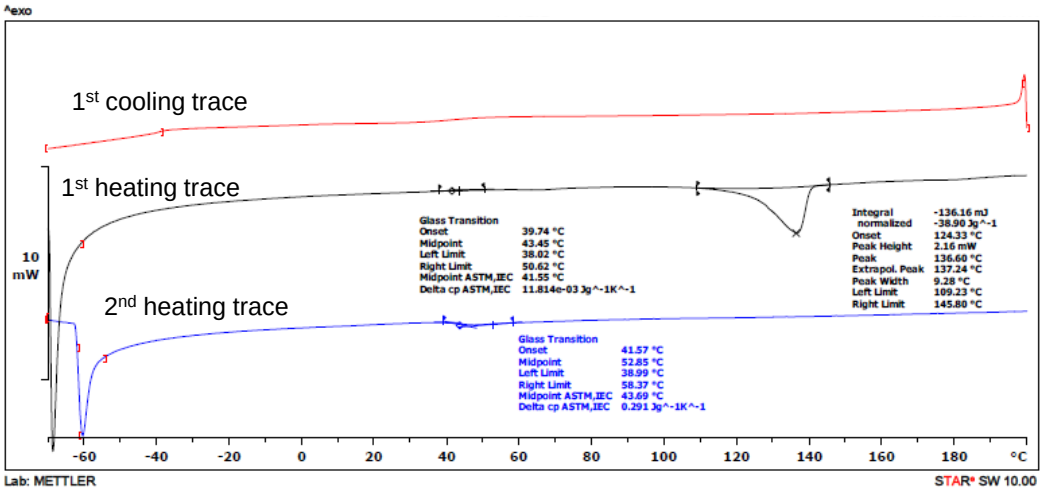

Figure 3-19. DSC traces of poly(**1d**-**2b**) (Table 3-2, entry 1).

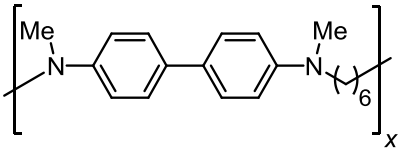

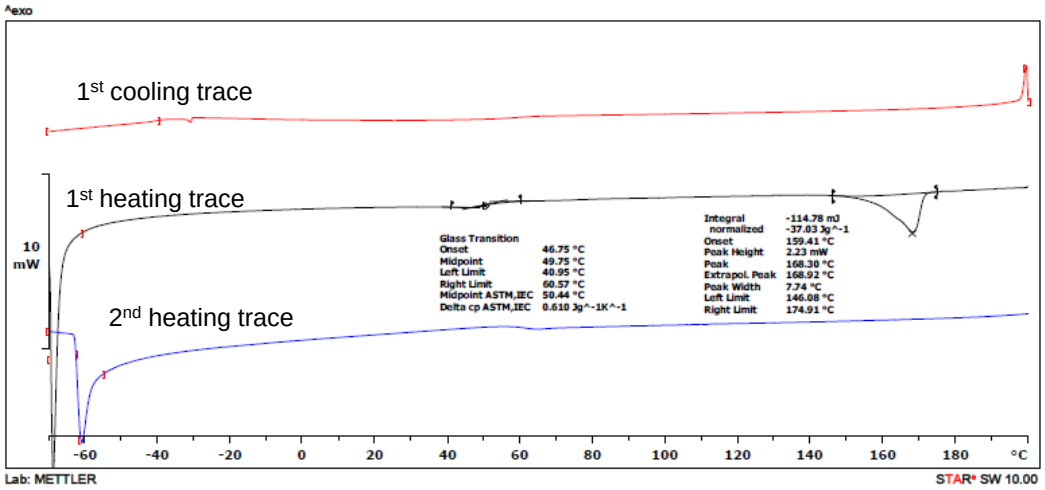

Figure 3-20. DSC traces of poly(**1d**-**2c**) (Table 3-2, entry 2).

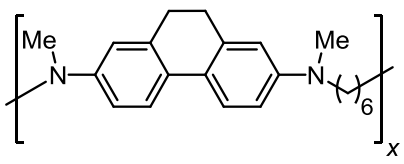

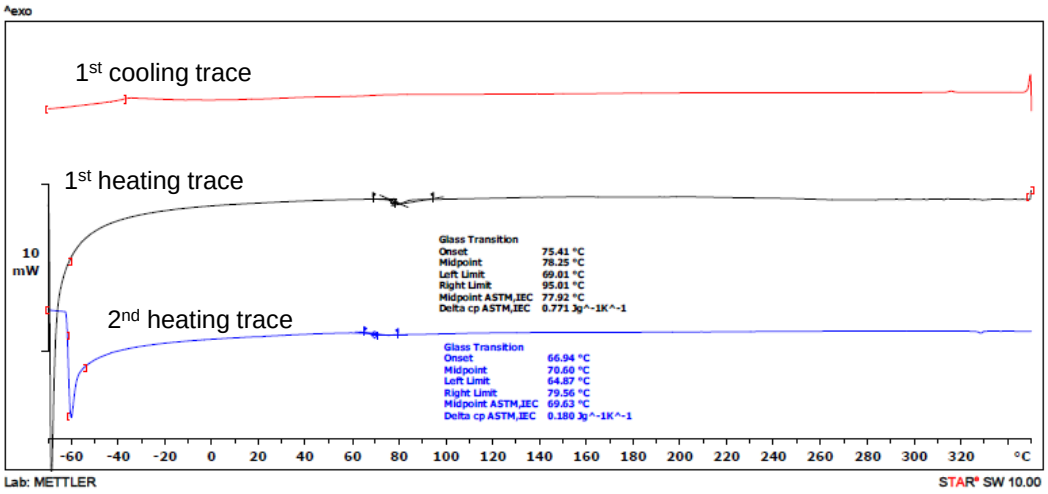

Figure 3-21. DSC traces of poly(**1d**-**2d**) (Table 3-2, entry 3).

This sample used the following heating program: −70 °C to 350 °C at 10 °C/min, 350 to −70 °C at 10 °C/min, and then −70 °C to 350 °C at 10 °C/min.

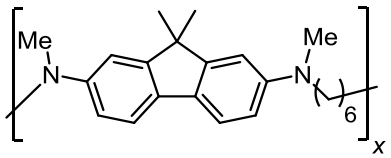

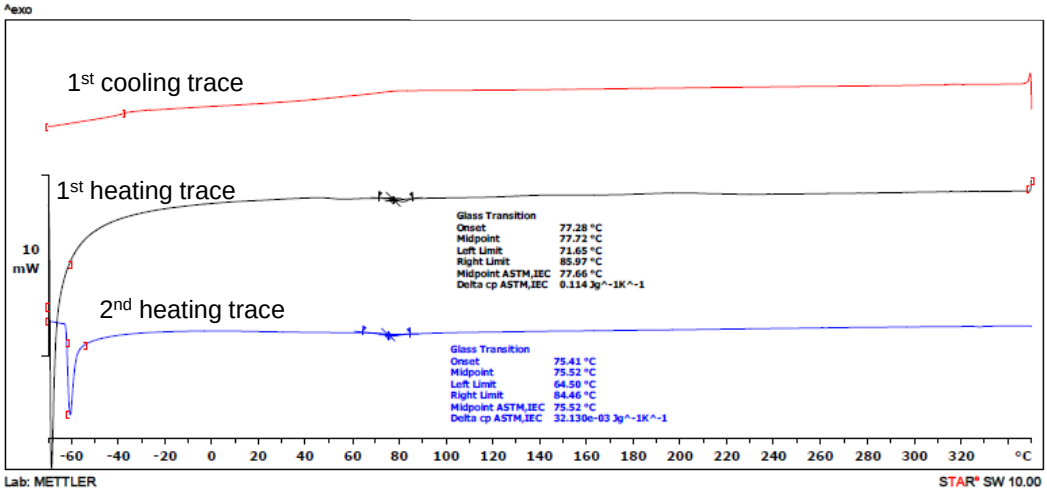

Figure 3-22. DSC traces of poly(**1d**-**2e**) (Table 3-2, entry 4).

This sample used the following heating program: −70 °C to 350 °C at 10 °C/min, 350 to −70 °C at 10 °C/min, and then −70 °C to 350 °C at 10 °C/min.

3-8. ^{1}H and ^{13}C NMR Spectra of Poly(arylamines)

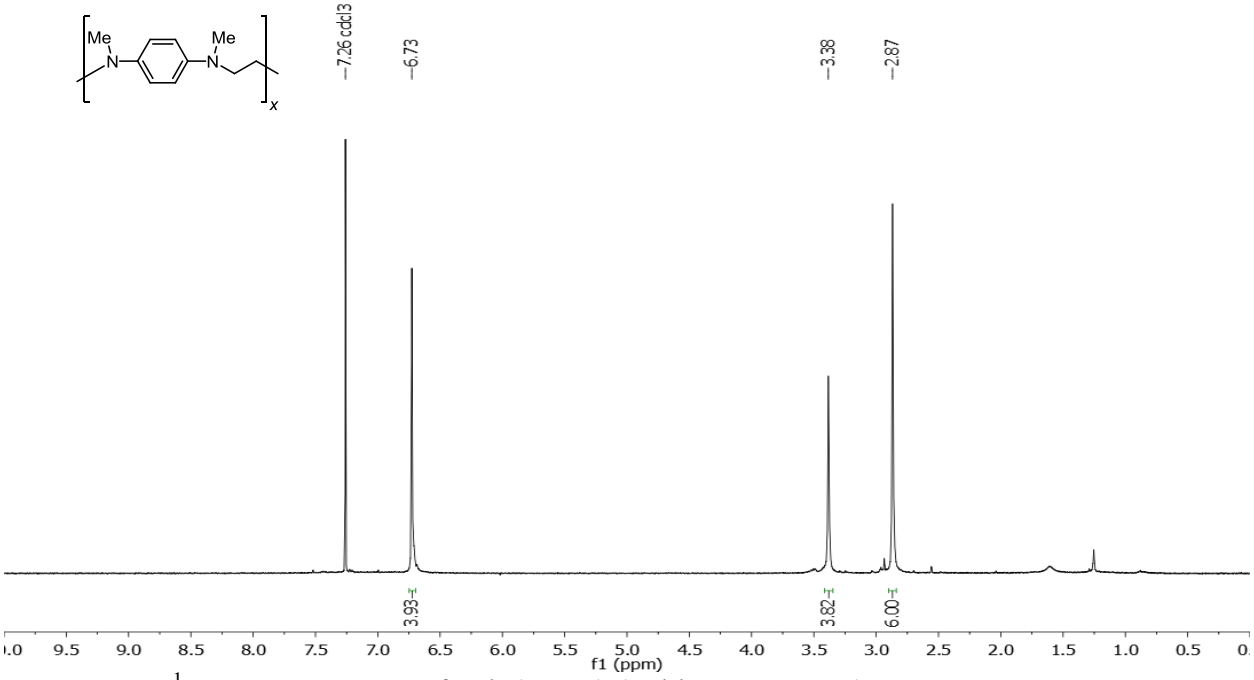

Figure 3-23. ^{1}H NMR spectrum of poly(**1a-2a**) (Table 3-1, entry 1).
^{1}H NMR spectrum ($CDCl_3$, 400 MHz): δ 6.73 (s, 4H), 3.38 (s, 4H), 2.87 (s, 6H).

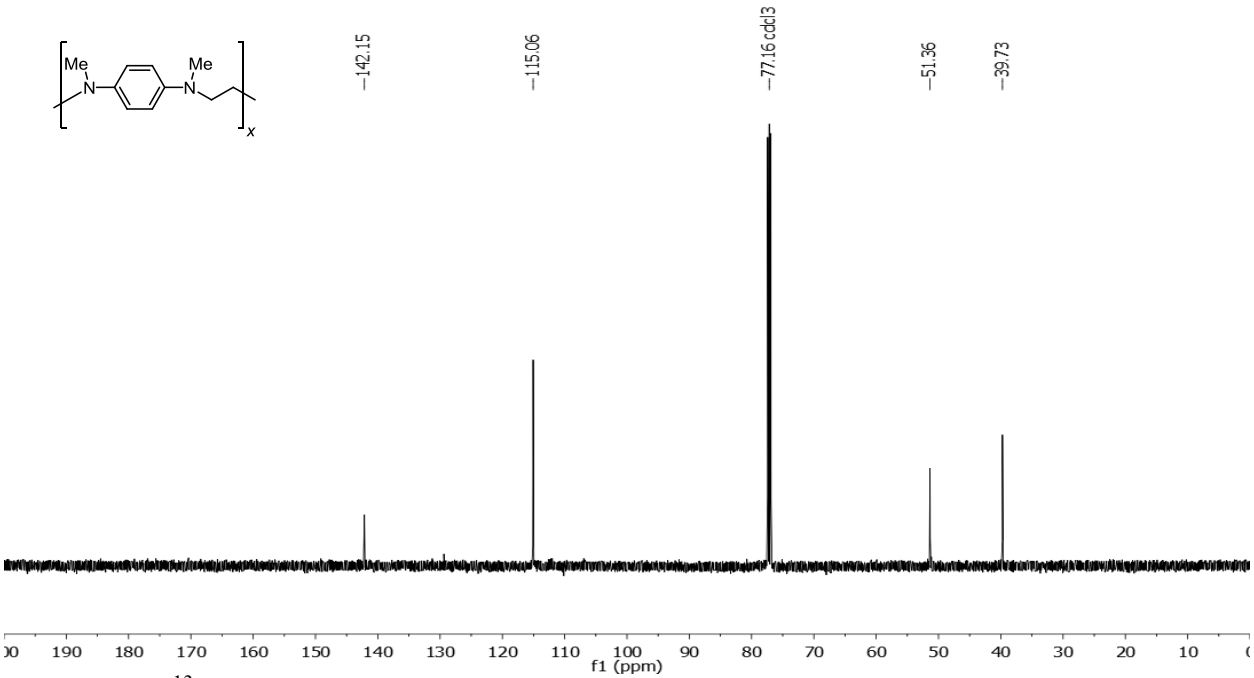

Figure 3-24. ^{13}C NMR spectrum of poly(**1a-2a**) (Table 3-1, entry 1).
^{13}C NMR ($CDCl_3$, 125 MHz): δ 142.15, 115.06, 51.36, 39.73.

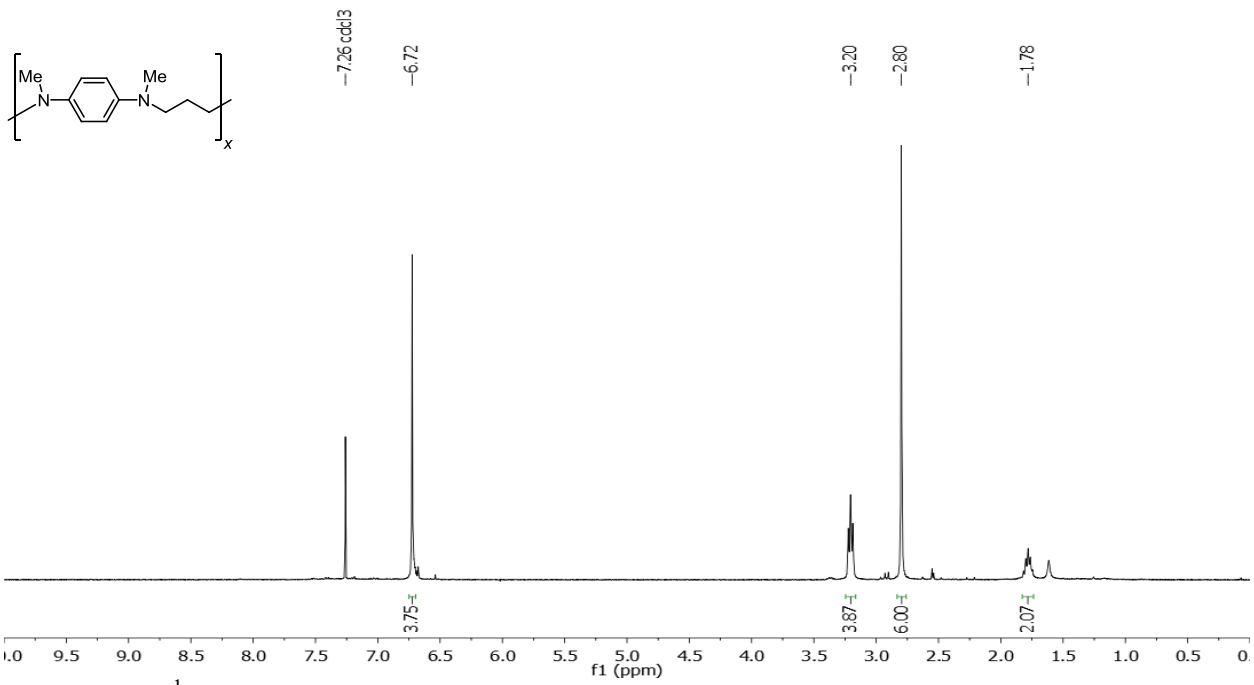

Figure 3-25. ^{1}H NMR spectrum of poly(**1b**-**2a**) (Table 3-1, entry 2).
^{1}H NMR spectrum ($CDCl_3$, 400 MHz): δ 6.72 (s, 4H), 3.20 (t, 4H), 2.80 (s, 6H), 1.75-1.82 (p, 2H).

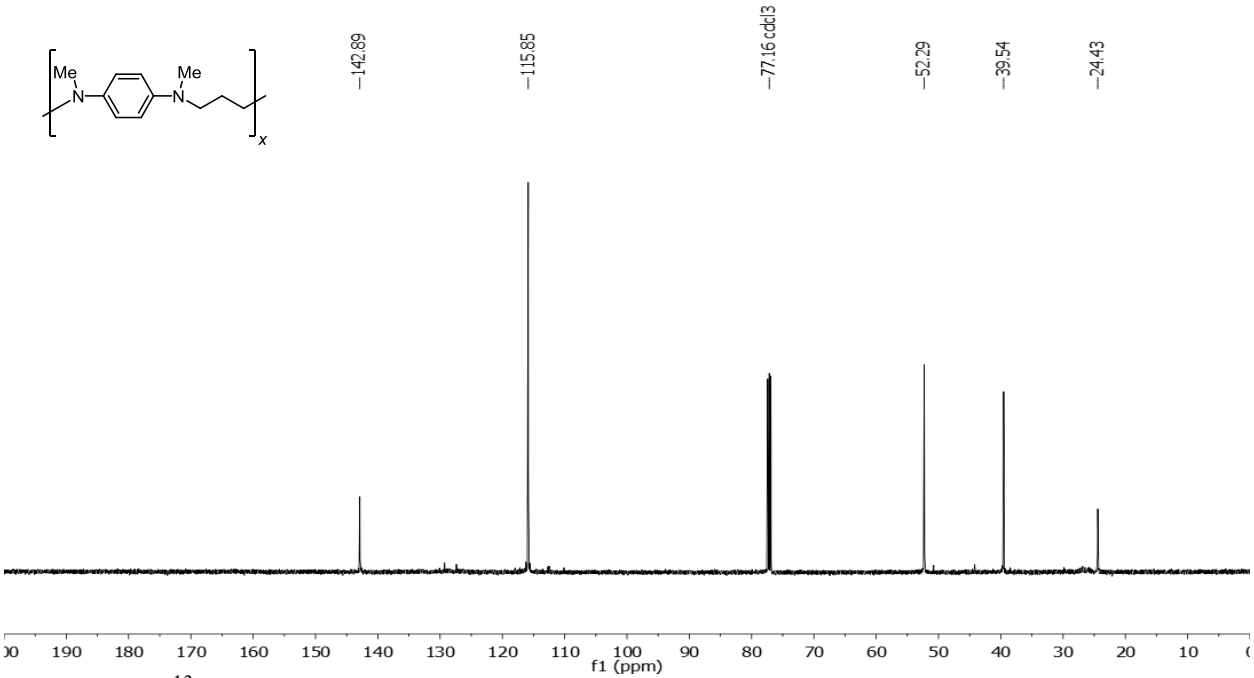

Figure 3-26. ^{13}C NMR spectrum of poly(**1b**-**2a**) (Table 3-1, entry 2).
^{13}C NMR ($CDCl_3$, 125 MHz): δ 142.89, 115.85, 52.29, 39.54, 24.43.

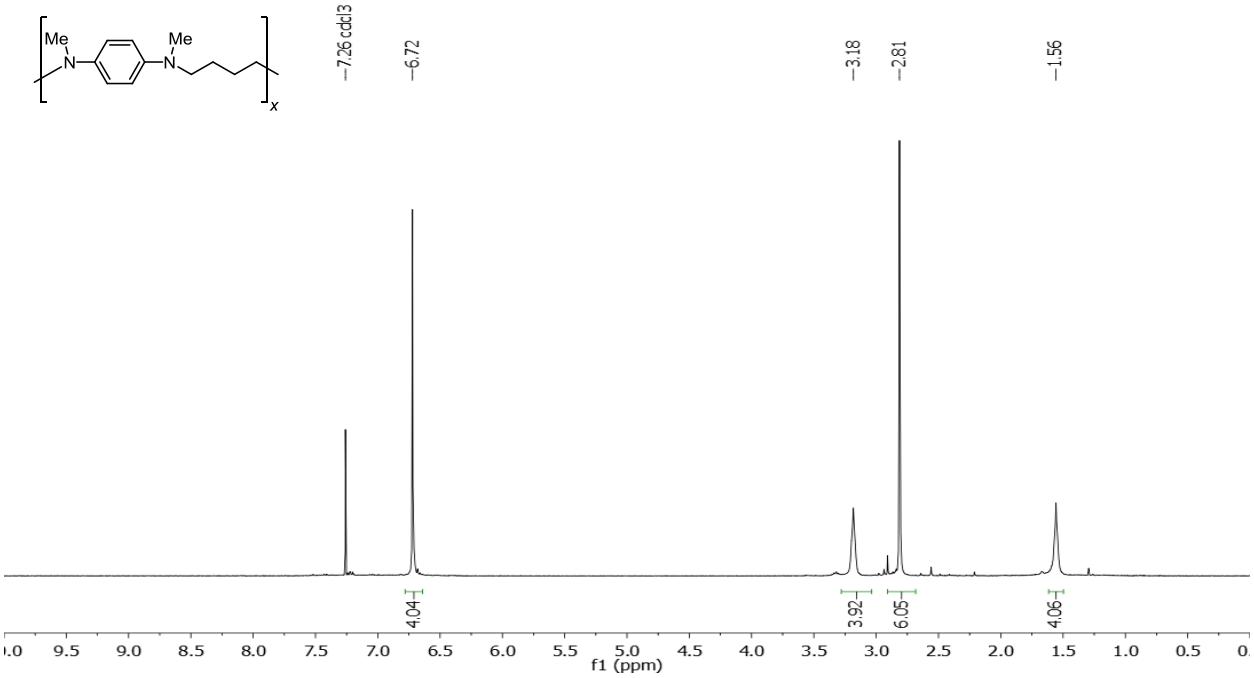

Figure 3-27. ^{1}H NMR spectrum of poly(**1c**-**2a**) (Table 3-1, entry 3).
^{1}H NMR ($CDCl_3$, 400 MHz): δ 6.72 (s, 4H), 3.16-3.21 (m, 4H), 2.81 (s, 6H), 1.53-1.58 (m, 4H).

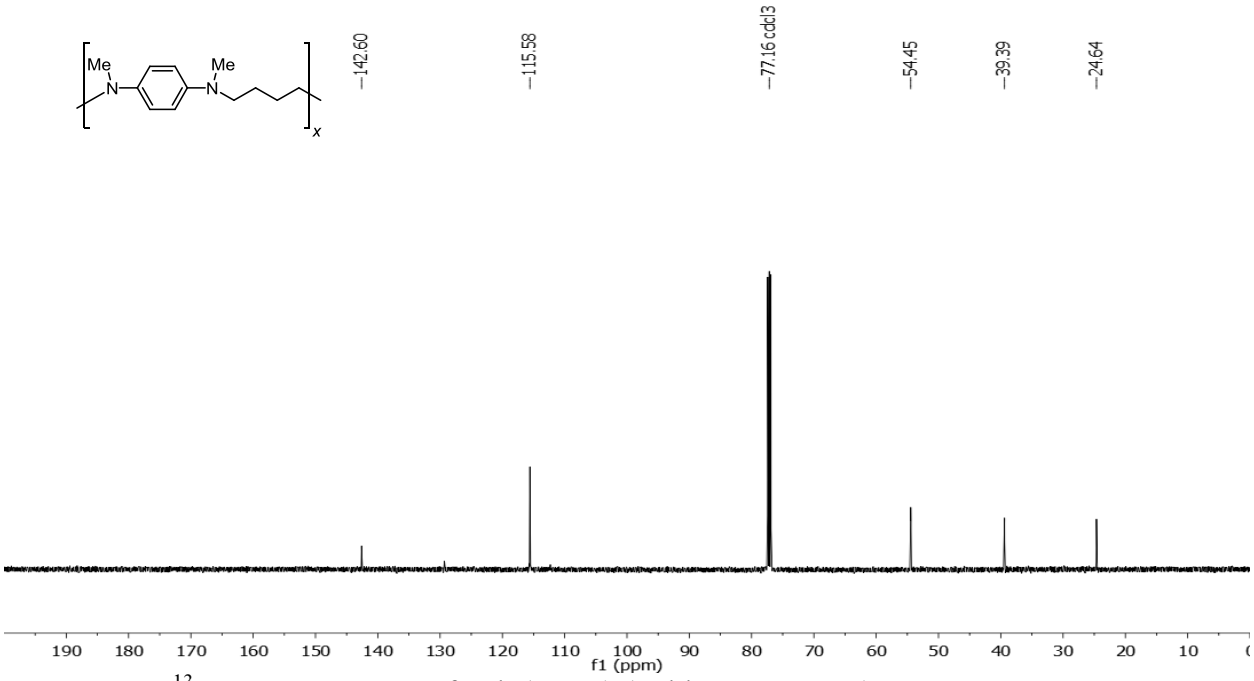

Figure 3-28. ^{13}C NMR spectrum of poly(**1c**-**2a**) (Table 3-1, entry 3).
^{13}C NMR ($CDCl_3$, 125 MHz): δ 142.60, 115.58, 54.45, 39.39, 24.64.

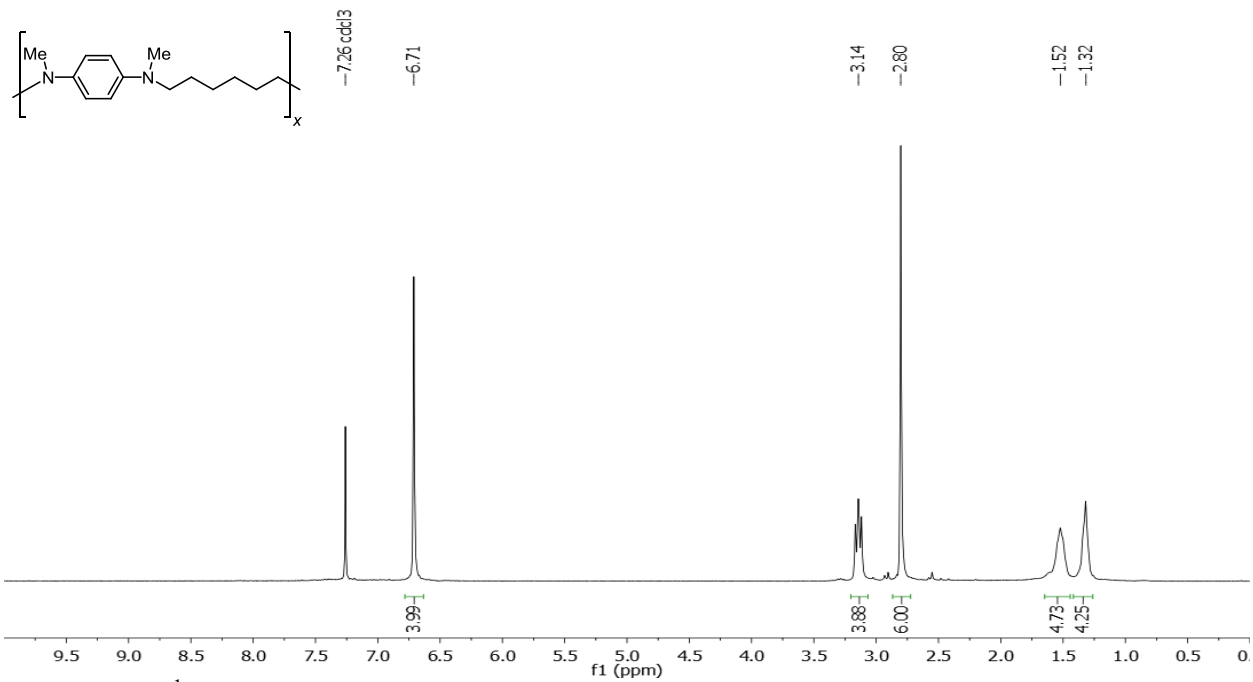

Figure 3-29. ^{1}H NMR spectrum of poly(**1d-2a**) (Table 3-1, entry 4).
^{1}H NMR spectrum ($CDCl_3$, 400 MHz): δ 6.71 (s, 4H), 3.14 (t, 4H), 2.80 (s, 6H), 1.48-1.56 (m, 4H), 1.29-1.35 (m, 4H).

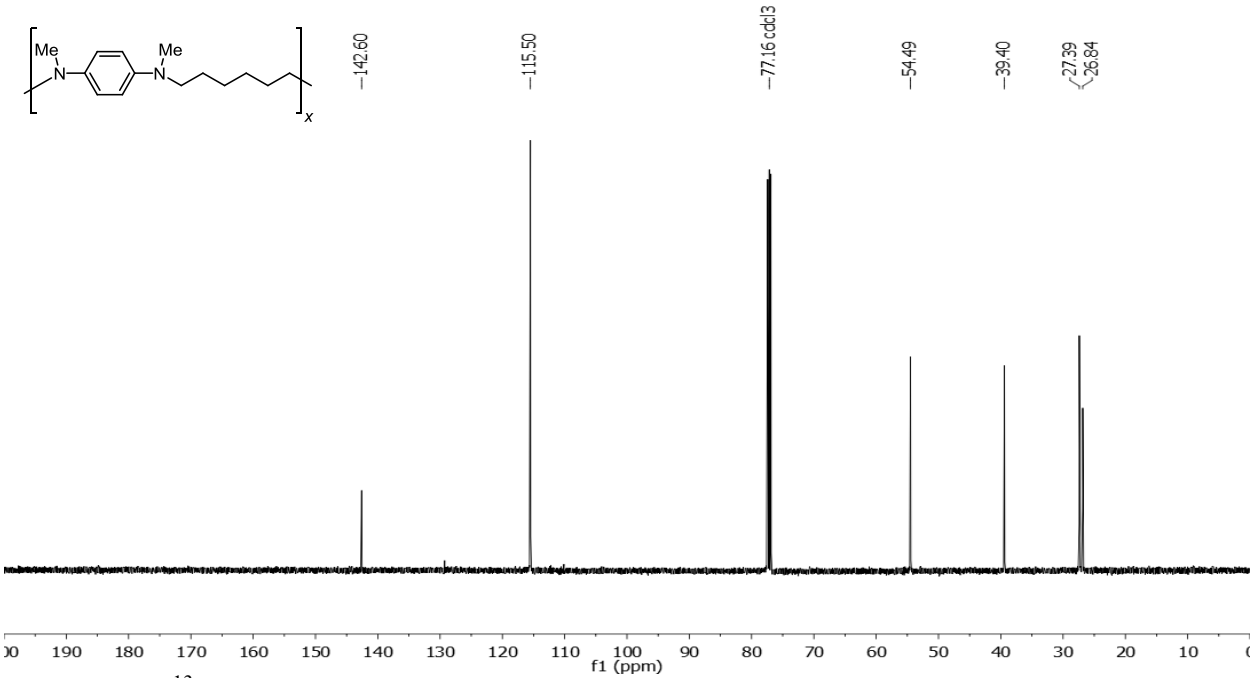

Figure 3-30. ^{13}C NMR spectrum of poly(**1d-2a**) (Table 3-1, entry 4).
^{13}C NMR ($CDCl_3$, 125 MHz): δ 142.60, 115.50, 54.49, 39.40, 27.39, 26.84.

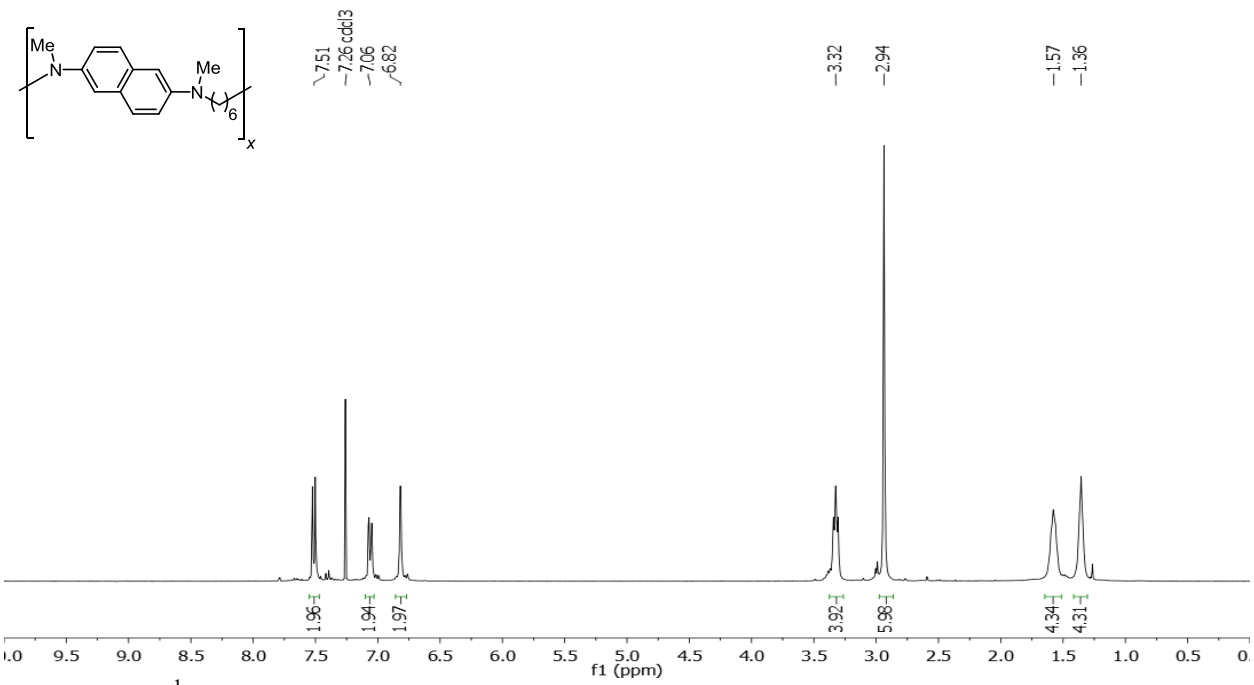

Figure 3-31. ^{1}H NMR spectrum of poly(**1d**-**2b**) (Table 3-2, entry 1).
^{1}H NMR spectrum ($CDCl_3$, 400 MHz): δ 7.51 (d, 2H), 7.06 (m, 2H), 6.82 (d, 2H), 3.32 (t, 4H), 2.94 (s, 6H), 1.54-1.61 (m, 4H), 1.34-1.37 (m, 4H).

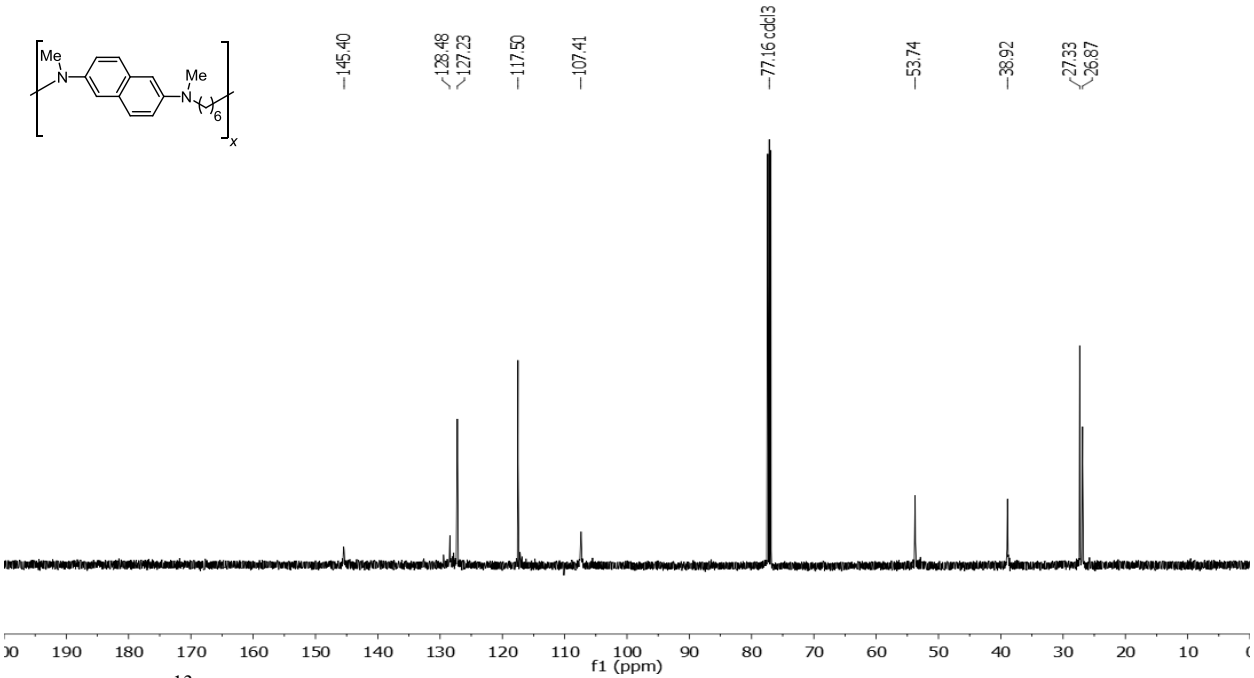

Figure 3-32. ^{13}C NMR spectrum of poly(**1d**-**2b**) (Table 3-2, entry 1).
^{13}C NMR ($CDCl_3$, 125 MHz): δ 145.40, 128.48, 127.23, 117.50, 107.41, 53.74, 38.92, 27.33, 26.87.

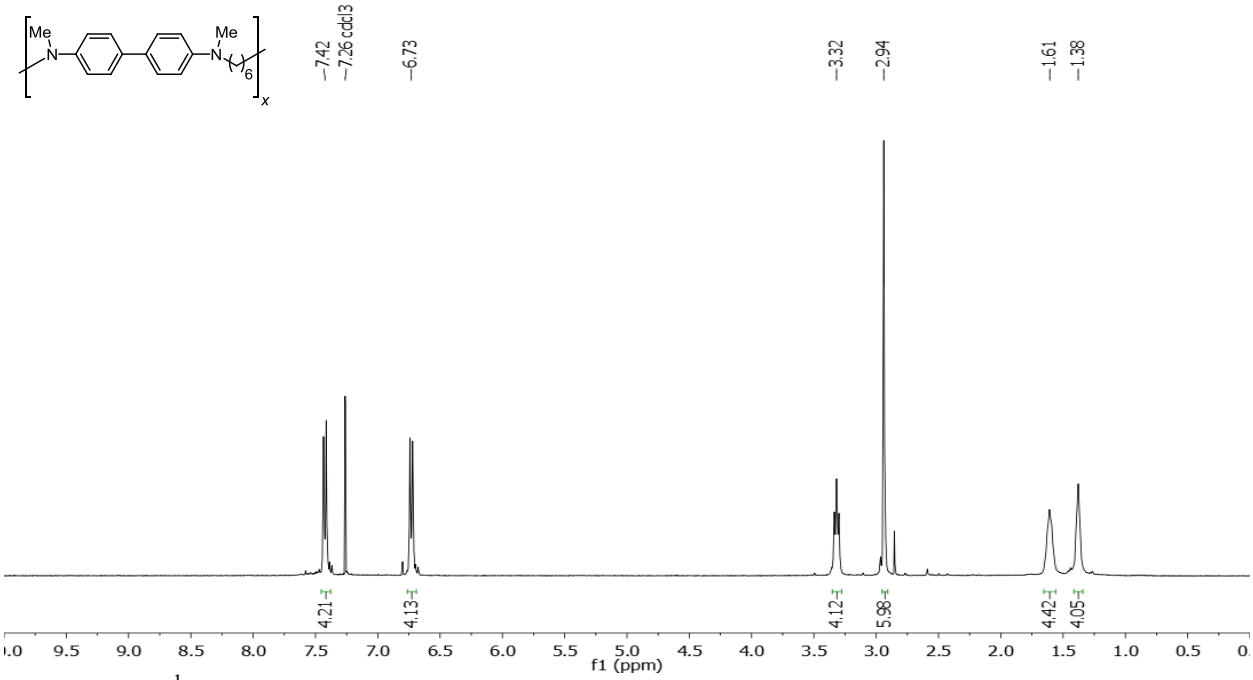

Figure 3-33. ^{1}H NMR spectrum of poly(**1d-2c**) (Table 3-2, entry 2).
^{1}H NMR spectrum ($CDCl_3$, 400 MHz): δ 7.42 (d, 4H), 6.73 (d, 4H), 3.32 (t, 4H), 2.94 (s, 6H), 1.58-1.63 (m, 4H), 1.36-1.40 (br s, 4H).

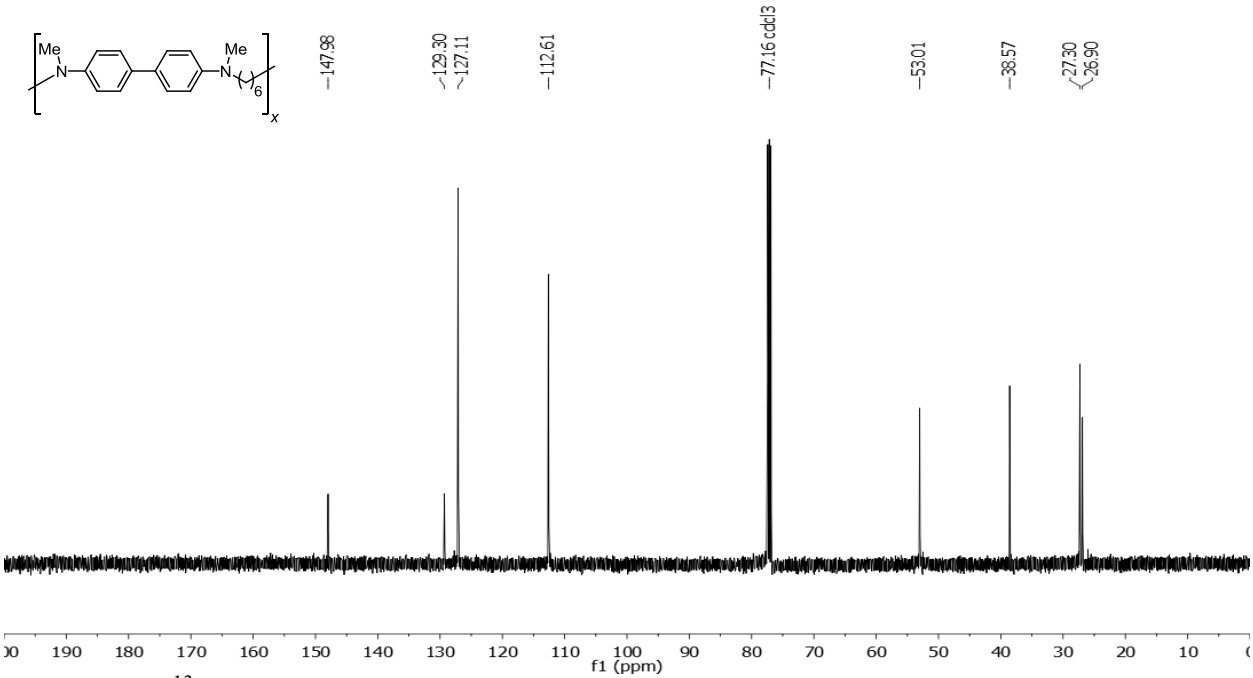

Figure 3-34. ^{13}C NMR spectrum of poly(**1d-2c**) (Table 3-2, entry 2).
^{13}C NMR ($CDCl_3$, 125 MHz): δ 147.98, 129.30, 127.11, 112.61, 53.01, 38.57, 27.30, 26.90.

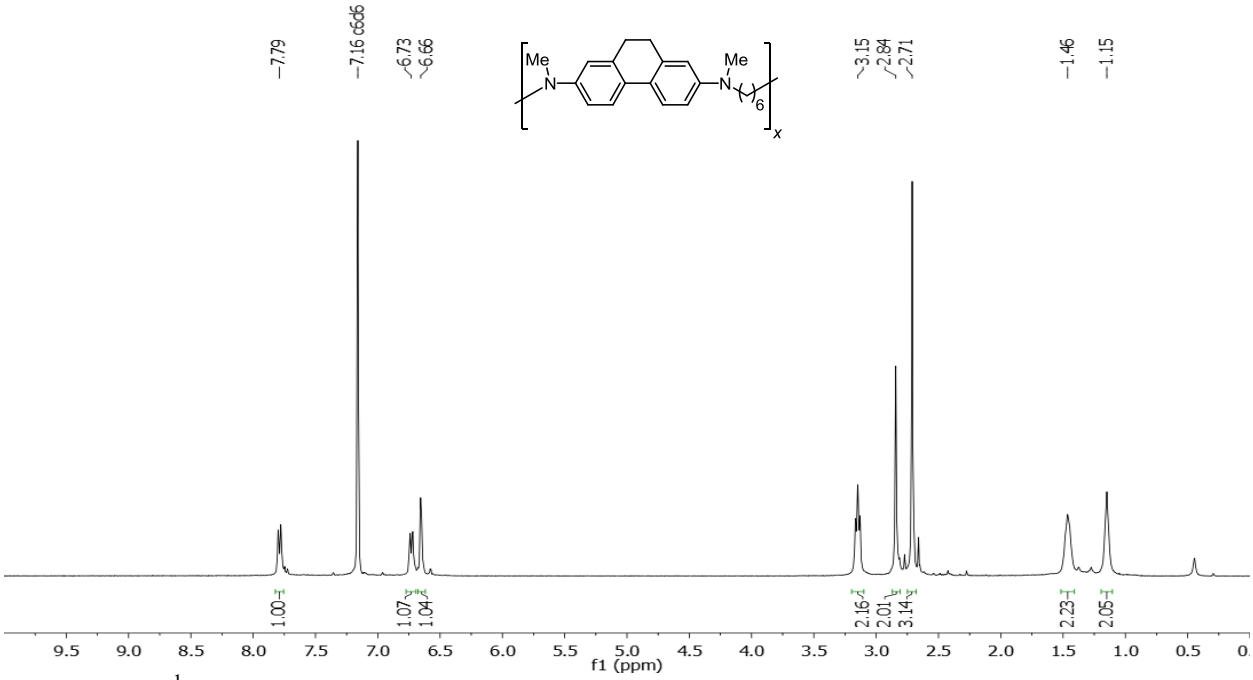

Figure 3-35. ^{1}H NMR spectrum of poly(**1d**-**2d**) (Table 3-2, entry 3).
^{1}H NMR spectrum (C_6D_6, 400 MHz): δ 7.79 (d, 2H), 6.73 (d, 2H), 6.66 (s, 2H), 2.16 (t, 4H), 2.01 (s, 4H), 2.71 (s, 6H), 1.44-1.49 (m, 4H), 1.13-1.17 (m, 4H).

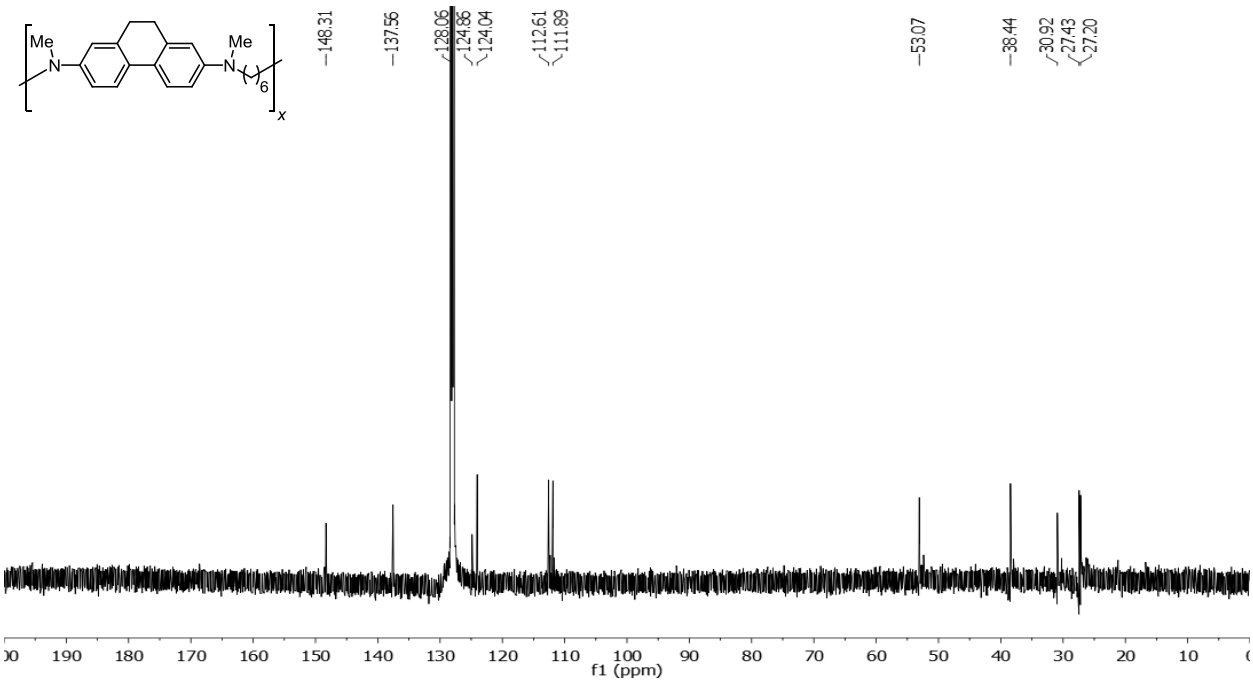

Figure 3-36. ^{13}C NMR spectrum of poly(**1d**-**2d**) (Table 3-2, entry 3).
^{13}C NMR ($CDCl_3$, 125 MHz): δ 148.31, 137.56, 128.06, 124.86, 124.04, 112.61, 111.89, 53.07, 38.44, 30.92, 27.43, 27.20.

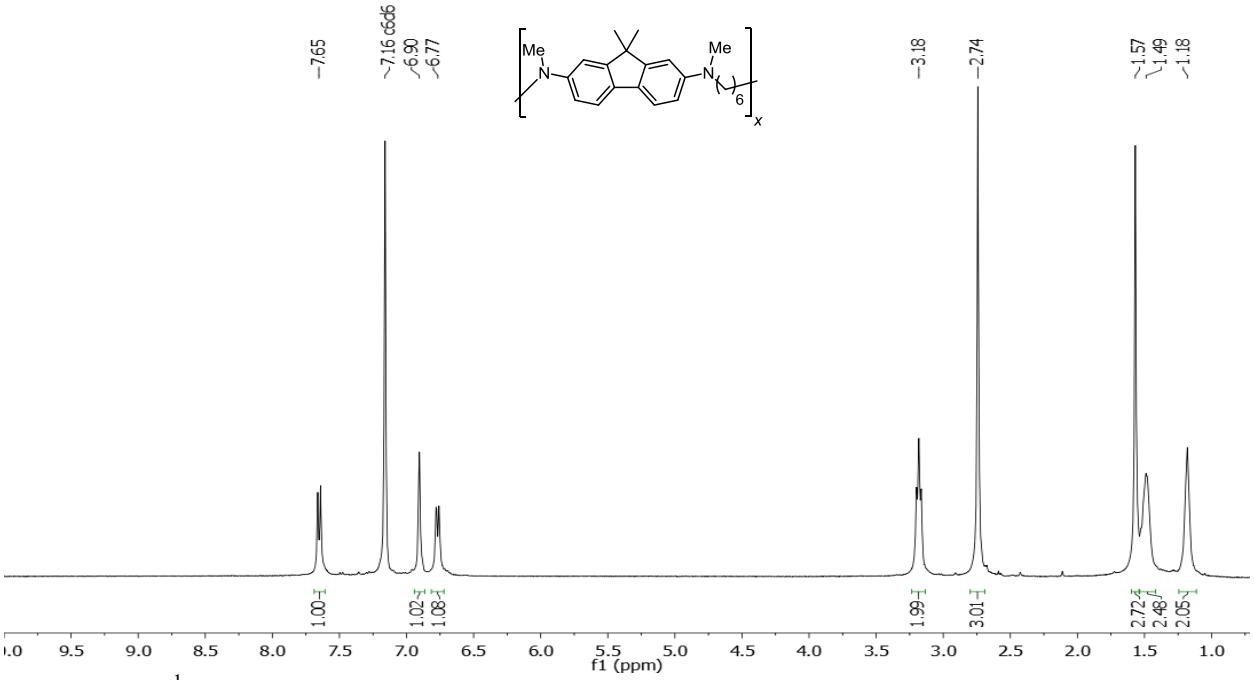

Figure 3-37. ^{1}H NMR spectrum of poly(**1d-2e**) (Table 3-2, entry 4).
^{1}H NMR spectrum (C_6D_6, 400 MHz): δ 7.65 (d, 2H), 6.90 (s, 2H), 6.77 (d, 2H), 3.18 (t, 4H), 2.74 (s, 6H), 1.57 (s, 6H), 1.46-1.51 (m, 4H), 1.16-1.20 (br s, 4H).

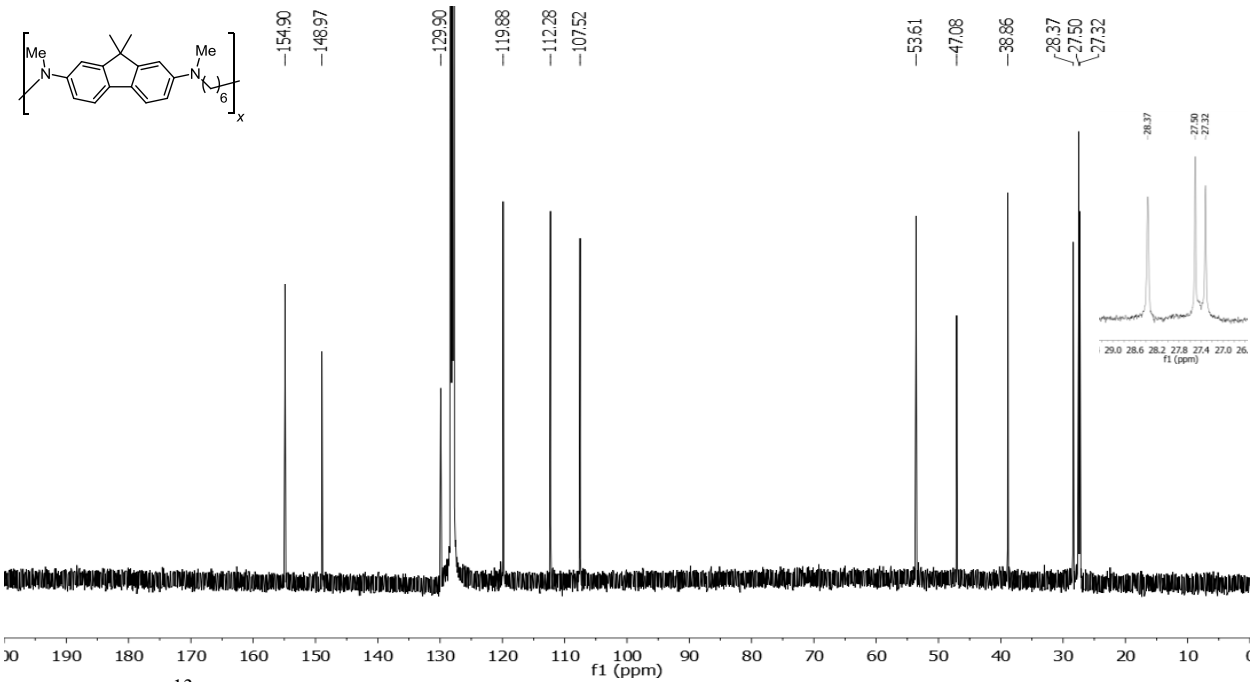

Figure 3-38. ^{13}C NMR spectrum of poly(**1d-2e**) (Table 3-2, entry 4).
^{13}C NMR (C_6D_6, 125 MHz): δ 154.90, 148.97, 129.90, 119.88, 112.28, 107.52, 53.61, 47.08, 38.86, 28.37, 27.50, 27.32.

REFERENCES

(1) Armand, M.; Tarascon, J. M. *Nature* **2008**, *451*, 652-657.

(2) Larcher, D.; Tarascon, J. M. *Nat. Chem.* **2015**, *7*, 19-29.

(3) Tarascon, J. M. *ChemSusChem* **2008**, *1*, 777-779.

(4) Tarascon, J. M.; Armand, M. *Nature* **2001**, *414*, 359-367.

(5) Liang, Y.; Tao, Z.; Chen, J. *Adv. Energy Mater.* **2012**, *2*, 742-769.

(6) Song, Z.; Zhou, H. *Energy Environ. Sci.* **2013**, *6*, 2280-2301.

(7) Novák, P.; Müller, K.; Santhanam, K. S. V.; Haas, O. *Chem. Rev.* **1997**, *97*, 207-282.

(8) Janoschka, T.; Hager, M. D.; Schubert, U. S. *Adv. Mater.* **2012**, *24*, 6397-6409.

(9) Nakahara, K.; Oyaizu, K.; Nishide, H. *Chem. Lett.* **2011**, *40*, 222-227.

(10) Burkhardt, S. E.; Lowe, M. A.; Conte, S.; Zhou, W.; Qian, H.; Rodríguez-Calero, G. G.; Gao, J.; Hennig, R. G.; Abruña, H. D. *Energy Environ. Sci.* **2012**, *5*, 7176-7187.

(11) Conte, S.; Rodríguez-Calero, G. G.; Burkhardt, S. E.; Lowe, M. A.; Abruña, H. D. *RSC Adv.* **2013**, *3*, 1957-1964.

(12) Truong, T.-T.; Coates, G. W.; Abruña, H. D. **2015**, *Submitted*.

(13) Michaelis, L.; Schubert, M. P.; Granick, S. *J. Am. Chem. Soc.* **1939**, *61*, 1981-1992.

(14) Ito, A.; Sakamaki, D.; Ino, H.; Taniguchi, A.; Hirao, Y.; Tanaka, K.; Kanemoto, K.; Kato, T. *Eur. J. Org. Chem.* **2009**, *2009*, 4441-4450.

(15) Muci, A. R.; Buchwald, S. L. In *Cross-Coupling Reactions*; Miyaura, N., Ed.; Springer Berlin Heidelberg: 2002; Vol. 219, p 131-209.

(16) Hartwig, J. F. *Acc. Chem. Res.* **2008**, *41*, 1534-1544.

(17) Kanbara, T.; Izumi, K.; Narise, T.; Hasegawa, K. *Polym J* **1998**, *30*, 66-68.

(18) Goodson, F. E.; Hauck, S. I.; Hartwig, J. F. *J. Am. Chem. Soc.* **1999**, *121*, 7527-7539.

(19) Zhang, X.-X.; Sadighi, J. P.; Mackewitz, T. W.; Buchwald, S. L. *J. Am. Chem. Soc.* **2000**, *122*, 7606-7607.

(20) Chang, G.; Luo, X.; Zhang, L.; Lin, R. *Macromolecules* **2007**, *40*, 8625-8630.

(21) Hoyos, M.; Sprick, R. S.; Wang, C.; Turner, M. L.; Navarro, O. *J. Polym. Sci., Part A: Polym. Chem.* **2012**, *50*, 4155-4160.

(22) Feng, J. K.; Cao, Y. L.; Ai, X. P.; Yang, H. X. *J. Power Sources* **2008**, *177*, 199-204.

(23) Roberts, M. E.; Wheeler, D. R.; McKenzie, B. B.; Bunker, B. C. *J. Mater. Chem.* **2009**, *19*, 6977-6979.

(24) Su, C.; Yang, F.; Ji, L.; Xu, L.; Zhang, C. *J. Mater. Chem. A* **2014**, *2*, 20083-20088.

(25) Merz, A.; Bard, A. J. *J. Am. Chem. Soc.* **1978**, *100*, 3222-3223.

(26) Peerce, P. J.; Bard, A. J. *J. Electroanal. Chem. Interfacial Electrochem.* **1980**, *112*, 97-115.

(27) Zweig, A.; Maurer, A. H.; Roberts, B. G. *J. Org. Chem.* **1967**, *32*, 1322-1329.

(28) Bard, A. J.; Faulkner, L. R. *Electrochemical Methods: Fundamentals and Applications, 2nd Edition* - 2nd ed.; Wiley: New York, 2001.

(29) Dietrich, M.; Heinze, J.; Fischer, H.; Neugebauer, F. A. *Angew. Chem., Int. Ed.* **1986**, *25*, 1021-1023.

(30) Henning, T. P.; Bard, A. J. *J. Electrochem. Soc.* **1983**, *130*, 613-621.

(31) Meerholz, K.; Heinze, J. *Angew. Chem., Int. Ed.* **1990**, *29*, 692-695.

(32) D. Abell, A.; Brandt, M.; A. Levy, M.; A. Holt, D. *J. Chem. Soc., Perkin Trans. 1* **1997**, 1663-1668.

(33) Abruna, H. D.; Denisevich, P.; Umana, M.; Meyer, T. J.; Murray, R. W. *J. Am. Chem. Soc.* **1981**, *103*, 1-5.

CHAPTER FOUR

CONCLUSIONS AND FUTURE OUTLOOK

4-1. Overview

The research presented in this dissertation focused on the development of new, high-capacity, organic cathode materials for electrochemical energy storage applications. These polymers contained redox-active arylamine moieties, such as *N,N,N′,N′*-tetramethyl-*p*-phenylenediamine and *N,N,N′,N′*-tetramethylbenzidine. Correspondingly, they exhibited two reversible one-electron transfers at high potentials (>3.3 V vs. Li/Li^+) and fast charging/discharging rates. The electrochemical performance of the polymers was dependent on the alkyl linker between arylamine groups and longer alkyl spacers were necessary to obtain well-defined redox processes. In these studies, the polymers displayed good cycling capability and the potential to be used as cathode materials in electrochemical energy storage devices.

4.2 Future Studies

The ideal organic cathode material should have high energy and power densities, and can be cycled for thousands of cycles with minimal capacity fade. Additional work is needed to improve the performance of the polyarylamines presented in this work to achieve those goals. The biggest challenge for these polyarylamines is to improve their cycling capability and correspondingly, their insolubility.

The electropolymerized benzidine polymers could be cycled for one hundred cycles at the rate of 1,000 C, and retained 92% of its initial capacity. Three methods to improve the cycling performance are to optimize the electropolymerization in order to deposit an insoluble polymer film, enhance stability of the dicationic polymer species

and to prevent charge trapping. Using the conditions described in chapter two, a polymer film of **PDA-6** was deposited directly on conductive substrates. The polymer films had good adhesion to the electrodes; the films had to be scrubbed off the electrodes with Kimwipes to remove the polymer films. **PDA-6** exhibited >99% capacity retention when cycled around the first redox couple. However, there was a steady decrease in capacity when **PDA-6** was cycled around both redox couples, which suggested that the dicationic polymer has higher solubility in the electrolyte. Controlling the electropolymerization to obtain higher molecular weight polymers, which should improve the insolubility of the material, could increase the cycling performance of these polymers. Furthermore, enhancing the electrolyte-polymer interactions in a favorable manner (e.g. to prevent dissolution and to stabilize the charged species) should improve the cycling performance. Carbonyl-based organic cathode materials utilized salt formation during cycling to prevent dissolution of active material (as reviewed in chapter one).

Some of the polyarylamines presented in chapters two and three displayed charge trapping effects, where the monocation radical polymer could be oxidized to

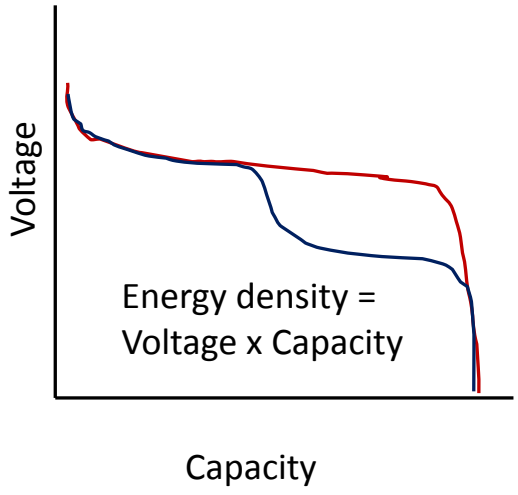

Figure 4-1. The discharge curves for compounds that undergo (red) two-electron transfer and (blue) two one-electron transfers.

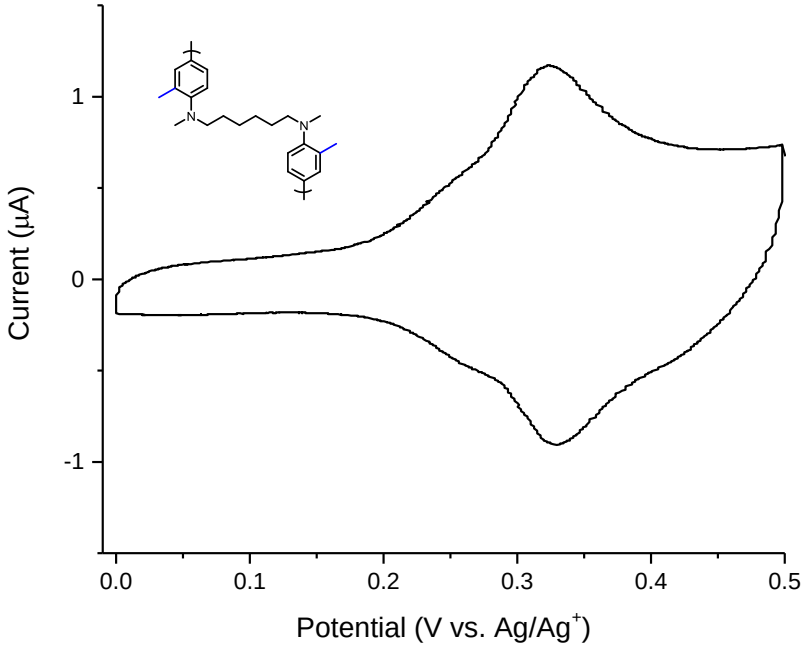

Figure 4-2. The cyclic voltammogram of the substituted benzidine polymer film in 0.5 M $[NBu_4][PF_6]$ in CH_3CN at 20 mV s^{-1}.

the dication polymer but not reduced to the neutral polymer without a large driving force. The cause of this phenomenon is still under investigation. One strategy to overcome the charge trapping effect and improve the energy densities of the system is to use polymers that undergo two-electron transfers in one step. This should eliminate the charge trapping of the monocation radical polymer. Since energy density is the product of voltage and capacity, this system would have a larger energy density compared to polymers with two one-electron transfers (Fig. 4-1.) There is precedence for substituted benzidines to be oxidized to the dication in one step.[1] We can vary the substituents on di- and tri-anilinoalkanes to synthesize a benzidine polymer that exhibits a two-electron transfer. Additionally, substituents can shift the redox processes to very positive potentials for application in high voltage batteries. Fig. 4-2 shows the cyclic voltammogram of an electropolymerized dimethylbenzidine polymer that exhibited only one redox couple at ~330 mV vs. Ag/Ag^+ (approximately where the second redox couple occurs for **PDA-6**). These preliminary results show the

viability of this route to synthesize higher energy density polymers that exhibit a two-electron transfer.

Thin films of electropolymerized benzidine polymers can be deposited on conductive substrates. These films could potentially be used in flexible or 3D batteries. Preliminary tests of **PDA-6** on high surface area electrodes (reticulated vitreous carbon) showed that 50x more polymer was deposited than on GCEs, and the films retained ~75% of its initial capacity after 100 cycles (Fig. 4-3).

Chapter three presented work on Pd-catalyzed cross-coupling to synthesize polyarylamines. These polymers demonstrated promising electrochemical performance as cathode materials. However, the low molecular weight polymers were soluble in electrolytes. The polymers need to be insoluble to be used in practical EES

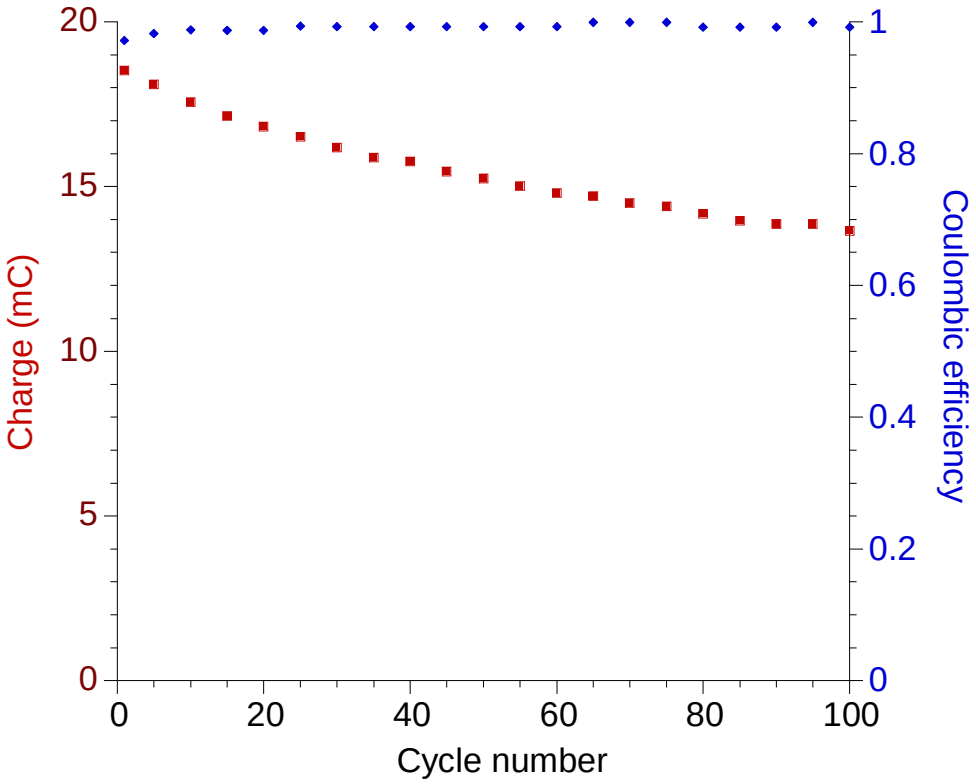

Figure 4-3. The charge (red) and Coulombic efficiency (blue) of PDA-6 deposited on high surface area reticulated vitreous carbon electrodes, cycled in 0.5 M $[NBu_4][PF_6]$ in CH_3CN at 10 mV s^{-1}.

devices. The two methods to synthesize insoluble polymers are to re-submit oligomers in the polycondensation reaction and to crosslink the oligomers (Fig. 4-4). After obtaining these insoluble polymers, they can be tested as cathode materials in coin cell devices. The results from the device testing can provide new insight into the development of improved polyarylamines as cathode materials.

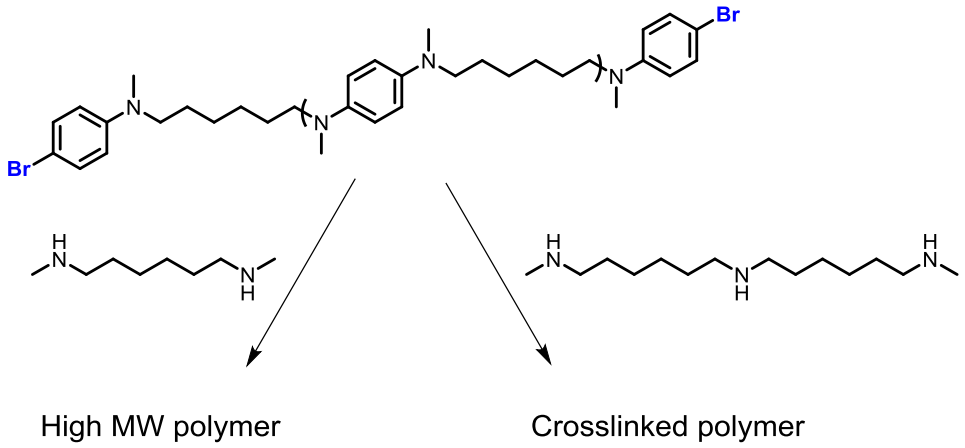

Figure 4-4. The cyclic voltammogram of the substituted benzidine polymer film in 0.5 M $[NBu_4][PF_6]$ in CH_3CN at 20 mV s^{-1}.

REFERENCES

(1) Macías-Ruvalcaba, N. A.; Evans, D. H. *J. Phys. Chem. C* **2007**, *111*, 5805-5811.